MULTINUCLEAR NMR SPECTROSCOPY STUDIES OF SOME ALUMINIUM COMPLEXES IN SOLUTION

PhD thesis

Andrea Bodor

University of Debrecen
Debrecen, 2000

MULTINUCLEAR NMR SPECTROSCOPY STUDIES OF SOME ALUMINIUM COMPLEXES IN SOLUTION

Értekezés a doktori (PhD) fokozat megszerzése érdekében
a kémia tudományágban

Írta: Bodor Andrea okleveles vegyész, kémia tanár

Készült a Debreceni Egyetem kémia doktori programja
(koordinációs kémia K/2 alprogramja) keretében

Témavezető: Dr. Tóth Imre

Jelölt a doktori szigorlatot 2000. ….. ….. – n eredményesen letette:

a bizottság elnöke: Dr. ……

Az értekezés bírálói:

Dr. …….
Dr. …….

A bírálóbizottság:

elnök: Dr. …….
tagok: Dr. …….
Dr. …….
Dr. …….
Dr. …….

Az értekezés védésének időpontja: 2000. ….. …..

Ezen értekezést a Debreceni Egyetem kémia doktori program koordinációs kémia (K/2) alprogramja keretében készítettem 1995 – 2000 között és ezúton benyújtom a Debreceni Egyetem doktori (PhD) fokozatának elnyerése céljából.

Debrecen, 2000. szeptember 7.

Bodor Andrea
doktorjelölt

Tanúsítom, hogy Bodor Andrea doktorjelölt 1995 – 2000 között a fent megnevezett doktori alprogram keretében végezte munkáját. Az értekezésben foglaltak a jelölt önálló munkáján alapulnak, az eredményekhez önálló alkotó tevékenységével meghatározóan hozzájárult. Az értekezés elfogadását javaslom.

Debrecen, 2000. szeptember 7.

Dr. Tóth Imre
egyetemi docens
témavezető

Table of Contents

I. INTRODUCTION

Approaching the topics from linguistic point of view the name aluminium derives from the Latin word *alum*, the double sulphate $KAl(SO_4)_2 \cdot 12H_2O$, which was used as an astringent in ancient Greece and Rome (*alumen* meaning bitter salt), as a fireproofing agent for wood and also as a mordant in dyeing. When speaking about aluminium the first non chemical observation is that some people call it aluminium, others refer to it as aluminum. It was Humphry Davy who although unsuccessful in isolating the metal called it alumium, then aluminum. Later this name was changed to aluminium, and this was adopted internationally; but in North America the ACS decided to use the old version, which has persisted up to the present day.

Pure metal aluminium is not found in nature, it was isolated for the first time in 1854 by the French chemist, Deville. On the other hand aluminium is the most abundant metal in the earth's crust (8.3% m/m) and it is a major component of many minerals, such as feldspars and micas. Under conditions of extreme weathering silicon is leached out and a mixture of hydrated oxides is formed, called bauxite. This is the starting material in metal aluminium production performed on huge scales following the Bayer process. Metal aluminium is used widely mainly in five major areas: (i) building and construction, (ii) containers and packaging, (iii) transportation, (iv) electrical conductors and (v) machinery and equipment. It is an attractive metal to recycle because the remelting of scrap requires only some 5% of the energy needed to produce the same weight of primary aluminium from bauxite.[1,2]

On the other hand aluminium is rarely found in any life forms. That is the reason why no organisms have developed protection against it. Problems began when as a consequence of rain containing significant amounts of sulfur and/or nitrogen oxoacids the soil and water pH values have decreased in large areas with poorly buffering (aluminosilicate) bedrocks. The result of interaction of strong acids with Al–containing minerals and/or with organic matter containing complexed and/or absorbed aluminium was the increased geochemical mobility of Al^{3+}. It was also found, that soluble Al^{3+} has toxic effects:

In case of plants at the surface of roots it antagonises calcium binding, which is essential for cell surfaces under these conditions. In this way aluminium can be responsible for forest damage and root damage in general.[3] Some polymeric

hydroxo complexes appear to have toxic effects as well.[4] Tea plants accumulate Al^{3+}, although it is not uniformly distributed. The aluminium content of older leaves is about 3%, while young leaves contain only 0.01%. Typical tea infusions contain about 50 times as much Al^{3+} as do infusions from coffee. Addition of milk to tea should immobilise Al^{3+} as insoluble phosphate, while addition of lemon forms a dangerous, strong citrate complex.[5]

In case of animals the circulating fluids are protected against aluminium as they are high in calcium and magnesium and are maintained at pH > 7. However, high aluminium content in streams and lakes is a causal factor in decline of fish stocks in these areas. The exact mechanism by which Al exerts its toxic effect may vary depending on the organism and its life stage, but also on which Al form is dominating. For example organically complexed Al is less toxic to brook trout (*Salvelinus fontinalis)* than the inorganic forms.[6] It was also reported that natural organic acids didn't reduce Al toxicity to juvenile rainbow trout (*Salmo gairdneri*), although the effect was delayed. The presence of silicate also reduces aluminium toxicity to fish.[4]

In humans the 'normal' plasma concentrations of aluminium are 10–20 μgdm^{-3}, thus reducing retention and deposition to a minimum. In foodstuffs aluminium levels of 10 mg per kg are rarely exceeded, and given the very low uptake of the element these probably represent safe levels. On the other hand it is known since Roman times that Al^{3+} is added to drinking water to improve its appearance. In individuals with chronic renal disease who had been exposed to dialysis fluid made with untreated or only softened tap water an accumulated aluminium level was found in the brain. This is associated with the 'dialysis dementia syndrome', called also dialysis encephalopathy. The complex bone softening state – particular fracturing variant of osteomalacia – which usually accompanies dialysis treated chronic renal failure is believed to represent the effects of accumulating tissue aluminium. Another recognised aspect of aluminium toxicity is iron–adequate anaemia which is probably due to inhibition in the bone marrow of the haemoglobin synthetic process. It has been also reported that the intra cellular content of aluminium is raised in certain nerve cells. The most important neurodegenerative condition linked to aluminium is Alzheimer's disease.[7,8]

It appears that Al^{3+} can be assimilated and transported using the iron pathways, but not stored in the same way, and it is this point that the toxic effects

manifest themselves by disrupting the biochemistries of other metal ions such as Ca^{2+} and Mg^{2+} and possibly also phosphate biochemistry.

For studying the chemistry of the different Al systems a proper experimental technique is required. Finding a good method might be an easier problem for some other metals, but aluminium is a 'hard metal' in this way also. Owing to the electronic structure of $1s^2 2s^2 2p^6$ and the absence of extended delocalised electronic structure in most of the ligands, UV–VIS spectroscopy is useless. There are no oxidation – reduction processes in these systems, so application of redoxy potential measurements is dropped. Regarding to the slow formation reactions potentiometric methods can be very time consuming, still this is the way how most equilibrium constants are determined. Aluminium is silent in ESR. ^{27}Al is a 100% abundant NMR nucleus having a quadrupolar moment (I = 5/2). The disadvantage is, that in most cases no information can be obtained from the observed very broad signals. Therefore, it is very useful if studies can be performed from the side of the ligand (*e.g.* ^{1}H, ^{13}C, ^{19}F NMR).

Among the naturally occurring ligands fluoride, oxalate and citrate have outstanding importance both from bioinorganic and geochemical point of view. Their complexes with aluminium were studied earlier, but the complete solution chemistry of these systems is still not elucidated. In this study we try to carry out detailed equilibrium, structural and dynamic characterization of several systems by multinuclear NMR. Our aim is: *i*) to investigate and reinvestigate some debated equilibria (Al^{3+} – oxalate – fluoride, Al^{3+} – fluoride), *ii*) to evaluate kinetics including both inter– and intra–molecular processes (Al^{3+} – fluoride, Al^{3+} – oxalate, Al^{3+} – citrate), *iii*) to find correlation between the kinetic behaviour of ligands and their coordination mode (Al^{3+} – oxalate, Al^{3+} – citrate) and *iv*) to solve the solution structures of some polynuclear species (Al^{3+} – citrate) by 1D and 2D NMR techniques using ^{1}H, ^{13}C and ^{19}F NMR.

II. BIBLIOGRAPHIC REVIEW

Bearing in mind the presented environmental and bioinorganic implications it is obvious why the solution chemistry of Al^{3+} became important. Modern books[1,2] and recent reviews[3,9] summarise the basic concepts about Al^{3+}. Evidences about the scientific activity in this research field are given by the number of recently published PhD works,[4,10–16] which cover a large area both geographically and scientifically. Without claiming to enumerate entirely all groups, those with the highest impact on this thesis are listed. Thus, most of the potentiometric evidences come from Umeå; Australian groups in Perth are concentrated on industrial relations of concentrated Bayer liquiors; a Californian team is interested in geochemical implications and adsorption properties; while research of some bioinorganic aspects is done in Hungary, at Debrecen, and Szeged.

Solution coordination chemistry studies give information about the distribution, speciation, structure and kinetics of the complexes. Having small size and high charge, Al^{3+} is a 'hard' ion, ligands possessing hard donor atoms will easily coordinate. Such naturally occurring ligands are F^-, the O containing hydroxide, oxalate, citrate, organic and inorganic phosphate, transferrin, humic acids, etc.

The equilibrium is very well founded in many Al^{3+} systems, stability constants resulting mainly from potentiometric titrations, using NMR, LAXS (X–ray on concentrated solutions) and single–crystal measurements as complementary, or supporting methods. For illustrating the variety and complexity of these systems a few examples are invoked. In Al^{3+} – H^+ – gallic acid system dinuclear and polynuclear complexes are formed. Moreover, an *o* – diphenolic complexation has been supposed.[17,18] The powerful complexing ability of two *ortho* – coordinated phenolic groups has been confirmed in the case of Al^{3+} – 1,2 dihyroxynaphtalene-4-sulfonate – OH^- system[19] as well. In addition, it is stated that the corresponding oxidized compounds, *o* – diquinones, do not form any complexes with Al^{3+}. The *ortho* – coordination is met in the aluminium – pyrocatechol system, where hydrolyzed species and a trinuclear complex has been detected as well. In these solutions the existence of several degrees of polymerization can be assumed.[20] The absence of polynuclear species is reported for the aluminium – salicylate system, where the coordination of a phenolic group and a carboxylate was studied. In this

case besides the binary compounds only the ternary, hydrolyzed, species are present.[21]

From structural point of view the chemistry of Al^{3+} is dominated by the formation of six coordinated, octahedral or distorted octahedral species, although direct structural confirmation *in solution* is rather sparse. Five coordinated Al^{3+} is the most uncommon coordination and can be found in some minerals (andalusite), or in fully hydrolysed zeolite A.[15] Four coordination with tetrahedral geometry is met in $Al(OH)_4^-$, but it is rare in other compounds. In *nonaqueous* solution tetrahedral AlF_4^- has been shown to exist.[22,23]

The main kinetic feature in these systems is the slow formation of the complexes and the slow ligand exchange reactions (observed already for $Al(H_2O)_6^{3+}$).[24] Kinetic studies of complex formation for Al^{3+} were performed in pure solvents and solvent mixtures with ligands possessing one or more coordination sites. Complexation with the unidentate sulphate ion was studied in water,[25] water – formamide, water – dimethylsulfoxide and water – hexamethylphosphoric triamide solvent mixtures.[26] The complexation of bidentate salicylic acid, 5 – sulfosalycilic acid and 5 – nitrosalycilic acid was also studied.[27-29] Secco and Venturini proved that complexation with salicylate follows a dissociative mechanism since the rate constant of ligand penetration is in excellent agreement with the rate constant of water exchange of the $Al(H_2O)_6^{3+}$. Perlmutter–Haymann and Tapuhi studying the complex formation with 5 – sulfosalycilic acid calculated a second order rate constant with a factor of 2 higher than the one obtained from water – ligand exchange. This is interpreted as a support of the 'internal hydrolysis' idea reffering to a metal which reacts with the anion of a weak acid.[30] Later, comparing the results for the above enumerated salicylate ligands, Perlmutter–Haymann and Tapuhi gave an alternative explanation originating from the fact that higher values were obtained for the anation reaction rate constants compared to the water exchange rate constant. They concluded, that an associative interchange mechanism is operative for all tervalent ions in their unhydrolyzed form. Moreover, it was found that the hydrolysed species $Al(OH)(H_2O)_5^{2+}$ undergo anation reaction faster than the aqua ions $Al(H_2O)_6^{3+}$ by more than two orders of magnitude. The reason is attributed to the mutual ligand interaction due to the OH^- ligand which in the same time labilases the water molecules around the metal ion.

Following this general review the specific bibliographic background is given for the studied systems separately.

II.1. The Aluminium – Fluoride System

Of more than sixty metal ion species, Al^{3+} binds F^- the most strongly, and its fluoride complexes are much stronger than those with other halides. When present, Al^{3+} is the main complexing agent of F^- in drinking water. Fluoride in drinking water is thought to reduce the incidence of dementia. Naturally occurring fluoride reduces toxicity to fish and also to plants such as tea and wheat.[31]

The biological importance of fluoroaluminates and fluoroberyllates has been recognised in so far as they act as phosphate analogues in enzymic reactions, possibly mimicking either the γ–group of a nucleoside triphosphate when a nucleoside diphosphate is present or an inorganic phosphate in the absence of any nucleotide. Still the role of AlF_4^- as an active inhibitory species has been questioned.[32,33]

Complexation of Al^{3+} by F^- also plays an important role in the Watts-Utley titration procedure which is widely used for monitoring of the Bayer process.[34] The final stage of this procedure is to determine Al^{3+} by titration of the OH^- released by the addition of an excess of F^-. The reaction is normally represented as :

$$Al(OH)_4^- + 6F^- \rightarrow AlF_6^{3-} + 4OH^-$$

The fluoride complexes of Al^{3+} have been intensively studied using a variety of experimental methods. The system is deceptively simple with many studies showing that it is well represented by the formation of a series of complexes ($i \geq 1$):

$$AlF_{i-1}^{(4-i)+} + F^- \rightleftharpoons AlF_i^{(3-i)+} \qquad \text{(II.1.)}$$

The values of the stepwise equilibrium constants corresponding to the equilibria in equation II.1. obtained by various types of potentiometric measurements, have been critically reviewed and are in excellent agreement for the lower order complexes ($i \leq 3$). However, some uncertainty exists with respect to the higher order complexes ($i \geq 4$). Thus, although all studies report formation of AlF_4^- (aq), estimates of K_4 vary by an order of magnitude. Despite the existence of higher order fluoro - aluminate species in the solid state and in high temperature melts there is, apart from an early potentiometric study by Brosset and Orring,[35] little evidence for the existence of complexes with $i \geq 5$ in *aqueous* solution. On the other hand, unlike the analogous Al^{3+}/OH^- system, no polynuclear species appear to form.

The Al^{3+}/F^- system has been investigated by NMR spectroscopy on a number of occasions. The earlier measurements have been reviewed thoroughly by Akitt.[9] Unfortunately, owing to the technological limitations of the times the early NMR work is only of qualitative use. For example, Yamazaki and Takeuchi[36] working in fairly concentrated aqueous solutions (c_{Al} = 0.5 –1 M, HF/Al = 1-6) found complexes with i = 1–4. Petrosyants and her colleagues published a series of papers dealing with ^{19}F-NMR studies of $AlF_i^{(3-i)+}$ complexes in aqueous solution and organic solvents.[37–40] Evidence for the existence of AlF_6^{3-} in solution has been provided by Konhsin and Tsernisov.[41] Their ^{27}Al – and ^{19}F – NMR spectra, measured in 90% H_2O_2 at *ca.* –40 °C, showed coupling consistent with a central Al^{3+} coordinated to six equivalent fluoride ligands, with $^1J_{Al-F}$ = 19 Hz. More recently, a high field study by Martinez *et al.*[42] confirmed the existence of ^{19}F signals for $AlF_i^{(3-i)+}$ (aq) with i = 1 and 2 but, significantly, noted difficulties in obtaining signals for higher species. They attributed other signals to the formation (at pH > 2) of mixed $Al(OH)F_i^{(2-i)+}$ complexes.

The kinetics of the formation of AlF^{2+} (aq) was studied by Shurukhin *et al.*[43] using a fluoride ion-selective electrode. Plankey and Pattersson[44] reinvestigated the system, also by potentiometry, and suggested I_a and I_d mechanisms for the reaction of F^- with Al^{3+} and $Al(OH)^{2+}$, respectively. On the basis of conventional kinetic measurements (followed by ^{19}F NMR) Zbinden[45] proposed a reactivity order towards F^- of $Al(H_2O)_6^{3+}$ << $Al(H_2O)_5F^{2+}$<< $Al(H_2O)_4F_2^+$.

No quantitative studies have been made on the kinetics of the formation or exchange reactions of the $AlF_i^{(3-i)+}$ (aq) complexes on spectroscopic time scales. However, Yamazaki and Takeuchi showed that complexes with i = 1–3 are in the "slow exchange regime" on the 60 MHz NMR time scale. The observed ^{19}F temperature-dependent line widths suggested the presence of ligand exchange reactions. Similar effects were observed by Martinez *et al.* who explained the temperature-dependent line broadening by proton exchange reactions (i.e. between ligated OH^- and H_2O) .

A number of questions clearly remain unanswered about the Al^{3+}/F^- system. Is there unambiguous evidence for the existence of $AlF_i^{(3-i)+}$ (aq) with i > 4 ? What are the structures and reaction dynamics of the $AlF_i^{(3-i)+}$ (aq) species which can be definitely identified?

II. 2. The Aluminium – Oxalate System

Oxalate is studied from many points of view, as a consequence its related literature is vast. It is one of the most abundant low molecular weight organic acids present in organic matter in soils. Oxalate is a major metabolic product of fungi in natural environments, and it is highly biodegradable. It was found that it weathers biotite more rapidly than other organic acids, and even HCl. Oxalic acid is present as nutritional stress in many crop plants, and has been found to be involved in the attacking mechanism of several phytopathogenic fungi.[46] As deposited in some concentration, or resulting from secretions of the biological organisms present in atmosphere oxalate is one of the dominant corrosion products of carbonate stone.[47] Massive research is done in the crystallization of calcium oxalate at different nephron levels, and investigation was done about forming either harmless crystals excreted with urine, or calcium stones, having more dramatic medical effects.[48]

Oxalate forms strong complexes with Al^{3+}. Aluminium extractability and solubility from different type of soils is studied in many cases by applying oxalate extraction.[49] Surface soils were analyzed for extractable Al hoping to test their use as geochronometers and paleoenvironmental indicators. Unfortunately, the study did not appear to give reliable results.[50] Investigations in cell biology proved that in the case of Al – stressed *Pseudomonas fluorescens* cells there is an increased oxalic acid production.[51] For appreciating these findings it is vital to know the possible complexes present under the investigated circumstances. Several groups worked on this project, and determination of species was done by potentiometric titrations. In the study of Bottari and Ciavatta the method of competitive reactions was used.[52] Sjöberg and Öhman combined the e.m.f. titration technique with ^{27}Al NMR measurements, as in this way it was possible to investigate solutions with very high and low acidities.[53] In a recent study of Ciavatta et al. ternary hydroxo oxalate species were again confirmed.[54]

Several structures for the Al oxalate species were determined. In all cases aluminium is six coordinated and $AlOx_3^{3-}$ trihydrate compound had been crystallized with different cations, but showing always the same structure with three bidentate oxalate ligands.[55–57] A structure with bridging oxalate was also detected for a tris oxalato aluminium sodium crystal.[58]

Oxalate shows different kinetic behaviour, and it seems to be very much metal dependent. For example in the case of titanium (III) the kinetics of complex

formation occurs via reaction with monoprotonated ligand, as in the studied pH range deprotonated oxalate is negligible and the fully protonated ligand is a very weak nucleophile. Substitution at the $Ti(OH_2)_6^{3+}$ proceeds by an associative interchange mechanism, while substitution of water in $TiOx(OH_2)_4^{+}$ proceeds by a predominantly dissocative mechanism, presumably because of the lower positive charge and the unimportance of the nucleophilic strength of the entering ligand at this stage.[59] In the vanadate(V) – oxalate system complexes similar to aluminium – oxalate species are detected VO_2Ox^- and $VO_2Ox_2^{3-}$. In the case of the second complex both intra– and inter – molecular ligand exchange are detected. The exchange within $VO_2Ox_2^{3-}$ is lowered only at temperatures around –5 °C. The activation entropy does not differ greatly from zero, $\Delta S^* = 40$ J mol^{-1} K^{-1}, a value characteristic for fluxional changes. In the case of the inter–molecular exchange a dissociative mechanism is preferred, which is in agreement with the positive activation entropy, $\Delta S^* = 30$ J mol^{-1} K^{-1}, and it is less probable that the relatively large oxalate ion enters into the already saturated coordination shell of vanadium.[60] For the aluminium – oxalate system the rate of water exchange for $AlOx(H_2O)_4^{+}$ species has been studied. It is found that the reactivity of Al(III) – oxygen bonds to water is dramatically increased by addition of a dicarboxylic chelate in the inner–sphere of the metal.[61]

In this study we would like to characterize the aluminium – oxalate species and to complete the kinetic information available in this field studying ligand exchange reactions by ^{13}C NMR measurements. Moreover, possessing equilibrium and kinetic data of both binary aluminium – fluoride and aluminium – oxalate species an equilibrium study of the more complex aluminium – fluoride – oxalate system is performed trying to use NMR measurements for complementary information to potentiometric titrations.

II.3. The Aluminium – Citrate System

Tricarboxylic citrate is widely found in geochemical and biological systems. Citric acid is capable to form soluble complexes with Al from clay minerals. In biological fluids citrate is the main small molecule of aluminium

transport and it is the lowest molecular weight metal binder in blood plasma. Citrate ion has four potential donor sites, two terminal and one central carboxylate and an alcoxy group on the central carbon. The carboxylate parts are available at low pH, but they bind Al(III) less strongly than the more basic hydroxyl group, which is protonated at low pH, therefore it is not available. Various coordinations are known from structural studies performed on complexes of citrate with transition metals and main group metals. Thus, for example, citrate was found to be bidentate in the mononuclear Sb(III) – Cu(II) complex[62] with the deprotonated alcoxy group and the central carboxyl group as coordinating sites. The deprotonated alcoxy group is able to take bridging positions as it was shown for the dimeric Ga(III) complex.[63] Moreover, the hydroxyl group can coordinate in protonated form as well, a feature demonstrated for the Co(III) complex.[64] The optimum combination of chelate ring size is presented in the tridentate form. The use of one terminal carboxyl group and the carboxyl and alcoxy groups from the central carbon gives this favourable positioning found for example in the case of deprotonated alcoxy for V(IV) complex[65] and for the protonated one in the Fe(II) complex.[66] Tetradentate coordination is indicated in the Ni(II) complex, where anions consisting of two Ni_4 clusters are linked by bridging carboxyl and alcoxo groups.[66] For aluminium citrate species two X ray structures are known. One is the monomeric $Al(Cit)_2^{5-}$ with tridentate fully deprotonated citrates with the above mentioned favourable positioning.[67] The other is the trimeric anion $Al(H_{-1}Cit_3)(OH)(H_2O)^{4-}$ indicating four dentate citrate ligands – each of them are distinct in their coordination – with three deprotonated alcoxy oxygen donor atoms, hydroxide ion in bridging position and a water molecule to complete the octahedral coordination sphere around the three metal centers.[68] It is interesting to point out that both crystals were precipitated at pH ~ 8. The trimer was obtained from an equimolar Al : citric acid mixture neutralized with aqueous ammonia and the mononuclear species precipitated at a metal : ligand ratio 1 : 2. Considering this, it may not be surprising that divergent data appeared concerning the existing species in solution. The equilibrium of the Al-citrate system was studied by different groups,[69–72] and different species distribution was reported. The reason for this is that aluminium citrate species form very slowly and under some conditions equilibrium is established in more than 20 hours. Reflecting to this, it seems understandable that Powell and Gregor and Motekaitis and Martell described only mononuclear forms by their potentiometric studies considering that the allowed

time for equilibration was 10 minutes and 4 hours, respectively. Polynuclear species were detected when a longer time was permitted for equilibration. Thus, the reliable model was given by Öhman and his data are used - and confirmed - in this study as well. According to this work monomeric and trimeric forms are present. $Al_3(H_{-1}Cit)_3(OH)^{4-}$ indicated four dentate citrate ligands. At pH > 7 another polynuclear complex appears $Al_3(H_{-1}Cit)_3(OH)_4^{7-}$ having coordinated citrates through two carboxylate and one deprotonated hydroxyl groups. This shows similar coordination pattern than that of $Al(Cit)_2^{3-}$, species existent in equilibrium at pH = 2.5 – 6.5 (and not at ~ 8.0).

The outcome of the different coordination could be different kinetic behaviour. Nevertheless, there is no information about the dynamics in the Al–citrate system. Searching for an answer to this question we identified the species existent in solution by means of ^{1}H and ^{13}C NMR measurements. Furthermore, an investigation and comparison of the behaviour of different coordinated citrate ligands was performed in inter- and intra- molecular exchange reactions.

III. EXPERIMENTAL SESSION

III.1. Used Chemicals

All chemicals used in this work were of the highest purity, purchased from Merck, or Aldrich. Several substances were prepared, as follows:

Aluminium chloride was prepared from 99.9999% purity Al wire (Ajka, Hungary). A weighed quantity of wire was reacted with a stoechiometric quantity of HCl in a Pt boat kept in a glass vessel. As well as acting as a container the Pt served as a catalyst to speed the reaction time to 1 day. The vessel was cooled and protected against the introduction of impurities by allowing the H_2 formed to evolve *via* a gas-washing bottle containing dilute HCl. A stock aluminium solution of 0.400 M, containing a minimum of free acid, was prepared and its concentration checked by EDTA titration.

$(NH_4)_5[Al_3(H_{-1}Cit)_3(OH)(H_2O)]NO_3{\cdot}5H_2O$ was prepared by the method of Feng *et al*.[68] *$Na_5[Al_3(H_{-1}Cit)_3(OH)(H_2O)]\ NO_3{\cdot}5H_2O$* was prepared similarly to the recipe given by Feng *et al.* 19.2 g (0.0768 mol) solid H_3Cit was dissolved in 87 cm^3 5M NaOH solution and 37.52 g (0.0933 mol) $Al(NO_3)_3{\cdot}9H_2O$ was added to this solution. The resulted pH was ≈ 4.5. The solution was kept 1 hour at 80 °C, while pH decreased to ≈ 2.5. By addition of NaOH pellets pH ≈ 8 was set and solution was stirred for 1 day. No precipitation occurred. To addition of ethanol precipitation started and the slurry was kept 2 days at constant stirring. The precipitated substance was filtered and dried at 90°C. The number of crystal water molecules was determined by drying 5 parallel samples at 150°C, and weighing them before and after heating. Yield: 14%. In our studies the Na^+ salt was used. In this case we didn't have to take into account the buffer capacity of the NH_4^+ ion and the $NH_4^+ + OH^- \rightleftharpoons NH_3 + H_2O$ reaction in the pH dependent studies. The ^1H and ^{13}C NMR spectra of both salts were identical.

III.2. pH Measurements

Free hydrogen ion concentrations in solutions of moderate acidity were measured by a combined glass electrode (Radiometer), or in the case of fluoride containing samples with a HF-resistant combined glass electrode (Ingold, HF-405-60-57) connected to a pH meter and calibrated by the method of Irving *et al* [73] to

give $pH = -log[H^+]$. If solutions were prepared in D_2O then pH was calculated using the relation: pH = pD + 0.4 [74] Occasionally the pH had to be measured in samples with little or no buffer capacity, or in very acidic solutions. In such cases pH can be measured *in situ* by monitoring the observed time-averaged (^1H, ^{13}C, ^{19}F) NMR shift (δ_{obs}) of a properly chosen HL/L^- signal. The requirement toward this substance is the absence of reactions with the species existent in solution. However, in some cases this species was present in the solution as being the investigated ligand. One can use the signal of the free ligand also to follow pH, if the exchange between the free ligand and ML_i is slow on the actual NMR time scale. Providing the proton exchange is rapid it is readily shown that:

$$pH = pK_{HL} - log[\delta_L - \delta_{obs}]/[\delta_{obs} - \delta_{HL}] \quad \text{(III.1.)}$$

where δ_L is the chemical shift of the deprotonated form, L^-, in extreme basic solution and δ_{HL} is the chemical shift of the protonated form, HL, in the extreme acidic solution and δ_{obs} is the measured value. This method is sensitive to pH-change in the pH range corresponding to: $pK_{HL} \pm 1.9$. Characteristics of this HL/L^- species are collected in Table III.1.

Table III.1. The observed nuclei of the chosen HL/L^- substances, their pK_{HL} values at the respective ionic strength and temperature and the extreme chemical shifts

NMR nucleus	HL	Ionic media	pK_{HL} 298 K	δ_{HL}(ppm)	δ_L(ppm)
^{13}C	$H^{13}CN$	3 M KCl	10.01	115.35	167.83
	$H^{13}COOH$	1 M NaCl	3.58	168.89	174.14[75]
^{19}F	HF	1 M NaCl	2.89	-44.10	0.00
		3 M KCl	3.32	-43.08	0.40

III.3. NMR Measurements

^1H NMR spectra were recorded at 360 and 500 MHz, ^{13}C NMR spectra at 80 and 125 MHz; ^{19}F NMR spectra at 470 MHz; ^{27}Al NMR spectra at 130 MHz with Bruker AMX360, DMX500 and DRX500 spectrometers using a 5 mm inverse probehead and a 10 mm BBO probehead (for ^{27}Al measurements) in locked mode. Characteristic parameters (flip angle, pulse repetition time, spectral window, number of scans) were chosen as to obtain high quality spectra and quantitative

integration where possible. The temperature of the probehead was checked by the ′methanol-thermometer method′.[76]

The chemical shifts are reported in ppm for ^{1}H and ^{13}C spectra toward higher frequencies with respect to TMS* as an external standard (0.00 ppm in both cases); in ^{27}Al NMR referring to $Al(H_2O)_6^{3+}$ at 0.00 ppm and in ^{19}F NMR toward lower frequencies using an aqueous alkaline solution of 0.01 M NaF (δ = 0.00 ppm) as an external standard. For ^{19}F measurements samples were introduced in PTFE NMR tubes, which were inserted into conventional 5 mm glass tubes.

Assignation and structural analysis. The simplest and most often applied measurement is the one pulse ^{1}H experiment. The pulse sequence contains the preparation period (d1) followed by the radio frequency pulse p1 and the detection period (aquisition).

d1 – p1 – aq

Optimal values has to be set for parameters d1 and p1. For this it is advised to previously determine the 90° pulse and the T_1 relaxation time. Assignments and structural information are drawn from the chemical shifts, coupling constants and the integrated values of the individual proton resonances. If signals in 1D spectra are overlapping and assignation seems hopeless the 2D homonuclear correlation H, H – COSY experiment is required. This sequence establishes the H/H coupling network as cross peaks appear if spin coupling is present. The basic COSY sequence for magnitude processing is:

d1 – p1 – t1 – p2 – aq

where p1 is the 90° pulse and p2 can have different values. If it is set to the 90° value than the sensitivity is maximized; if it has the value of 45° then structured cross peaks are yielded and diagonal peaks are suppressed. t_1 is set to 1/[2·sw1]. For separation of the spin–spin coupling from chemical shift 2D *J*–resolved spectra is acquired, as on the F_2 axis only the chemical shift information is present and on the F_1 axis the spin –spin coupling information. The sequence is:

d1 – p1 – t1/2 – p2 – t1/2 – aq

where t1 evolution is 1/[2·sw1] and a p2 = 180° pulse is set in the center for refocusing the effect of chemical shift but not the one of the homonuclear J–coupling (spin–echo). Another advantage of this method is the separation of homonuclear and heteronuclear couplings.

The one pulse ^{13}C NMR experiment is identical to the basic ^{1}H experiment, except that the pulse is applied at the ^{13}C frequency. In this way the heteronuclear HC couplings are present, and the resulted spectra is crowded. As in most cases the C resonances are interesting, H decoupled spectra are recorded. If only a qualitative picture is desired than a power gated decoupled or a DEPT (**D**istorsionless **E**nhancement by **P**olarization **T**ransfer) spectrum is run. In the DEPT sequence polarization transfer from protons to the ^{13}C nucleus is used to increase the signal strength:

^{1}H: d1 – p1 – d2 – p2 – d2 – p3 CPD

^{13}C: p4 – p5 – d2 AQ

where CPD stays for the composite pulse decoupling; p1, p2 are the 90° and 180° ^{1}H decoupler pulses; p4, p5 are the 90° and 180° ^{13}C transmitter pulses; d2 = $1/(2J_{CH})$ with J_{CH} = 140 Hz. This sequence has the advantage that the different CH_n groups can be distinguished by the variation of p3 pulse length. Thus, the p3 = 45° ^{1}H decoupler pulse will give the signals of CH, CH_2, CH_3 groups positive, setting the 90° value gives only the signals of CH groups and for the 135° value the signals of CH and CH_3 groups are positive and the signals of CH_2 groups are negative.

Recording quantitative ^{13}C spectra is not as straightforward as in the case of ^{1}H NMR, because both nuclear Overhauser enhancement (nOe) and the varying relaxation times of the different carbon environments complicate the situation. For quantitative analysis the inverse gated technique is used. The sequence is:

^{1}H: CPD

^{13}C: d1 – p1 – aq

where p1 is the 45° ^{13}C transmitter pulse. In this experiment the composite pulse decoupling is applied only during the short aquisition time and not during the delay d1. Coupling information is immediately eliminated by the decoupling field and the build up of nOe requires a time similar to the spin-lattice relaxation. Therefore, setting the d1 delay at least 10 times the aquisition time, ^{1}H decoupled spectra without nOe can be recorded.

Connectivities between H and C atoms in a molecule, through one or more chemical bonds, are elucidated by 2D heteronuclear correlation techniques. The corresponding experiments use either the large $^{1}J_{CH}$ or the smaller long range $^{n}J_{CH}$ couplings for polarisation transfer. A variety of sequences exist, which differ in the detected interaction ($^{1}J_{CH}$ or $^{n}J_{CH}$) and the mode of detection (^{13}C or ^{1}H detected,

magnitude or phase mode, phase cycling or gradients for coherence selection). A basic HETCOR experiment yields cross signals for all protons and ^{13}C nuclei which are connected by a C,H coupling over one bond. The assignment of one member of a spin-coupled pair leads immediately to the assignment of the other. The basic ^{13}C detected sequence is:

^{1}H: d1 – p1 – (t1)/2 – (t1)/2 – d2 – p2 – d3 CPD

^{13}C: p3 – p4 – d2 AQ

where p1, p2 is the 90° ^{1}H decoupler pulse, p3 is the 180° ^{13}C transmitter pulse; p4 is the 90° ^{13}C transmitter pulse. Delay d1 is about 2s, and delays d2, d3 are $1/(2J_{CH})$ and $1/(3J_{CH})$, respectively. The increment for t1 evolution is 1/(2SW1). Heteronuclear couplings are 'removed' in both dimensions by the addition of the p3 pulse in the middle of the t1 evolution period and by ^{1}H broadband decoupling during data aquisition.

The inverse detection mode is a more suitable solution as acquisition is on the ^{1}H channel - meaning shortened measuring time - and it is based on multiple quantum transitions. The most common experiments are HSQC (**H**eteronuclear **S**ingle **Q**uantum **C**oherence), or HMQC (**H**eteronuclear **M**ultiple **Q**uantum **C**oherence). The challenge of these inverse detected experiments is the suppression of the large unwanted signals induced by protons not directly bound to a ^{13}C nucleus and originating almost exclusively from all the ^{12}C isotopomers. The ^{1}H detected and gradient enhanced experiments are currently the best methods to apply.

Long range coupling patterns are determined in the same way, the only difference is the adjustment of delays to values appropriate to those of $^{2}J(C,H)$ and $^{3}J(C,H)$.

NMR can also be used to determine the spatial structure of a molecule. The purpose of a two dimensional NOESY spectra is to establish connectivities between the spins via cross – relaxation. The pulse sequence of the NOESY experiment is:

$$d1 - p1 - t1 - p1 - \tau_{mix} - p1 - aq$$

The experiment starts with a relaxation delay, followed by a p1 = 90° pulse from direction X to create transverse magnetization. This concludes the preparation stage, followed by the evolution stage , during which spins become labeled with their offset frequencies. The second 90° pulse from –X creates again Z magnetization During the mixing period magnetization is transferred from one spin

to another via cross – relaxation. The third 90° pulse brings the magnetization back in the XY plane and the precession can be monitored during aquisition. A phase sensitive NOESY is advantageous to record, as in this case one can distinguish between nOe effects (if they are positive) and exchange effects. Thus, when the diagonal peaks have positive intensities, the nOe crosspeaks will show negative intensities and crosspeaks due to chemical exchange exhibit positive intensities. If NOESY does not give a result, then the application of the rotating frame variant: ROESY is suggested. For this nOe effects are measured under spin – locked conditions:

$$d0 - p1 - t1 - spinlock - aq$$

In the case of studying exchange reactions in 2D, the pulse sequence of the EXSY is the same as for the NOESY.

The 100% abundant, spin ½ nucleus, ^{19}F presents some experimental problems. Because of the similarity in the magnetogyric ratios of ^{1}H and ^{19}F (26.751 and 25.1665 respectively), the resonance frequencies are very close and ^{19}F is not usually regarded as an X – nucleus. Consequently, when measuring this nucleus, first a ^{1}H file is loaded and the resonance frequency of 500 MHz is tuned to around 480 MHz. After this, following the correct connection of the cables, on a ^{19}F file the corresponding 470 MHz is tuned. From now on the simple ^{1}H pulse sequences can be run, of course with the corresponding pulse parameters.

^{27}Al is a quadrupolar nucleus with spin 5/2. As a consequence, the relaxation times are short and broad signals are resulted, preventing accurate measurement of chemical shift and the resolution of scalar coupling splittings. However, in highly symmetrical environments the quadrupolar relaxation mechanism becomes less effective, relaxation times become longer and linewidth become smaller. This is the case of the easy observed hexacoordinated $Al(H_2O)^{3+}$ at 0.0 ppm and the tetracoordinated $Al(OH)_4^-$ at 80.0 ppm.[77–82]

Equilibrium. Although NMR spectroscopy does not usually have the precision of potentiometric measurements it can provide an important independent check on their validity. Providing the signal assignments are correct, measurement of the integrated intensities as a function of pH and/or concentrations enables the stability constants of all detected species to be determined.[83] (see also Chapter IV)

Dynamics. It is a common use of NMR to study dynamic processes in equilibrium systems. Rate constants between 1 and 10^{10} can be measured. The following situations can take place: if the rate is much slower compared to the

difference between the chemical shift of the individual species, then two separate narrow peaks are observed. The other extreme is the case when the exchange rate is much faster than the shift difference and only one narrow averaged peak is detected. In between, there is a broadening of both peaks, followed by a coalescence resulting a common broad peak. Thus, line broadening measurements provide kinetic information. In the case of *n* exchanging species the line broadening is described by the relation:

$$LB_i = \frac{1}{\pi} k_i^{obs} \qquad \text{(III.2.)}$$

where k_i^{obs} is the pseudo first order rate constant of all parallel reactions from site *i.* Once the chemical reactions which can transfer magnetisation from one site to the other are found the reaction rates can be written and the expression with the concentration, LB and *k* values are fitted, and calculated. Calculations were done using MATLAB microprograms. Detailed description is found in chapter IV.1.2.

There are situations where the chemical exchange is too slow to affect the line shape and information on T_2 *transverse relaxation* time scale are not obtained. If the rate of exchange is of the same order of magnitude as the *longitudinal relaxation* rate ($1/T_1$) than the rate constants can be evaluated by magnetization transfer experiments. That means that exciting one peak it will relax and parallely exchange is also happening. This is observed on the peak of the exchange partner, as the intensity of that one is decreasing. Technically this selective excitation – 180° inversion – is performed in several ways. The DANTE[77] (**D**elays **A**lternating with **N**utation for **T**ailored **E**xcitation) sequence consists of a train of *n* hard pulses of very small flip angle with constant phase and constant separation. The acronym DANTE is a reference to Dante Alighieri's *La Divina Comedia*, where in the second part, the *Purgatorio*, heaven (transverse magnetization) is reached progressively via intermediate stages (RF pulses and delays).

$$180° (n\tau_p) \text{ - VD - } 90° \text{ - aq}$$

where VD stands for variable delay, and the non–selective 90° reading pulse generates observable peaks. If the VD time is very small compared to relaxation time and the life time of the individual exchange site than there is no time for negative magnetisation to be transferred, and the spectrum will consist of one negative and one or more positive peak(s). Increasing the VD period the intensity of the inverted signal will increase and the one(s) of the exchange partner(s) will

decrease. If the VD value is long enough for complete relaxation than both peaks will appear with their initial intensities in positive phase.

In case of studying strictly a two site system, the method of 3 hard (90°) pulses can also be used, with the τ_i delay chosen as half the distance between the peaks, setting the transmitter to one of the signals:

$$90°_x - \tau_i - 90°_y - VD - 90°_x - aq$$

Data analysis is based on the fact that the change of longitudinal magnetization with time is described by the matrix equation:

$$\mathbf{M}_\infty - \mathbf{M}_\mathbf{t} = \exp(-\mathbf{R} \cdot t) \cdot (\mathbf{M}_\infty - \mathbf{M}_\mathbf{0})$$

where **M** stays for the magnetization vector of site *i* at time t and at equilibrium, and the values are the integrated intensities of the corresponding signals. **R** is the rate matrix with rate constants k_{ij} ($i \neq j$) as off -diagonal elements and the sum of the exchange rates k_{ji} and the relaxation rates $(1/T_1)_i$. Values of **R** matrix are determined by non-linear least square analysis. Parameter fitting can be done keeping at fixed, constant values either the relaxation times or the initial or final magnetisations. (See also chapter IV.1.2.)

III. 4. Potentiometric Measurements

Titrations are carried out in a thermostated box at 25°C, using two measuring electrodes. The free H^+ concentration, h, is determined by measuring the e.m.f. of the cell:

(-) RE // equilibrium solution // ME (+)

where ME is one measuring electrode and RE is the reference electrode. The ME electrode is formed from quinhidrone crystals (recrystallised quinhidrone from water at 70°C) and a Pt foil electrode, which is washed in hot aqua regia and water then dried in ethanol flame before each titration. The quinhidrone electrode is used in order to avoid problems with the glass electrode in connection with fluoride solutions. The RE is:

Ag, AgCl / 0.01M Cl^-, 0.59 M ClO_4^- // 0.6M NaCl

Free F^- concentration, f, is determined using the following cell:

(-) RE // equilibrium solution // ME' (+)

where ME' is a F^- selective electrode and RE is the reference electrode described before.

Titrations are done in a teflon vessel in N_2 atmosphere. Occasional impurities from N_2 were stopped by passing the gas through three washing solutions: 10 % NaOH, 10 % H_2SO_4 and 0.6 M NaCl and a G_4 filter, respectively.

Titrations are performed and controlled by computer. E.m.f. values are monitored every 5 minutes. 4 equilibrium points are collected and the maximum equilibrium time is allowed to be 90 minutes. In general equilibrium is established in 5 minutes. The maximum slope for equilibrium is fixed as being $5 \cdot 10^{-5}$ mV/s.

Calibration of the electrodes. The standard potentials, E_0, of the electrodes are calculated using the Gran method.[84] As a starting point the Nernst equation is used. For E_0^H this looks like:

$$E = E_0^H + g \cdot \lg[H^+] + E_j \quad \text{with } g = 59.1597 \text{ mV}$$

and the corresponding Gran plot is: $(V_0 + V_i) \cdot 10^{E/g} = f(V_i)$. This graphical representation leads to calculate the interesting values as:

$$E_0 = g \cdot \lg\left(\frac{\text{slope}}{c_i}\right) \; ; \; c_0 = \frac{\text{intercept}}{V_0 \cdot 10^{\frac{E_0}{g}}} \qquad \text{(III.1.)}$$

As the measurements are done in a pH domain of 2.5 – 3.5, no junction potential is included. For E_0^F analogous calculations are done. In this case the Nernst equation is: $E = E_0^F - g \cdot \lg[F^-]$. Moreover, the effect of oxalate on the fluoride electrode is tested by measuring the E_0^F in presence of oxalate ion. Only a negliglible change of 0.071 mV is observed.

Titration of the aluminium –fluoride – oxalate system. For realization of these titrations two possibilities appear: to prepare first the binary Al – fluoride species and titrate this solution with oxalate, or to form first the Al – oxalate complexes followed by titration with fluoride. Both ways are checked with the following technical arrangements:

i) titration of $AlF_p^{(3-p)}$ complexes with Ox^{2-} is realised in three steps:

a) first E_0^H is determined by titrating the 0.6 M NaCl solution with HCl. From these data the concentration of the titrant HCl solution can be refined also.

b) the final solution a) is titrated further with NaF in order to determine E_0^F.

c) to solution b) the necessary amount of $AlCl_3$ is added. After waiting 1 hour for equilibration, the solution is titrated from one buret with a mixture of $AlCl_3$ and NaF; thus keeping the c_{Al} and c_F constant; and from the other buret with a buffer of HOx^-/Ox^{2-} (pH ≅ 4). In this way dilution problems are eliminated.

ii) titration of $AlOx_q^{(3-2q)}$ species with F^- titrations are done in two-steps:
a) E_0^H is determined as mentioned above.
b) to solution a) $AlCl_3$ and a buffer of HOx^-/Ox^{2-} (pH ≅ 4) is added, then titration from one buret with a mixture of Al^{3+} and Ox^{2-} and from the other buret with a solution of NaF follows. In this case E_0^F is determined before and after each titration by a titration of a NaCl solution with NaF.

Once E_F and E_H values are measured, and knowing the volume of the titrant at each addition using the initial concentrations of each component and the initial volumes it is possible to fit the stability constants using the LETAGROP program.[85] The database consists also from the protonation constants of fluoride and oxalate, the stability constants of hydroxo aluminium species, binary fluoride and oxalate complexes, and the estimated constants of the assumed ternary species together with the set of measured points from one or more titrations. These estimated constants are fitted and refined by choosing the total fluoride concentration as error carrying variable. This is a reasonable choice, as the error in the emf measurements is small compared to the analytical error in the titrants.

III.5. ICP Measurements

ICP measurements were performed with a Spectroflame ICP-AES instrument (Spectro GmbH, Germany) on the 396.152 nm line of Al. Crossflow nebulizer was used for aerosol production. Gas flow values were set to 0.6 l/min for nebulization, 1.5 l/min for plasma and 15 l/min for cooling and plasma stabilization. Sample introduction was done by impulse technique.[86] 100 µl sample was introduced at once from a teflon tray. Five standard solutions of concentrations between 1 - 30 ppm (0.04 – 1.11 mM) were used for setting up the calibration curve.

III.6. Data Set of Overall Stability Constants

Literature values logβ (defined for components Al^{3+}, H^{+}, L^{n-}) used for concentration distribution calculations and for LETAGROP refinements.

OH^{-}	–13.997	
$Al(OH)^{2+}$	–5.52	
$Al(OH)_2^{+}$	–11.3	
$Al(OH)_3$	–17.3	
$Al(OH)_4^{-}$	–23.46	
$Al_3(OH)_4^{5+}$	–13.57	
$Al_{13}O_4(OH)_{24}^{7+}$	–109.2	[99]
HF	3.17	
HF_2	3.75	
AlF^{2+}	6.11	
AlF_2^{+}	11.07	
AlF_3	14.92	
AlF_4^{-}	17.27	
AlF_5^{2-}	18.60	
AlF_6^{3-}	(19.07)	[35]
HOx^{-}	3.57	
H_2Ox	4.54	
$AlOx^{+}$	5.97	
$AlOx_2^{-}$	10.93	
$AlOx_3^{3-}$	14.88	
$HAlOx^{2+}$	5.94	[53]
H_2Cit^{-}	9.298	
$HCit^{2-}$	5.217	
H_3Cit	12.067	
AlCit	7.147	
$Al(Cit)_2^{3-}$	11.604	
$AlHCit^{+}$	9.387	
$Al(H_{-1}Cit)^{-}$	3.587	
$Al(OH)(H_{-1}Cit)$	–2.643	
$Al_3(OH)(H_{-1}Cit)_3^{4-}$	14.431	
$Al_3(OH)_4(H_{-1}Cit)_3^{7-}$	–10.909	[71,72]

IV. RESULTS AND DISCUSSION

IV.1. The Aluminium – Fluoride System

IV.1.1. Equilibrium Studies

Stepwise formation of $AlF_i^{(3-i)+}$ species can be easily followed by ^{19}F NMR, however, it is vital that such measurements be performed under carefully controlled conditions of pH, temperature and ionic strength. Changing c_F/c_{Al} at constant pH or changing pH at constant c_F/c_{Al} enables the assignment of NMR peaks to specific complexes. More importantly, the sensitivity of high field ^{19}F NMR makes possible measurements at concentrations comparable to those used in classical thermodynamic studies.

The lower complexes are easily detected in solutions of high acidity. Figure IV.1.1. shows a typical series of spectra at c_{Al} = 5 mM, c_F/c_{Al} = 3 in 3 M KCl solutions at 298 K measured as a function of HCl concentration.

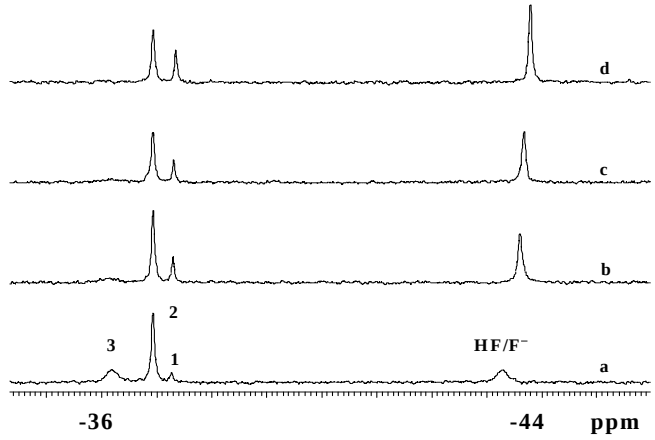

Figure IV.1.1. ^{19}F NMR spectra of a solution with c_{Al} = 5 mM, c_F = 15 mM, 3 M KCl at 298 K, at different total acid concentrations, c_H : (a) 0.1 M, (b) 0.3 M, (c) 0.4 M, (d) 0.6 M. Numbers **1** , **2**, **3** refer to species AlF^{2+}, AlF_2^+, AlF_3^0.

Four signals, corresponding to AlF^{2+}, AlF_2^+, AlF_3^0 and HF, are observed. As expected, the higher the acid concentration, the lower the intensity of the signals of the higher order species. Considering this signals **1**, **2**, and **3** can be assigned as being species AlF^{2+}, AlF_2^+, AlF_3^0. The chemical shift of the ′free′

fluoride, HF/F^-, changes slightly at lower acidities due to exchange with the small amounts of unprotonated F^-, but those of the $AlF_i^{(3-i)+}$ species do not vary significantly. This is a certain indication that these species do not take part in protonation equilibria.

For detection of higher $AlF_i^{(3-i)+}$ species it is an obvious way to prepare samples with higher c_F/c_{Al} ratios and/or at higher pH. Accordingly, c_F was varied at constant c_{Al} and with the pH held constant at 4.5 with 0.05 M HAc/Ac^- buffer in 3 M KCl. At $c_F/c_{Al} \leq 3$ no new signals were detected. Further, at higher ratios, $c_F/c_{Al} \leq 8$, the signals of the $AlF_i^{(3-i)+}$ complexes disappeared! This phenomenon was also reported by Martinez *et al.*[42] who attributed it to exchange processes. However, as the chemical shift differences for the various $AlF_i^{(3-i)+}$ species are relatively small, a few ppm, a complete loss of intensity by broadening seems to be very unlikely. Close inspection of the semi-translucent plastic NMR tubes indicated the presence of a fine, colourless precipitate at such concentrations. Analysis by ICP AES of filtered solutions indicated virtually no Al(III) in solution. Dissolution of the solid in 1M HNO_3 followed by ICP AES accounted for all the 'missing' Al(III). The nature of the solid was not investigated further but AlF_3, Na_3AlF_6 (and therefore perhaps K_3AlF_6) and a range of $Al^{3+}/OH^-/F^-$ solids are all sparingly soluble in near-neutral aqueous solutions.[87]

Following Brosset and Orring and others who reported greater solubilities in R_4N^+ media,[35,37,38] a series of solutions were prepared in 0.6 M TMACl, 0.05 M HAc/Ac^- buffer at pH ≈ 6.0. No precipitation at c_{Al} = 5 mM occurred, even up to c_F = 600 mM. More importantly, at 278 K, in addition to the three signals observed for $AlF_i^{(3-i)+}$ with i ≤ 3 in 3 M KCl media at 298 K (Figure IV.1.1.), two further signals were detected (Figure IV.1.2.). At low c_F (≤ 5 mM), signals **1** (AlF^{2+}) and **2** (AlF_2^+) were dominant with minor amounts of signal **3** (AlF_3^0). As c_F was increased to 15 mM, signals **1** and **2** progressively decreased whilst signal **3** increased along with that of a new signal **4**. At c_F = 25 mM (c_F/c_{Al} = 5) signal **4** became dominant with signal **3** decreasing and a further resonance **5** beginning to grow. Signal **5** continued to grow up to c_F = 40 mM, but remained quite broad. No evidence for a sixth signal was found even up to c_F = 600 mM (c_F/c_{Al} = 120). In the absence of excessive line broadening or precipitation, no missing ^{19}F NMR intensity could be detected within the limits of precision of the integration (± 5%). The most obvious explanation for signals **4** and **5** is to attribute them to the species AlF_4^-(aq) and AlF_5^{2-}(aq) respectively. However, at the pH employed (~6.0), the

formation of ternary $AlF_i(OH)_j^{(3-i-j)+}(aq)$ species must also be considered. Formation of such complexes is favoured at higher pH and modest c_F. Accordingly, series of solutions were prepared in 0.6 M TMACl at c_F/c_{Al} = 40/5 and 20/5 and 3.7 ≤ pH ≤ 6.5 at 278 K. The line widths and relative intensities of the signals obtained changed but the chemical shifts were independent of pH. Thus, ternary complexes do not account for signals **4** and **5** and it is concluded that they can be ascribed to AlF_4^- (aq) and AlF_5^{2-} (aq).

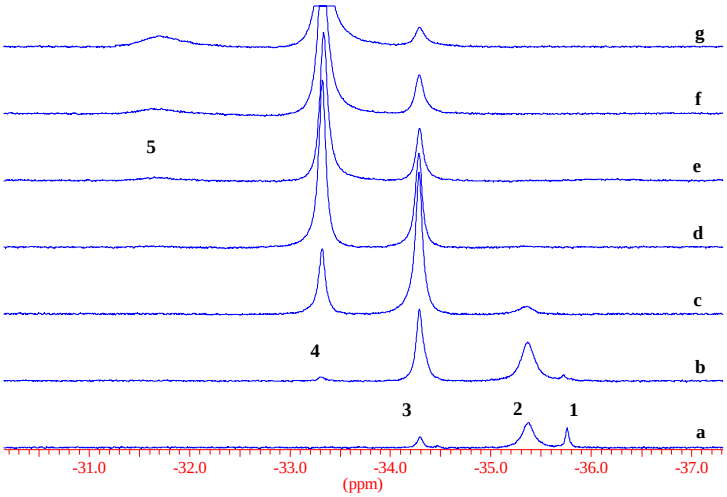

Figure IV.1.2. ^{19}F NMR spectra of a solution with c_{Al} = 5 mM, HAc/Ac^- buffer 0.05 M, pH ≈ 6.1, 0.6 M TMACl at 278 K, at different c_F: (a) 5 mM, (b) 10 mM, (c) 15 mM, (d) 20 mM, (e) 25 mM, (f) 30 mM, (g) 40 mM. Numbers **1** , **2**, **3**, **4**, **5** refer to species AlF^{2+}, AlF_2^+, AlF_3^0 , AlF_4^-, AlF_5^{2-}. The narrow signal of free fluoride at δ ~ 0 ppm is not shown.

The assignments of signals **1 - 5** and their chemical shifts are summarised in Table IV.1.1. The chemical shifts for the lower order complexes (i ≤ 3) are similar to those of previous studies; quantitative agreement would not be expected given the widely varying concentrations, temperatures, pH, counterions and chemical shift standards, and the absence of a constant ionic medium in the earlier studies.

Table IV.1.1. Equilibrium Constants and Chemical Shift Values of $AlF_i^{(3-i)+}$ Complexes

Peak	Species	$\log K_i$[a]	δ (ppm)	$\log K_i \pm$ est.err. 0.6 M TMACl; 278 K	δ(ppm)	$\log K_i \pm$ est.err. 3 M KCl; 298 K
1	AlF^{2+}	6.11	-35.76	6.42 ± 0.03 (3 points)	-37.27	6.35 ± 0.08 (8 points)
2	AlF_2^+	4.96	-35.36	5.41 ± 0.09 (7 points)	-36.93	5.25 ± 0.07 (30 points)
3	AlF_3^0	3.85	-34.29	3.99 ± 0.09 (6 points)	-36.18	4.11 ± 0.12 (7 points)
4	AlF_4^-	2.35	-33.32	2.50 ± 0.05 (8 points)	–[b]	–
5	AlF_5^{2-}	1.33	-31.66	0.84 ± 0.20 (9 points)	–[b]	–
6	AlF_6^{3-}	(0.47)	not detected	–	–[b]	–

[a] literature values for I = 0.5 M (KNO_3); 298 K[35, 88, 89].
[b] precipitation occurred

Recording high quality and quantitative spectra and performing the identification of peaks it is possible to calculate the equilibrium constants. The system is represented by the formation of complexes ($i \geq 1$):

$$AlF_{i-1}^{(4-i)+} + F^- \rightleftharpoons AlF_i^{(3-i)+} \qquad \text{(IV.1.1.)}$$

with stepwise equilibrium constants:

$$K_i = \frac{[AlF_i^{(3-i)+}]}{[AlF_{i-1}^{(4-i)+}][F^-]} \qquad \text{(IV.1.2.)}$$

where [ ] denote concentrations. In acid solutions it is convenient to represent the formation of these complexes as:

$$AlF_{i-1}^{(4-i)+} + HF \rightleftharpoons AlF_i^{(3-i)+} + H^+ \qquad \text{(IV.1.3.)}$$

for which the corresponding stepwise equilibrium constants are:

$$K_i^H = \frac{[AlF_i^{(3-i)+}][H^+]}{[AlF_{i-1}^{(4-i)+}][HF]} \qquad \text{(IV.1.4.)}$$

Introducing the protonation constant of fluoride:

$$K_{HF} = \frac{[HF]}{[H^+][F^-]} \qquad \text{(IV.1.5.)}$$

combination with (IV.1.2.) and (IV.1.4.) gives:

$$\log K_i = \log K_i^H + \log K_{HF} \qquad \text{(IV.1.6.)}$$

The concentrations of the individual complexes, $[AlF_i^{(3-i)+}]$ and [HF] are determined from the integrated intensities, I_i:

$$[AlF_i^{(3-i)+}] = \frac{I_i c_F}{i I_T} \qquad \text{(IV.1.7.)}$$

where I_T is the total integrated intensity summed over all ^{19}F NMR signals.
Combining eqs (IV.1.4.) and (IV.1.7.) gives:

$$K_i^H = \frac{i-1}{i} \cdot \frac{I_i}{I_{i-1}} \cdot \frac{I_T}{I_{HF}} \cdot \frac{[H^+]}{c_F} \qquad \text{(IV.1.8.)}$$

where $[H^+]$ is calculated from the mass balance equation:

$$[H^+] = c_H - [HF] \qquad \text{(IV.1.9.)}$$

The values of K_i obtained in this way at 278 K in I = 0.6 M TMACl and at 298 K in I = 3 M KCl are summarised in Table IV.1.1. Although a detailed comparison with previous data is beyond the scope of the present work, given the differences in the media and the relatively low precision of NMR integrations of broad signals, the agreement with reliable literature values for the lower order complexes ($i \leq 4$) is excellent. Note that temperature effects are small (< *ca*. 0.1 in $logK_i$ for a temperature difference of 20 K) based on the known values of ΔH_i.[89] It is interesting to note and almost certainly significant that the present value of K_5 is about a factor of 3 lower than the only previous report of this constant.

As noted earlier no evidence has been obtained for the existence of AlF_6^{3-} (aq) at T ≥ 255 K and $c_F/c_{Al} \leq 120$. Still, one can ask whether the sixth complex really exists in solution, or not. It is possible to check whether this complex appears in more concentrated solutions. The starting solution was prepared from $AlF_3 \cdot 3H_2O$, and to avoid precipitation further fluoride was added in the form of tetra n buthyl ammonium fluoride trihydrate: $C_{16}H_{36}FN \cdot 3H_2O$. The former value of c_{Al} 5mM was changed to 0.1 M, and c_F was varied between 0.3 and 1 M. Figuring a concentration distribution taking into account the binary species with the above calculated equilibrium constants, species HF, HF_2, $Al(OH)_i^{(3-i)+}$ ($i \leq 4$) and $AlF_i(OH)_j^{(3-i-j)+}$ ($i, j \leq 3$) and assuming that K_6 = 0.5, then the AlF_6^{3-} complex should form at c_F > 0.5 M in a quantity of ~ 10%. The calculated distribution is shown on Figure IV.1.3.:

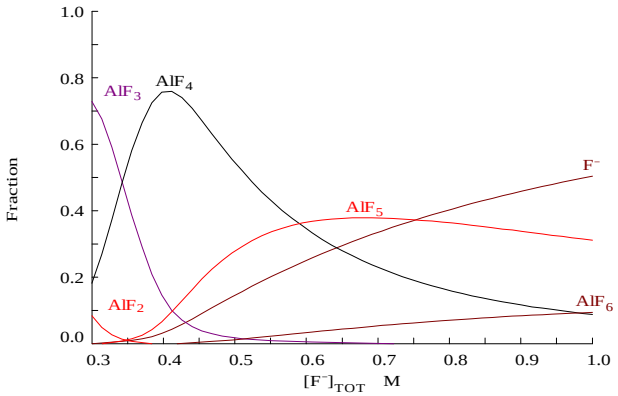

Figure IV.1.3. Typical concentration distribution diagram (showed for F – fraction) calculated using the equilibrium constants from Table IV.1.1., considering $K_6 = 0.5$

If this is so, this complex can be detected by NMR. Measured spectra are shown on Figures IV.1.4.*a* and *b*:

a) *b)*

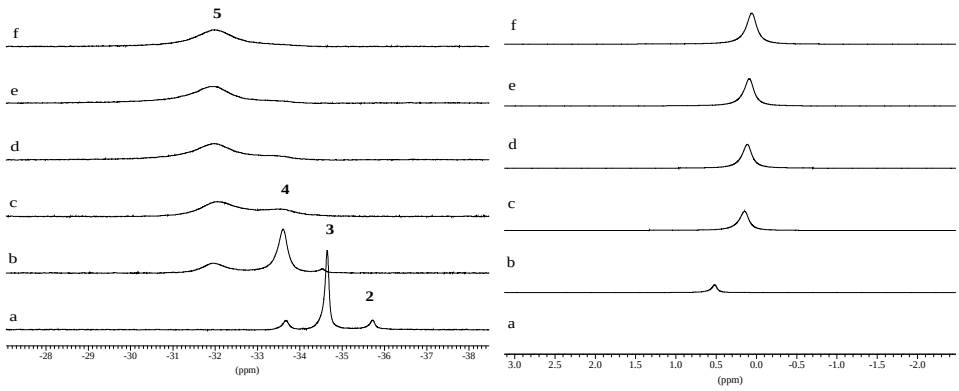

Figure IV.1.4. ***a)*** ^{19}F NMR spectra of solutions with c_{Al} = 0.1 M at 278 K, at different c_F : (a) 0.3 M, (b) 0.4 M, (c) 0.7 M, (d) 0.8 M, (e) 0.9 M, (f) 1 M. Numbers **2**, **3**, **4**, **5** refer to species AlF_2^+, AlF_3^0 , AlF_4^-, AlF_5^{2-}, respectively. Free fluoride signals are shown on figure ***b)***.

The chemical shifts for the binary complexes in these solutions are: AlF_2^+ –35.73 ppm, AlF_3^0 = –34.65 ppm, AlF_4^- = –33.4 ppm, AlF_5^{2-} = –31.94 ppm. These values differ from those given in Table IV.1.1., but the ionic strength was not kept

constant here, its value was somewhere between 0.6 and 3 M. With increasing fluoride concentration complexes **4** and **5** appear, both of them being broad. The broadening of **4** varies possibly as a consequence of inter–molecular exchange with the third complex. Signal **5** shows a large and more or less constant broadening which can not be explained by inter–molecular exchange with the free fluoride. Another explanation may be the existence of an intra–molecular exchange between a pentagonal and octahedral structure. It is useful to note, that increasing the temperature to 298 K only one, time–averaged broad signal of the complexes is detected, while free fluoride signal remains narrow. Thus, the kinetics for $AlF_i^{(3-i)+}$ ($i \geq 4$) at higher pH, where these complexes become dominant, could be different form the kinetics for $i \leq 3$ discussed in the followings. Nevertheless, even under these extreme conditions there is no indication about the existence of the sixth complex. The only reasoning that can be composed is that if this AlF_6^{3-} complex exists in aqueous media, then K_6 must be lower than 0.5.

IV.1.2. Dynamic Studies

As seen from Figure IV.1.1. the line widths of the signals except that of AlF^{2+} vary with acidity. With increasing acid concentration the HF signal narrows, whereas those of AlF_2^+ and AlF_3^0 broaden. This is a certain indication of the presence of exchange processes. As the number of peaks is equal to the number of species reported by equilibrium studies, the "slow exchange" situation is valid. In this case the line width of the signal for the species i (LW_i) is:

$$LW_i = \frac{1}{\pi}\left(\frac{1}{T_{2,i}} + \frac{1}{\tau_{inh}} + \frac{1}{\tau_{ex,i}}\right) \qquad \text{(IV.1.10.)}$$

where: $T_{2,i}$ is the transverse relaxation time of species i , τ_{inh} the relaxation time due to inhomogeneity of the magnetic field and $\tau_{ex,i}$ is the contribution of chemical exchange to the transverse relaxation.

The line broadening of species i (LB_i) resulting from chemical exchange is defined as the difference between the observed line width and the non-exchange line width:

$$LB_i = LW_i - \frac{1}{\pi}\left(\frac{1}{T_{2,i}} + \frac{1}{\tau_{inh}}\right) \qquad \text{(IV.1.11.)}$$

Line broadening is determined by the dynamic behaviour of the equilibrium system:

$$LB_i = \frac{1}{\pi}\sum_{\substack{i=0 \\ i \neq j}}^{n} k_{ij}^{obs} = \frac{1}{\pi} k_i^{obs} \qquad \text{(IV.1.12.)}$$

where n is the number of species, k_{ij}^{obs} is the pseudo first order rate constant of each reaction from site i to j and therefore k_i^{obs} is the pseudo first order rate constant of all parallel reactions from site i. The non-exchange line width is considered to be 12 Hz, which is the line width of HF/F^- at lower temperatures, where exchange processes are frozen and this value is the natural line width of the signal.

Knowledge of the speciation in the Al^{3+}/F^- system and the analysis of a series of exchange broadened spectra show that three sites take part in the exchange process in 3 M KCl at 298 K. The species AlF^{2+} is excluded, because its line width does not vary with concentration. Therefore Scheme IV.1.1. is an appropriate starting point for the kinetic analysis:

Scheme IV.1.1.

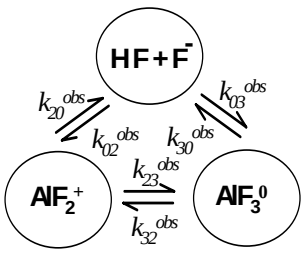

The next step is to find the chemical exchange reactions which can transfer magnetisation between the different sites. Three types of such processes are possible.

i) Ligand exchange between the complexes and 'free' ligand (HF and/or F^-) with no net chemical change (superscript H indicates exchange with HF):

$$*F^- + AlF_2^+ \underset{k_{20}}{\overset{k_{02}}{\rightleftharpoons}} AlF*F^+ + F^- \qquad \text{(IV.1.13.)}$$

$$H*F + AlF_2^+ \underset{k^H_{20}}{\overset{k^H_{02}}{\rightleftharpoons}} AlF*F^+ + HF \qquad \text{(IV.1.14.)}$$

$$*F^- + AlF_3^0 \underset{k_{30}}{\overset{k_{03}}{\rightleftharpoons}} AlF_2*F^0 + F^- \qquad \text{(IV.1.15.)}$$

$$H*F + AlF_3^0 \underset{k^H_{30}}{\overset{k^H_{03}}{\rightleftharpoons}} AlF_2*F^0 + HF \qquad \text{(IV.1.16.)}$$

ii) Complex formation (superscript c or cH):

$$F^- + AlF_2^+ \underset{k^c_{30},\, k^c_{32}}{\overset{k^c_{03},\, k^c_{23}}{\rightleftharpoons}} AlF_3{}^0 \qquad \text{(IV.1.17.)}$$

$$HF + AlF_2^+ \underset{k^{cH}_{30},\, k^{cH}_{32}}{\overset{k^{cH}_{03},\, k^{cH}_{23}}{\rightleftharpoons}} AlF_3^0 + H^+ \qquad \text{(IV.1.18.)}$$

iii) Ligand exchange between complexes, ′self - exchange′ with no net chemical change:

$$AlF_2^+ + AlF_2*F^0 \underset{k_{32}}{\overset{k_{23}}{\rightleftharpoons}} AlF*F^+ + AlF_3^0 \qquad \text{(IV.1.19.)}$$

Considering reactions IV.2.4. – 10, the reaction rates for the various species are:

$$w_0 = 2w_{02} + 2w_{02}^H + 2w_{03} + 2w_{03}^H + w_{02}^c + w_{02}^{cH} \qquad \text{(IV.1.20.)}$$

$$w_2 = 2w_{20} + 2w_{20}^H + w_{23}^c + w_{23}^{cH} + 2w_{23} \qquad \text{(IV.1.21.)}$$

$$w_3 = 2w_{30} + 2w_{30}^H + w_{30}^c + w_{30}^{cH} + 2w_{32} \qquad \text{(IV.1.22.)}$$

where w_0 represents the rate of ′disappearance′ of the ′free′ fluoride, T_F:

$$T_F = [F^-] + [HF] \qquad \text{(IV.1.23.)}$$

and w_2 is the rate of ′disappearance′ of $AlF_2{}^+$ and w_3 is that of $AlF_3{}^0$.

Expressing eqs IV.1.20. – 22 for reactions IV.1.13. – 19 the following relations are obtained:

$$w_0 = 2k_{02}[F^-][AlF_2^+] + 2k_{02}^H[HF][AlF_2^+] + k_{02}^c[F^-][AlF_2^+] + k_{02}^{cH}[HF][AlF_2^+] + \\ + 2k_{03}[F^-][AlF_3] + 2k_{03}^H[HF][AlF_3] = \left(k_{02}^{obs} + k_{03}^{obs}\right)T_F \qquad \text{(IV.1.24.)}$$

$$w_2 = 2k_{20}[AlF_2^+][F^-] + 2k_{20}^H[AlF_2^+][HF] + k_{23}^c[AlF_2^+][F^-] + k_{23}^{cH}[AlF_2^+][HF] + \\ + 2k_{23}[AlF_2^+][AlF_3] = \left(k_{20}^{obs} + k_{23}^{obs}\right)[AlF_2^+] \qquad \text{(IV.1.25.)}$$

$$w_3 = 2k_{30}[AlF_3][F^-] + 2k_{30}^H[AlF_3][HF] + k_{32}^c[AlF_3] + k_{32}^{cH}[AlF_3][H^+] + \\ + 2k_{32}[AlF_3][AlF_2^+] = \left(k_{30}^{obs} + k_{32}^{obs}\right)[AlF_3] \qquad \text{(IV.1.26.)}$$

where k_{ij} are the rate constants of the individual reactions and multiplication by 2 indicates that those exchanges are mutual, i.e., $k_{ij} = k_{ji}$.

The measured line broadenings, LB_i, are a function of the (equilibrium) concentration of each species taking part in the exchange reactions and the rates of those reactions. Combination of eqs IV.1.5. and IV.1.23. gives:

$$T_F = [F^-]\left(1 + K_{HF}[H^+]\right) \qquad \text{(IV.1.27.)}$$

which coupled with eqs IV.1.24. – 26. gives:

$$\pi \cdot LB_0 = [AlF_2^+]\left\{\left(2k_{02} + k_{02}^c\right)\frac{1}{1+K_{HF}[H^+]} + \left(2k_{02}^H + k_{02}^{cH}\right)\frac{K_{HF}[H^+]}{1+K_{HF}[H^+]}\right\} + \\ [AlF_3]\left\{2k_{03}\frac{1}{1+K_{HF}[H^+]} + 2k_{03}^H\frac{K_{HF}[H^+]}{1+K_{HF}[H^+]}\right\} \qquad \text{(IV.1.28.)}$$

$$\pi \cdot LB_2 = \left\{\left(2k_{20} + k_{23}^c\right)\frac{T_F}{1+K_{HF}[H^+]} + \left(2k_{20}^H + k_{23}^{cH}\right)\frac{T_F K_{HF}[H^+]}{1+K_{HF}[H^+]} + 2k_{23}[AlF_3]\right\} \qquad \text{(IV.1.29.)}$$

$$\pi \cdot LB_3 = \left\{2k_{30}\frac{T_F}{1+K_{HF}[H^+]} + 2k_{30}^H\frac{T_F K_{HF}[H^+]}{1+K_{HF}[H^+]} + k_{32}^c + k_{32}^{cH}[H^+] + 2k_{32}[AlF_2^+]\right\} \qquad \text{(IV.1.30.)}$$

Measurements of LB_i as functions of the acidity at known c_{Al} and c_F coupled with the equilibrium concentrations of each species (obtained from the integrated NMR intensities and K_{HF}) enable the rate constants to be determined by regression analysis of eqs IV.1.28. – 30.

Figure IV.1.5. shows the observed variation of LB_i against total acidity along with the broadenings calculated from the optimised parameters. The regression analysis showed no contribution from many processes, indicating that the following rate constants have a value of effectively zero: k_{02}^{H} , k_{20}^{H} , k_{23} , k_{32} , k_{02}^{c} , k_{02}^{cH} , k_{23}^{c} , k_{23}^{cH} , k_{32}^{c} , k_{32}^{cH} . Therefore, the best model to describe the system was :

$$LB_0 = p_1 \frac{2[AlF_2^+]}{1+K_{HF}[H^+]} + p_2 \frac{3[AlF_3]}{1+K_{HF}[H^+]} + p_3 \frac{3[AlF_3]K_{HF}[H^+]}{1+K_{HF}[H^+]} \qquad \text{(IV.1.31.)}$$

$$LB_2 = p_1 \frac{T_F}{1+K_{HF}[H^+]} \qquad \text{(IV.1.32.)}$$

$$LB_3 = p_2 \frac{T_F}{1+K_{HF}[H^+]} + p_3 \frac{T_F K_{HF}[H^+]}{1+K_{HF}[H^+]} \qquad \text{(IV.1.33.)}$$

with the empirical parameters p_x having the values: $p_1 = (5.6 \pm 0.9)\cdot 10^5$, $p_2 = (8.2 \pm 1.9)\cdot 10^5$, $p_3 = (1.4 \pm 0.1)\cdot 10^4$.

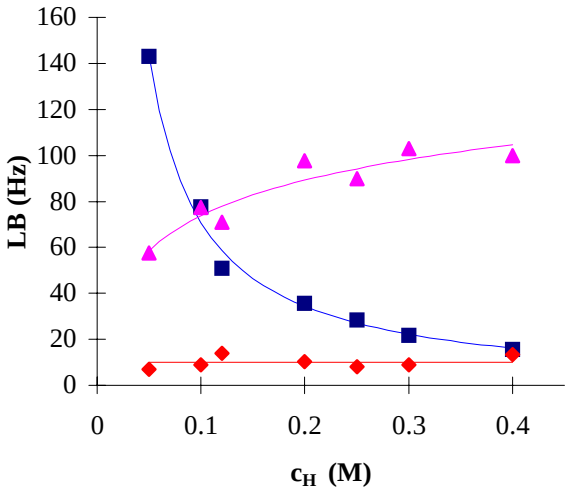

Figure IV.1.5. Dependence of line broadening on c_H. Points represent the measured values whilst lines show the calculated values. Symbols ■, ♦, ◆ refer to species HF/F^-, AlF_3^0 and AlF_2^+, respectively.

Note that up to this point the rate constants have been defined in classical kinetic terms, i.e., for ligand exchange processes of the type:

$$AlF_i^{(3-i)+} + *F^- \underset{}{\overset{k_{i0}}{\rightleftharpoons}} Al*FF_{i-1}^{(3-i)+} + F^- \qquad \text{(IV.1.34.)}$$

Such processes may be termed partial (or 'unspecified') exchange reactions. However, as has been pointed out by Lincoln and Merbach,[90] what is obtained from dynamic NMR methods is the rate constant for the complete (or 'specific') exchange:

$$AlF_i^{(3-i)+} + i*F^- \underset{}{\overset{k'_{i0}}{\rightleftharpoons}} Al*F_i^{(3-i)+} + iF^- \qquad \text{(IV.1.35.)}$$

The latter are smaller than those for partial exchange: $k'_{i0} = k_{i0}/i$. These so-called statistical factors must be kept in mind when comparing rate constants derived from dynamic NMR measurements on equilibrium systems with those obtained from traditional (non-equilibrium) kinetic measurements. Note that inclusion of these factors (*cf.* eq IV.1.31.) was found to be essential in performing the regression analysis. All rate constants quoted from now on refer to complete exchange reactions unless otherwise stated. Keeping this difference in mind the empirical rate equations corresponding to the observed broadenings are:

$$w_0 = 2k_{02}[AlF_2^+][F^-] + 2k_{03}[AlF_3][F^-] + 2k_{03}^H[AlF_3][HF] \qquad \text{(IV.1.36.)}$$

$$w_2 = 2k_{20}[AlF_2^+][F^-] \qquad \text{(IV.1.37.)}$$

$$w_3 = 2k_{30}[AlF_3][F^-] + 2k_{30}^H[AlF_3][HF] \qquad \text{(IV.1.38.)}$$

These rate expressions indicate that the observed LB_i are consistent with the occurrence of only three parallel reactions, IV.1.13, IV.1.15. and IV.1.16., with rate constants: $k'_{02} = k'_{20} = \pi p_1/2 = (8.8 \pm 1.4)\cdot 10^5\ M^{-1}s^{-1}$, $k'_{03} = k'_{30} = \pi p_2/2 = (1.3 \pm 0.3)\cdot 10^6\ M^{-1}s^{-1}$, $k'^H_{03} = k'^H_{30} = \pi p_3/2 = (2.2 \pm 0.16)\cdot 10^4\ M^{-1}s^{-1}$. It is notable that all these reactions are symmetrical, i.e., the processes responsible for line broadening are ligand exchange rather than complex formation reactions.

In an attempt to determine the influence of any slower processes, inversion transfer experiments were carried out by selective excitation of each peak, since the longitudinal relaxation time (T_1) is usually longer than the transverse relaxation time (T_2). A typical experiment is shown in Figure IV.1.6., where inversion was performed on the HF/F^- site. The magnetisation transfer to AlF_3^0 started before the initial observation time and equilibration between it and HF/F^- was complete in 4 – 5 ms consistent with the line broadening results. A decrease in the intensity of the AlF_2^+ signal in the range of 10 - 100 ms shows that this complex reacts slower than

AlF_3^0. Consistent with the absence of line broadening of the AlF^{2+} signal, no magnetisation transfer was observed to the AlF^{2+} site thus fixing an upper rate limit for its exchange processes. The total negative magnetisation 'leaked out' from the system in 2 – 3 s, illustrating the longer time scale.

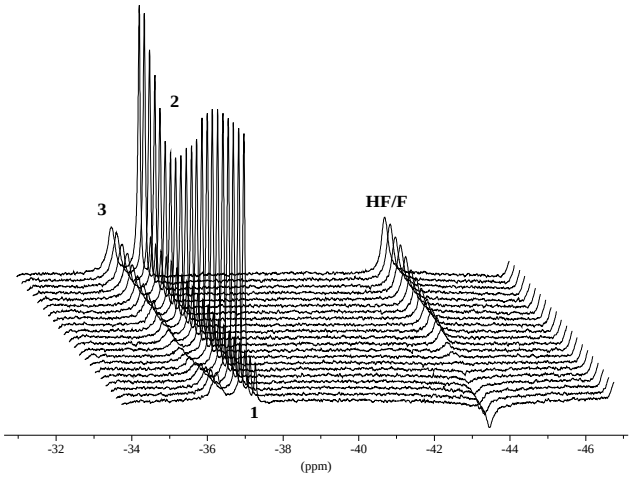

Figure IV.1.6. ^{19}F NMR serial plot of a magnetisation transfer experiment in a sample with c_{Al} = 5 mM, c_F = 15 mM, c_H = 0.1 M, 3 M KCl at 298 K. Numbers **1**, **2**, **3** refer to species AlF^{2+}, AlF_2^+, AlF_3^0 and the signal of HF/F^- was inverted with a shaped pulse sequence.

The change in longitudinal magnetisation with time is described by the matrix equation: $\mathbf{M}_\infty - \mathbf{M}_t = \exp(-\mathbf{R} \cdot t) \cdot (\mathbf{M}_\infty - \mathbf{M}_0)$. The matrix of pseudo first order rate constants (**R**) was determined by non-linear least squares analysis. Within experimental errors only two rate constants with values k_{30}^{obs} = 240 ± 14 s^{-1} and k_{20}^{obs} = 12 ± 0.2 s^{-1} were required to fit the data. Fitted values together with the measured intensities are represented on Figure IV.1.7.

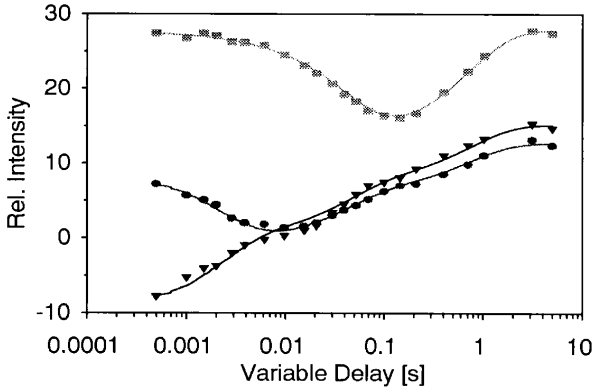

Figure IV.1.7. Intensities (arbitrary units) vs. delay time (s). Sample with c_{Al} = 5 mM, c_F = 15 mM, c_H = 0.1 M, 3 M KCl at 298 K. Numbers **2**, **3** refer to species AlF_2^+ and AlF_3^0. Symbols represent measured values.

We are now in the situation that 2 constants were determined by two different methods, namely by measurements on T_2 and T_1 time scales, respectively. It is useful to try a comparison between the obtained values. Therefore, a calculation of k_{30}^{obs} and k_{20}^{obs} values was performed using equations IV.1.12, 24.–26. and the k'_{ij} values determined from the line broadening. The resulted pseudo first order rate constants were: k_{30}^{obs} = 230 s^{-1} and k_{20}^{obs} = 35 s^{-1}. The agreement between the rate constants obtained from the line broadening and the magnetisation transfer data is excellent for k_{30}^{obs} but is less satisfactory for k_{20}^{obs}. However, it should be remembered that even though the T_1 time scale is more suitable for measuring such slow processes, the magnetisation experiments were performed on a single sample while the line broadening analysis was based on a series of samples.

In summary, the dynamics of the Al^{3+}/F^- system, at least for AlF_2^+(aq) and AlF_3^0(aq) is dominated by fluoride exchange (eqs IV.1.13.–16.) between the complexes and free fluoride (HF/F^-). Complex formation (water substitution) reactions (eqs IV.17.–18.) and fluoride exchange between complexes (eq IV.1.19.) are much slower. All processes are shown schematically on Scheme IV.1.2. Each of these processes will now be considered in detail along with the additional possibility of isomerisation.

Scheme IV.1.2.

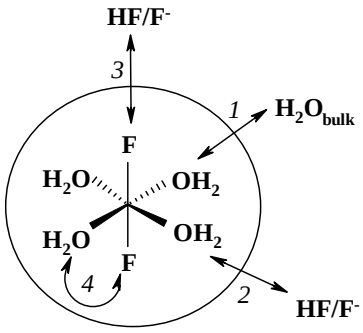

Fluoride complexation processes. In general the ligand substitution reactions of Al^{3+} in aqueous solution are known to follow the I_d mechanism. That is, the rate determining step (rds) of complex formation is the leaving of a coordinated water molecule from the outer sphere complex formed in a fast pre-equilibrium. Thus, for fluoride complexation the mechanism would be expected to be:

$$AlF_i(H_2O)_{6-i}^{(3-i)+} + F^- \overset{\text{fast}}{\rightleftharpoons} AlF_i(H_2O)_{6-i}^{(3-i)+}, F^- \qquad \text{(IV.1.39.)}$$

$$AlF_i(H_2O)_{6-i}^{(3-i)+}, F^- \xrightarrow{\text{rds}} AlF_{i+1}(H_2O)_{5-i}^{(2-i)+} + H_2O \qquad \text{(IV.1.40.)}$$

If the mechanism of complex formation is indeed dissociative in character, the first order rate constant of the rds, k_{rds}, is expected to be very close to the water exchange rate constant of $AlF_i(H_2O)_{6-i}^{(3-i)+}$. From eqs IV.1.39–40.: $k_{rds} = k/K_{os}$, where the equilibrium constant for IV.1.39., K_{os}, is usually estimated from one of the Fuoss-type equations.[91] Since the water exchange rates are known (Table IV.1.2.), the expected rate constants of the reactions for the formation of AlF_3^0 from AlF_2^+ (eqs IV.1.17–18.) can be calculated. For IV.1.17. this value is $k^c_{03} = k^c_{23} = 2.4 \cdot 10^4\ M^{-1}s^{-1}$; the value for IV.1.18. is even smaller (HF reacts more slowly than does F^-). As these values are considerably smaller than the experimental rate constant ($8.8 \cdot 10^5\ M^{-1}s^{-1}$) this accounts for why complex formation makes no significant contribution to the observed dynamics.

Another way of expressing the relative slowness of the complex formation reactions is to calculate the line broadenings caused by complex formation, assuming they follow the I_d mechanism (eqs IV.1.39–40.). These values, see Table IV.1.2. (column 5), calculated from the water exchange rate data (also in Table

IV.1.2.) indicate that none of the complex formation reactions contribute significantly to the observed line broadening .

Table IV.1.2. Rates of water exchange k_{ex} (H_2O) and calculated values of K_{os}, rate constants k_{0i}^{c} and HF/F^- line broadenings for formation reactions of various $AlF_i(H_2O)_{6-i}^{(3-i)+}$ species

Reaction	k_{ex} (H_2O) (s^{-1})[26]	K_{os} (M^{-1})	k_{0i}^{c} ($M^{-1}s^{-1}$)	LB (Hz)[a]
$Al(H_2O)_6^{3+} + F^- \rightleftharpoons Al(H_2O)_5F^{2+}$	2	20	$4\cdot10^1$	$<10^{-4}$, [b]
$AlF(H_2O)_5^{2+} + F^- \rightleftharpoons AlF_2(H_2O)_4^{+}$	$1\cdot10^2$	5	$5\cdot10^2$	$\sim 10^{-3}$
$AlF_2(H_2O)_4^{+} + F^- \rightleftharpoons AlF_3(H_2O)_3^{0}$	$2\cdot10^4$	1.2	$2.4\cdot10^4$	~ 0.1

[a] under the conditions of the inversion transfer experiments
[b] the concentration of the $Al(H_2O)_6^{3+}$ complex was estimated from the equilibrium constant

It is interesting to note that an *associative* (I_a) mechanism has been suggested by Plankey and Pattersson[92] for the formation of the first complex, $AlF(H_2O)_5^{2+}$ on the basis that the rate of substitution of H_2O on $Al(H_2O)_6^{3+}$ by F^- was greater than that of H_2O exchange, after the application of some statistical corrections. However, this difference was very small.

Fluoride exchange processes. A logical starting point to discuss fluoride exchange processes is to assume that they follow a mechanism *formally* similar to that of complex formation:

$$AlF_i(H_2O)_{6-i}^{(3-i)+} + *F^- \overset{\text{fast}}{\rightleftharpoons} AlF_i(H_2O)_{6-i}^{(3-i)+},*F^- \qquad \text{(IV.1.41.)}$$

$$AlF_i(H_2O)_{6-i}^{(3-i)+},*F^- \xrightarrow{\text{rds}} Al*FF_{i-1}(H_2O)_{6-i}^{(3-i)+} + F^- \qquad \text{(IV.1.42.)}$$

Note, however, this formalism does not indicate whether the rds is dissociative, associative or concerted.

Comparison of the rate constants for the following three processes:

$$AlF_3(H_2O)_3^0 + *F^- \rightleftharpoons Al*FF_2(H_2O)_3^0 + F^- \qquad k'_{30} = 1.3\cdot10^6\ M^{-1}s^{-1}$$

$$AlF_3(H_2O)_3^0 + H*F \rightleftharpoons Al*FF_2(H_2O)_3^0 + HF \qquad k'^{H}_{30} = 2.2\cdot10^4\ M^{-1}s^{-1}$$

$$AlF_3(H_2O)_3^0 + AlF*F^+ \rightleftharpoons Al*FF_2(H_2O)_3^0 + AlF_2^+ \qquad k'_{32} \approx 0$$

indicates that the rates of fluoride exchange reactions depend dramatically on the nature of the entering group, typical for associative interchange. (Note that as AlF_3^0 is neutral there is no significant correction to be made for the variation in the charge of the incoming group). A similar but more limited effect is observed for AlF_2^+,

$$AlF_2(H_2O)_4^+ + *F^- \rightleftharpoons Al*FF(H_2O)_4^+ + F^- \qquad k'_{20} = 8.8\cdot10^5\ M^{-1}s^{-1}$$

$$AlF_2(H_2O)_4^+ + H*F \rightleftharpoons Al*FF(H_2O)_4^+ + HF \qquad k'^{H}_{20} \approx 0$$

although here allowance must be made for the difference in charge. Nevertheless, on the basis of these two groups of results it may be concluded that fluoride exchange reactions are associatively activated.

The occurrence of an I_a mechanism for fluoride exchange is unusual given, as already noted,[92] that most, but possibly not all Al^{3+} substitution processes follow I_d behaviour. According to Lo and Swaddle[93] all substitution processes for octahedral M^{3+} species are I_a unless $r(M^{3+}) < 0.6$ Å. However, such substitution processes usually refer to the replacement of coordinated H_2O. Since F^- is smaller than H_2O and as $Al^{3+}$is only slightly smaller than 0.6 Å, it is possible that there is sufficient space in the coordination sphere of the Al^{3+} to accommodate an extra (incoming) F^-. The role of H-bonding is likely to be significant because all of the species under consideration, including HF^0 are very strongly solvated.

As the overall reaction embodied in eqs IV.1.41–42. is unaffected by the nature of the activation in the rds, the rate constants of the rds IV.1.42. can be calculated in a similar manner to those for the complexation reactions. The values so obtained are given in Table IV.1.3. for those exchange reactions for which the appropriate data are available. Comparison of the rate constants for AlF_2^+, the only complex for which numerical data are available, for F^- exchange (Table IV.1.3.) with those for water exchange (Table IV.1.2.) indicate that coordinated fluoride is more labile in these reactions than coordinated water by a factor of about 40, after allowing for the relevant statistical factor. However, similar trends are apparent for both types of bond breaking, i.e., the higher order the complex (the less positive the net charge on the complex), the more labile are both the coordinated F^- or water molecules.

It is notable that the present results show that F^- exchanges more quickly on AlF_i^{3-i}(aq) than does HF. This is opposite to that found for exchange on $UO_2F_i^{(2-i)+}$(aq), the only other system for which F^- exchange rates have been measured.[94] However, the latter is likely to involve some unusual H-bonding

effects. The present order is consistent with the reported rates of *substitution* reactions of F^- and HF with both Be^{2+} and Fe^{3+}. [95,96]

Table IV.1.3. Rate Constants of Ligand Exchange Reactions between Complexes and HF/F^-

Reaction	$k_{0\,i}$, $k_{0\,i}^{H}$ $(M^{-1}s^{-1})$ [b]	$k_{rds} = k_{0i}/K_{os}$ (s^{-1})
$AlF^{2+} + {}^*F^- \rightleftharpoons Al^*F^{2+} + F^-$ [a]	$\leq 1\cdot10^4$ [c]	$\leq 2\cdot10^3$
$AlF_2^+ + {}^*F^- \rightleftharpoons Al^*FF^+ + F^-$ [a]	$1.8\cdot10^6$	$1.5\cdot10^6$
$AlF_3^0 + {}^*F^- \rightleftharpoons AlF_2^*F^0 + F^-$	$3.9\cdot10^6$	$1.3\cdot10^7$
$AlF_3^0 + H^*F \rightleftharpoons AlF_2^*F^0 + HF$	$6.6\cdot10^4$	$2.2\cdot10^5$

[a] exchange of AlF^{2+} with HF/F^- and of AlF_2^+ with HF are too slow to be measured

[b] exchange constant for partial (unspecified) exchange

[c] Considering the magnetisation transfer experiment commented above, it is observable that in ~ 3 s the initial situation is re-established. Therefore, the half time ($t_{1/2}$) for this experiment is ~ 0.6 s and $k_{obs} = \ln 2/t_{1/2} \sim 1\ s^{-1}$. The accuracy of this type of measurements shows, that processes which have a first order rate constant less than ~ $0.1k_{obs}$ can not be detected on T_1 time scale. As the referred reaction is not detectable, we can calculate an upper limit for k_{01}. The rate equation is $w = 2k_{01}[AlF^{2+}][F^-]$ and $k_{obs} = \frac{w}{T_F} = 2k_{01}\frac{[AlF^{2+}]}{1 + K_{HF}[H^+]}$. Calculating the corresponding concentration values from the spectra we obtain $k_{01} \leq 10^4\ M^{-1}s^{-1}$.

Fluoride exchange between complexes. Once it is recognised that fluoride exchange processes occur via an associative mechanism then it is readily understood why the exchange of F^- between complexes is unimportant on the ^{19}F NMR time scale. The much greater bulkiness, *cf.* AlF_2^+ and F^- or HF, of an incoming complex inevitably means that in comparison such reactions will be extremely slow.

Isomerisation processes. The temperature dependence of the ^{19}F NMR spectra suggests another dynamic process in the $Al^{3+} - F^-$ system. Selected spectra are shown in Figure IV.1.8. At near ambient temperatures, broadened signals of HF and its exchange partners AlF_3^0 and AlF_2^+, indicate ligand exchange processes between the free and coordinated ligands (see above). Lowering the temperature causes the HF signal to narrow, until at ~ 262 K its half width becomes constant. The explanation for this temperature dependence is the lowered rate of exchange between HF and AlF_3^0 /AlF_2^+, i.e., the intermolecular exchange becomes frozen

on the T_2 time scale. (The chemical shift also shows some temperature dependence towards lower fields.) A similar decrease is expected for the line widths of the other sites, AlF_3^0 and AlF_2^+, involved in the exchange. In fact, these peaks do start to narrow as temperature is lowered from 306 to 298 K (not shown) but they broaden again at T < 287 K. Although it is not obvious from the raw ^{19}F spectra (Figure IV.1.8a) band shape analysis (Figure IV.1.8b) indicates that signal **2** (AlF_2^+) splits in two at T < 265 K. Signal **1** almost disappeared under the envelope of signal **2** but is revealed by the numerical analysis, with its correct intensity. The signals become slightly narrower with decreasing temperature down to the freezing point of the solutions, ~ 253 K. The most plausible explanation of the splitting of signal **2** is that the exchange between the *cis*- and *trans*- AlF_2^+ complexes enters into the "slow exchange regime" on the NMR time scale with decreasing temperature. If it is assumed that the *trans*- isomer is favoured because of its more symmetrical charge distribution then the *cis-/trans*- ratio of the AlF_2^+ isomers at 255 K, estimated from the deconvolution shown in Figure IV.1.8b is approximately 2:1. The linewidth of signal **3** shows a broadly similar dependence on temperature to that of signal **2**. However, as the reactions of AlF_3^0 are faster than those of AlF_2^+, signals for the *mer*- and *fac*- AlF_3^0 isomers can not be separated under our experimental conditions. Given that the present NMR measurements indicate that the free ligand (HF/F^-) is not involved in the isomerisation reaction of AlF_2^+ (and very likely also not for AlF_3^0 either) at lower temperatures, the probable isomerisation mechanism is an *intra*-molecular process rather than an *inter*-molecular ligand exchange reaction. The NMR measurements indicate that the temperature dependence for the *intra*- and *inter*-molecular fluoride exchange processes are different, indeed this difference allows their separation.

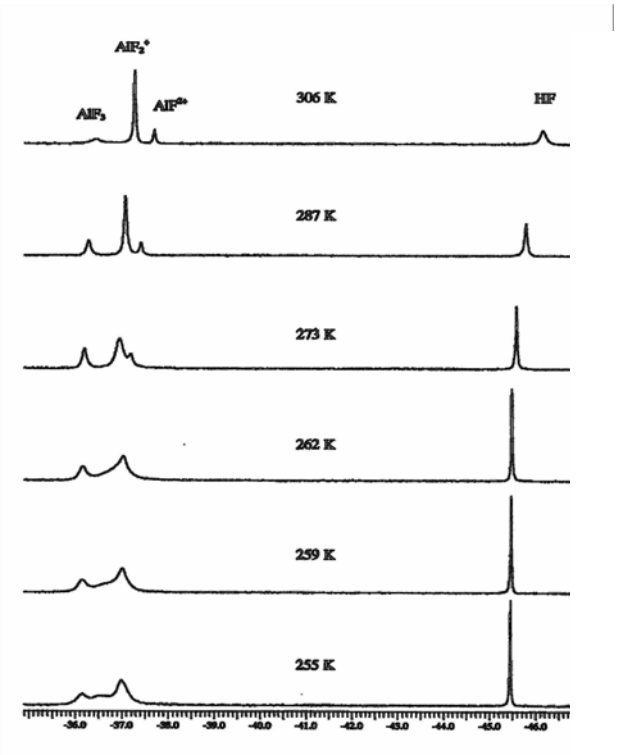

Figure IV.1.8a. ^{19}F NMR spectra of a solution with c_{Al} = 5 mM, c_F = 15 mM, c_H = 0.1 M, 3 M (KCl) at different temperatures T (a)= 255 K, (b) 259 K, (c) 262 K, (d) 273 K, (e) 287 K, (f) 306 K. Numbers **1**, **2**, **3** refer to species AlF^{2+}, AlF_2^+ and AlF_3^0, respectively.

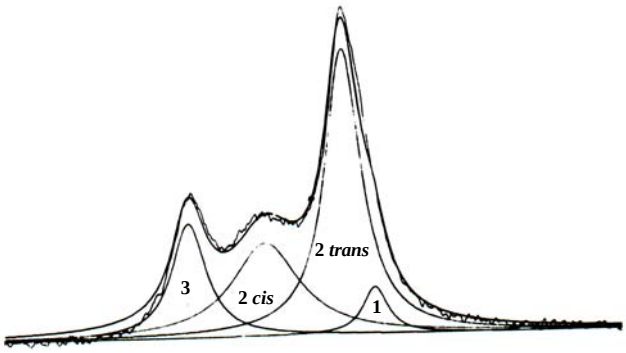

b. Band shape analysis for spectra at 255 K from **a**. Numbers **1**, **2**, **3** refer to species AlF^{2+}, AlF_2^+ (isomers *cis*-/*trans*-), AlF_3^0.

Geometry of the complexes. The existence of *cis*- and *trans* isomers of $AlF_2^+(aq)$ is a straightforward proof of its octahedral geometry and thus by implication that of $AlF^{2+}(aq)$ too. It has often been assumed by extension that this must also be true for the higher order complexes ($i \geq 3$). On the other hand, as noted earlier, complexes with geometries other than octahedral certainly exist in the solid state, in melts and in some *nonaqueous* solutions. The above presented measurements, like those of previous NMR investigations, do not provide any direct information on this matter. Thus, although the observed broadening of signal **3** implies their existence the *mer*- an *fac*- isomers of $AlF_3^0(aq)$ could not be positively identified under our experimental conditions. Similarly, whilst the existence of $AlF_5^{2-}(aq)$ implies octahedral geometry, failure to detect AlF_6^{3-} suggests that hasty conclusions on this subject may not be wise.

Comparison of the Al^{3+}/F^- and Al^{3+}/OH^- systems. It is interesting to contrast the behaviour of the Al^{3+}/F^- system with that of the industrially important Al^{3+}/OH^- system. Although unambiguous proof is not as readily available as commonly supposed, a variety of measurements indicate that $Al(OH)_4^-$ (aq) is tetrahedral.[97,98] Given that OH^- and F^- are isoelectronic and isochoric and show many parallelism in their chemistry, in both the solution and solid states, it is somewhat surprising that their interaction with $Al^{3+}(aq)$ should be so dissimilar. As noted by Tuck[1] this is a reflection of the very fine balance between the strength of interaction of Al^{3+} with the three hard donor ligands H_2O, OH^- and F^-. The values of $logK_i$ ($AlF_i^{(3-i)+}$) show the normal regular decrease with increasing *i* (Table IV.1.1.) which is *circumstantial* evidence for the preservation of octahedral geometry in this series of complexes. In contrast, the values of $logK_i$ ($Al(OH)_i^{(3-i)+}$) are 9.0, 8.7, 8.2 and 6.4 for i = 1 – 4, respectively.[99] This lack of variation has been noted by many authors and has been used as evidence of a change in geometry from the octahedral $Al(H_2O)_6^{3+}(aq)$ to tetrahedral $Al(OH)_4^-(aq)$. Where this change occurs is unknown because of experimental difficulties associated with solubility and polymer formation. This dissimilarity continues for the higher order complexes. Thus, $Al(OH)_6^{3-}(aq)$ exists but only at very high concentrations (>10 M) of OH^-.[100] No reliable evidence for $Al(OH)_5^{2-}(aq)$ exists. In contrast, as shown in this paper, $AlF_5^{2-}(aq)$ forms readily, yet $AlF_6^{3-}(aq)$ remains unproven.

IV.2. The Aluminium – Oxalate and Aluminium – Fluoride – Oxalate Systems

IV.2.1. The Aluminium – Oxalate System

The equilibrium study of the binary $Al^{3+} – C_2O_4^{2-}$ (referred to from now on as Ox^{2-}) system has already been performed by Öhman *et al.* by combined potentiometric and ^{27}Al NMR measurements.[53] Three binary species $AlOx^+$, $AlOx_2^-$, $AlOx_3^{3-}$ are detected in the acidic region, and two polynuclear hydroxo species are also found in the near neutral, alkaline solutions. At larger excess of oxalate only binary species are formed up to pH ≤ 6.5, see figures IV.2.1. a) and b).

a) ***b)***

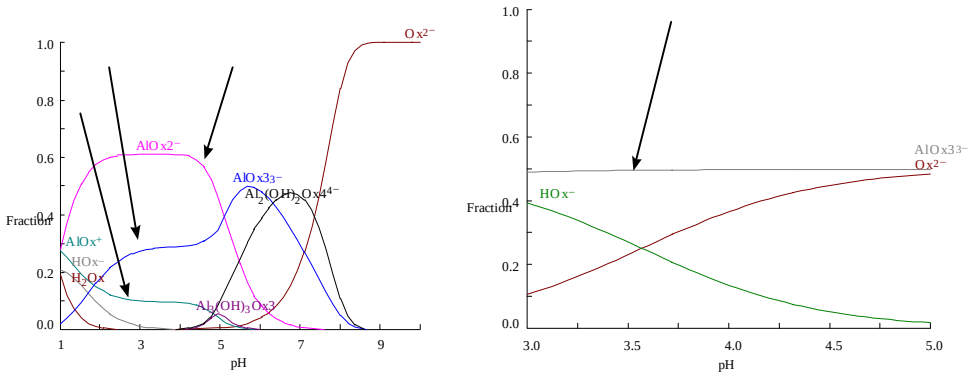

Figure IV.2.1. Distribution diagram as a function of pH (showed for oxalate fraction) for *a)* c_{Al} = 5 mM, c_{Ox} = 10 mM, and *b)* c_{Al} = 8 mM, c_{Ox} = 48 mM solutions. Arrows indicate the binary species.

Assignation of species. Using ^{13}C enriched Na_2Ox these species are identified by ^{13}C NMR. One can see from the concentration distribution curves that free oxalate, when present, can act as a good pH indicator. Its chemical shift varies depending on which of the three forms, Ox^{2-}, HOx^-, H_2Ox, is present. NMR titration of a 5 mM Na_2Ox sample in 0.6 M NaCl is shown on Figure IV.2.2. The δ – pH curve begins at pH = 1.36 and comes to the limiting shift at pH ~ 6. The protonation constants are evaluated from these data by least square fitting. The value for the first protonation constant, $\log\beta_{HOx} = 3.60 \pm 0.03$, is in excellent agreement with the literature value (see Chapter III.6). The second protonation constant can not be calculated properly from the available data, obtaining $\log\beta_{H2Ox} = 4.96 \pm 1.33$. It is worth to call the attention to a peculiarity of this pH titration, namely, that the ^{13}C

line width of the oxalate signal is substantially broader (5 – 8 Hz) than the usual width of either the carbonyl carbon peaks, or those of binary species (~ 0.6 Hz). This broadening is pH dependent, but the variation is not monotonic. To answer this finding a detailed study is needed, unfortunately, we have not cleared it up so far. Still, we believe it is an interesting proton exchange reaction related to H – bonding between the two carboxylate groups of oxalate.

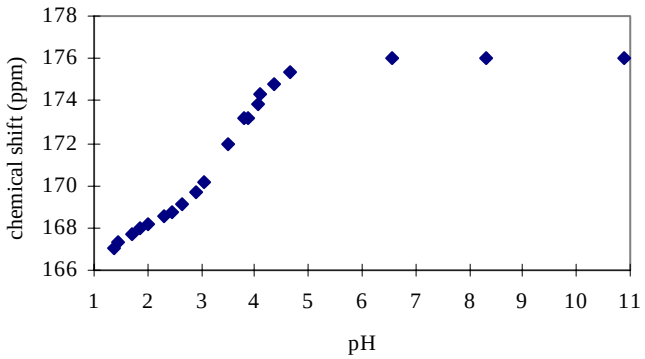

Figure IV.2.2. ^{13}C NMR titration curve of 5 mM Na_2Ox sample in 0.6 M NaCl

The assignation of species can be done by varying the metal/ligand ratio and pH. The results are summarised in Table IV.2.1. It is worthwhile to mention that these signals are very close to each other on the ^{13}C NMR chemical shift scale. Consequently, application of large line broadening before Fourier transformation can cause indistinct peaks. This might be happened in an earlier work of Phillips *et al.*[61]

Table IV.2.1. ^{13}C NMR shift values of the detected binary species

Species	Chemical shift (ppm)
$AlOx^+$	168.04
$AlOx_2^-$	168.10 168.16
$AlOx_3^{3-}$	168.26

Dynamics. As pH variation does not affect the position of the signals, the absence of protonation of these species is proved. Moreover, for species $AlOx_2^-$ two signals are detected in ratio 1:1. The most probable explanation for this is the existence of two isomers, such as:

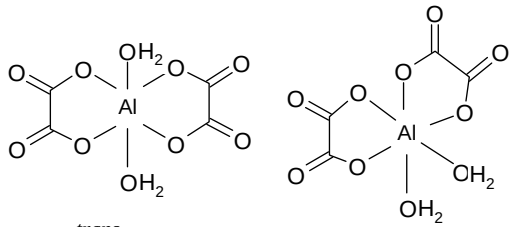

trans- *cis-*

Apart from the classical Werner type, inert Co(III) and Cr(II) complexes, the appearance of this kind of isomers has recently been detected by NMR for the vanadyl – oxalate, and uranyl – oxalate systems.[101] Observing two peaks mean that the *cis* and *trans* forms are in slow exchange at room temperature. To evaluate this intra–molecular exchange a temperature variation study has to be done.

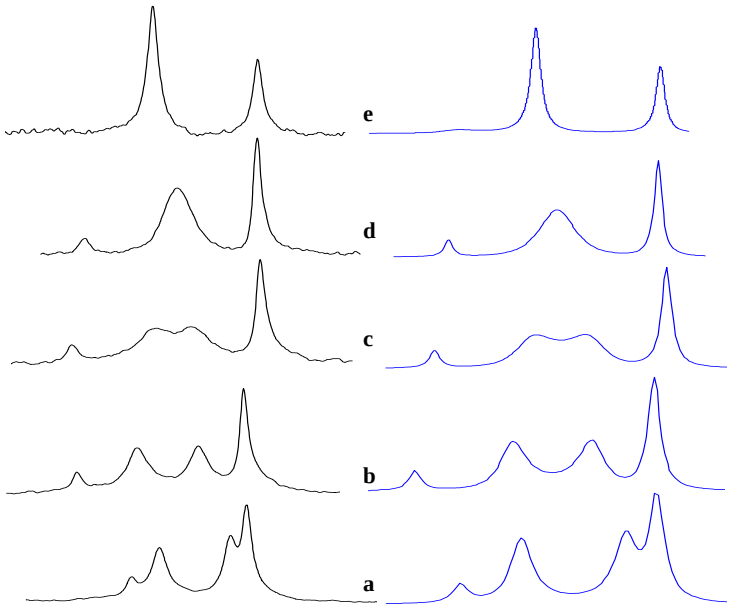

Figure IV.2.3. Measured (left) and simulated (right) ^{13}C NMR spectra of a solution with c_{Al} = 5 mM, c_{Ox} = 10 mM at pH = 2.02 at different temperatures: (a) 278 K, (b) 296 K, (c) 306 K, (d) 315 K, (e) 348 K.

In a sample prepared form 99% ^{13}C enriched oxalate and composition c_{Al} = 5 mM, c_{Ox} = 10 mM, pH = 2.02, the series of spectra shown on Figure IV.2.3 (left) is obtained. $AlOx_2^-$ is the dominant species, followed by $AlOx^+$ and a small quantity

of $AlOx_3^{3-}$. A negligible amount of HOx^- has to be present, but this is under detection limit. If it had appeared, it should have been under one of the signals of the binary species. The series of spectra is simulated by a MATLAB micropogram.[102] Species $AlOx^+$, $AlOx_2^-$ *cis* and *trans*, $AlOx_3^{3-}$ are symbolized as 1,2,3,4. The pseudo – first order intra–molecular rate constant is k_{23}. Inter – molecular exchange reactions are supposed between the first and second complex, and between the second and third complex with corresponding constants k_{12}, k_{13}, k_{34}, k_{24}. Both *cis* and *trans* forms of $AlOx_2^-$ take part with equal contribution to the exchange reactions. It is almost impossible that a reaction between the first and third complex exists, thus, this exchange is excluded. The obtained simulated spectra are shown on Figure IV.2.3. (right), and the goodness of fitting is certified by the coincidence of signal intensities and line width values. At temperatures higher than 306 K coalescent peak appears in the measured spectra. Their individual chemical shifts are calculated from the linear extrapolation of the shifts obtained at lower temperatures. Populations of the different sites is given from the deconvolution made at 296 K, which coincides with the concentration distribution, and it is kept constant for all other temperatures. Populations of *cis* and *trans* forms of $AlOx_2^-$ are the same. The fitted pseudo – first order rate constants are summarised in Table IV.2.2.

Table IV.2.2. Pseudo – first order rate constants for intra – molecular isomerisation of $AlOx_2^-$ and inter – molecular exchanges between binary species.

T (K)	k_{23} (s^{-1})	k_{12} (s^{-1})	k_{13} (s^{-1})	k_{24} (s^{-1})	k_{34} (s^{-1})
278	1.5	–	–	–	–
290	3	–	–	–	–
296	4	–	–	–	–
306	9	–	–	–	–
311	13	–	–	–	–
315	20	–	–	–	–
323	60	0.3	0.3	0.4	0.4
338	150	0.5	0.5	1	1
348	$1.00 \cdot 10^3$	1.5	1.5	2	2

As it is seen from Table IV.2.2. intra – molecular exchange measurements cover a temperature range of 70 K, thus, reliable activation parameters can be calculated. The following data are obtained from the Eyring plot: $\Delta H^{\#} = 67 \pm 5$ kJ mol^{-1} , $\Delta S^{\#} = -6 \pm 6$ J mol^{-1} K^{-1}. These are in the usual range considering fluxional

processes with pure intra–molecular character. For these activation entropy values are around zero. The calculation of $\Delta G^{\#}_{298}$ = 69 kJ mol^{-1} for this *cis/trans* rearrangement is more characteristic. This value is around the middle of the interval given in the literature for these rearrangements.[103] The *cis*/ *trans* exchange requires the mutual exchange of one water molecule and one carboxylate group of the oxalate ligand inside the inner coordination sphere of Al^{3+}, while the other carboxylate could be bound during isomerisation. The lability of water in $AlOx^{+}$ (and consequently probably in $AlOx_2^{-}$) is told to be much higher[61] (k_{H2O} = 109 s^{-1}) than the rate of the isomerisation ($k^{298}_{cis/trans}$ = 4 s^{-1}). The rate determining step should be the breaking of the Al–O(C=O) bond. Interestingly, Szabó *et al.* arrived to a different conclusion for the uranyl – L – fluoride system (L = oxalate, carbonate, picolinate), where the rate determining step of site exchange is the water exchange.[101] Thus, the *cis/trans* isomerisation can be described without any contribution of inter–molecular reactions. This indicates that bimolecular reactions like complex formation, *e.g.* $AlOx^{+} + Ox^{2-} \rightleftharpoons AlOx_2^{-}$, are quite slow at the ^{13}C NMR time scale at room temperature. However, in analogy to the $Al^{3+} – F^{-}$ system, one can expect ligand exchange reactions, *e.g.* $AlOx^{+} + {}^*Ox \rightleftharpoons Al{}^*Ox^{+} + Ox$, (Ox = H_2Ox, HOx^{-}, Ox^{2-}) to be much faster. This kind of reaction requires some free oxalate in the equilibrium system, condition fulfilled for solutions with c_{Ox}/c_{Al} > 3 and low pH. All our attempts to detect any exchange between complexes $AlOx_q^{(3-2q)+}$ and free Ox in pH = 1–4 range and c_{Ox}/c_{Al} = 3–6 using T_1 time scale of ^{13}C NMR fail. In this way only a limiting value τ > 3–5 T_1 ~ 120 s (k_{obs} ~ 1/τ < 0.008 s^{-1}) can be calculated. This shows how inert the 5 membered AlOx ring is!

Inter–molecular processes are also detected at temperatures higher than 323 K (see Table IV.2.2.), but these constants are purely of qualitative use. Inter – molecular exchange reaction between the free oxalate and one binary species is studied in a sample with c_{Al} = 8 mM, c_{Ox} = 32 mM at pH = 4.05. At this pH value only two signals appear in ^{13}C NMR, a narrow one of $AlOx_3^{3-}$ and a broader one of HOx^{-}/Ox^{2-}. The broadening could be attributed to H^{+} exchange. Magnetization transfer experiments (a typical one is shown on Figure IV.2.4.) are carried out at different temperatures for analyzing the reaction:

$$AlOx_3^{3-} + {}^*Ox^{2-} \underset{k_{0,3}}{\overset{k_{3,0}}{\rightleftharpoons}} Al{}^*OxOx_2^{3-} + Ox^{2-}$$

It is observed that ligand exchange is launched only at T ≥ 324 K. Evaluating the series of spectra recorded at different temperatures kinetic data appearing in Table IV.2.3. are obtained.

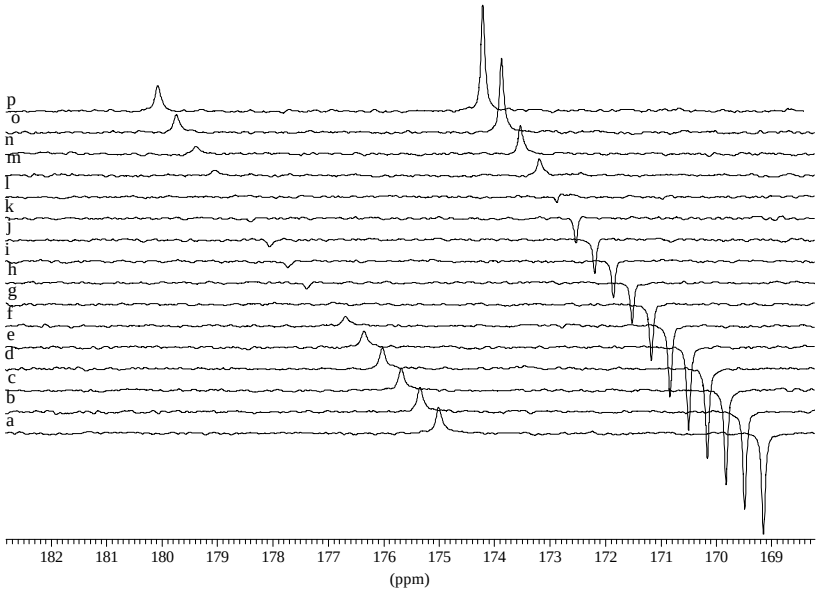

Figure IV.2.4. ^{13}C NMR spectra of a solution with c_{Al} = 8 mM, c_{Ox} = 32 mM, pH = 4.02, at 362 K. Corresponding values of the VD list are (a) 0.6 ms, (b) 0.01 s, (c) 0.03 s, (d) 0.05 s, (e) 0.1 s, (f) 0.2 s, (g) 0.4 s, (h) 0.8 s, (i) 1.2 s, (j) 1.5 s, (k) 2.5 s, (l) 5.0 s, (m) 8.0 s, (n) 10.0 s, (o) 20.0 s, (p) 30.0 s. The signal of $AlOx_3^{3-}$ is inverted.

Table IV.2.3. Pseudo – first order inter – molecular rate constants at different temperatures obtained from MT measurements**.**

T (K)	324	333	348	362
k_{30}^{obs} (s^{-1})	0.010±0.002	0.11±0.03	1.6±0.3	6.8±1.7

Remembering the lack of bimolecular reactions at room temperatures and the minor contributions of inter–molecular exchange found at higher temperatures (see Table IV.2.2.) these pseudo – first order rate constants might be considered as real

first order constants. Calculated activation parameters are $\Delta H^{\#} = 164\pm17$ kJ mol^{-1} , $\Delta S^{\#} = 225\pm51$ J mol^{-1} K^{-1}. These values are in accordance with a pure D, or I_d mechanism:

$$AlOx_3^{3-} \xrightarrow{\text{r.d.s.}} AlOx_2^{-\#} + Ox^{2-}$$

$$AlOx_2^{-\#} + {}^*Ox^{2-} \overset{\text{fast}}{\rightleftharpoons} AlOx_2{}^*Ox$$

In the first step dissociation of one oxalate is happening, while in the next fast step a new oxalate ligand will jump in the vacancy. The high value of $\Delta H^{\#}$ supports this dissociative step, as two bonds has to be broken. The activated complex will be more disordered, in agreement with the positive value of $\Delta S^{\#}$. Thus, this is a similar situation with the one met at the fully saturated $VO_2(Ox)_2$.[101]

IV.2.2. The Aluminium – Fluoride – Oxalate System

Equilibrium. Considering that H^+ is also present with varying concentration it would be more realistic to talk about quaternary system instead of the aluminium – fluoride – oxalate ternary one, as it is indicated in the title. The study of this complicated equilibria – approaching the situation met in nature – is based on potentiometric measurements, while supporting informations for the equilibrium model are provided by ^{19}F and ^{13}C NMR studies.

Potentiometric titrations are carried out in order to calculate the overall stability constants, $\beta_{p,q}$, of the general equilibrium:

$$Al^{3+} + pF^- + qOx^{2-} \rightleftharpoons AlF_pOx_q^{(3-p-2q)+} \qquad \text{(IV.2.1.)}$$

$$\beta_{p,q} = \frac{[AlF_pOx_q^{(3-p-2q)+}]}{[Al^{3+}][F^-]^p[Ox^{2-}]^q} \qquad \text{(IV.2.2.)}$$

Titrations of binary aluminium – fluoride system with oxalate (described in chapter III) fail, in agreement with observations mentioned in chapter IV.1. Precipitation occurs at ratios $c_F : c_{Al} \geq 2.7 - 3$ and equilibrium potentials are not reached even in 16 hours. Thus, the presented type *ii*) titrations are carried out, *i.e.* at constant c_{Al} concentration the c_{Ox} concentration is varied and the formed binary system is titrated with fluoride. The pH does not change too much, a variation between 2.2 – 2.7 is observed. Titration data are shown on Figure IV.2.5. covering the range $c_F : c_{Al} \leq 3$. If we consider six coordinated aluminium ions then species $AlF_pOx^{(1-p)+}$ with p = 1–4 and $AlF_pOx_2^{(-1-p)}$ with p = 1–2 should form. Due to

relatively acidic conditions mixed hydroxo species, $AlF_pOx_q(OH)_n^{(3-p-2q-n)+}$, are not taken into consideration. Moreover, there is no indication of the formation of protonated and polynuclear species in the working domain in LETAGROP refinements. Keeping fixed the stability constants of binary species and refining those for ternary ones, four complexes are enough and sufficient to describe the system: AlFOx, $AlFOx_2^{2-}$, AlF_2Ox^- and $AlF_2Ox_2^{3-}$. Fitted stability constants are shown in Table IV.2.4. Formation of complexes with higher fluoride content can not be excluded in the presence of other – larger – counterions, which prevent precipitation, as it is detected at the binary aluminium - fluoride system. However, under our experimental conditions only these species are present counting also solubility factors.

The reliability of the calculated stability constants can be represented by plotting the variation of the average number of coordinated ligand, $\bar{n}$, against the logarithm of the free ligand concentration. The $\bar{n}$ values for the measured points are calculated with expression IV.2.4. showed for fluoride coordination and resulting from the mass balance equation IV.2.3:

$$c_F = [F^-] + [HF] + 2\cdot[HF_2] + \sum_{p=1}^{5} p\cdot[AlF_p^{(3-p)}] + \sum_{p,q=1}^{4,2} p\cdot[AlF_pOx_q^{(3-2q-p)}] \qquad \text{(IV.2.3.)}$$

$$\bar{n} = \frac{c_F - [F^-]\cdot\{1 + K_{HF}[H^+] + K_{HF_2}[H^+]^2\}}{c_{Al}} \qquad \text{(IV.2.4.)}$$

The same formulas are applied for the fitted curve except that the corrected total fluoride concentrations are used, resulting from the output of LETAGROP calculations.

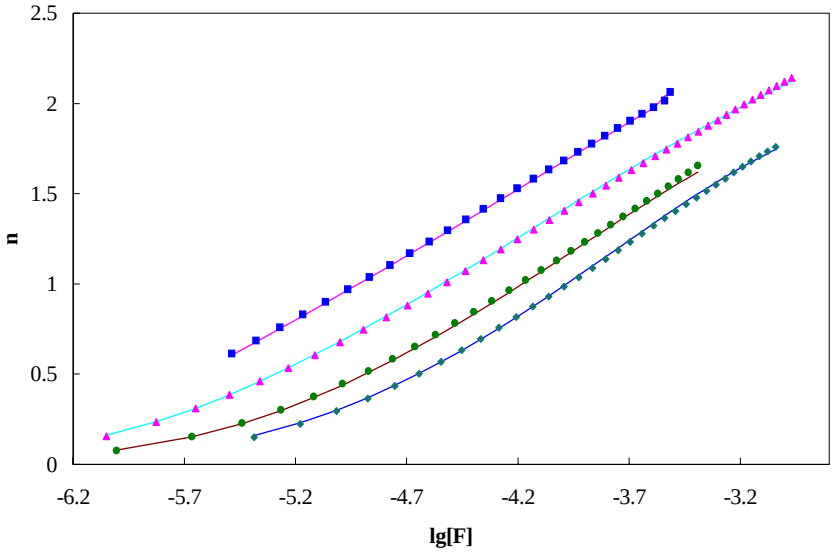

Figure IV.2.5. The average number of coordinated fluoride as a function of free fluoride concentrations at different Al^{3+} : Ox^{2-} ratios. c_{Al} = 5 mM, pH=2.2-2.7, 0.6 M NaCl at 25 °C, c_{Ox} varies: (■)5 mM, (♦)8 mM, (●) 12 mM, (◆) 15 mM.

Table IV.2.4. Overall stability constants, $\log\beta_{pq}$, of $AlF_pOx_q^{(3-p-2q)+}$ species determined in 0.6 M NaCl at 25 °C, and ^{19}F and ^{13}C NMR shifts and number of possible isomers.

Species	$\log\beta_{pq}$ [a]	δ_F (ppm)	δ_C (ppm)	isomers
AlFOx	11.53 ± 0.03	~ – 40	168.42	2
AlF_2Ox^-	15.67 ± 0.03	–38.60	168.77	4
$AlFOx_2^{2-}$	15.74 ± 0.02	–39.55	168.51	2
$AlF_2Ox_2^{3-}$	19.10 ± 0.04	–39.34	168.99	2

[a] The uncertainty is equal to three times the estimated standard deviations in the least squares refinement of the experimental data.

Typical concentration distribution curve calculated by the determined constants is shown on Figure IV.2.6a. It is easy to observe that at comparable c_{Ox} and c_F concentrations the mixed species are dominant. This dominance of the ternary complexes can also be demonstrated in a similar way at lower c_{Al} concentrations. Therefore, these ternary species might play important role in natural waters, in fluoride containing drinking waters and in biological fluids as

well. The formation of the ternary species can formally be described considering $AlOx_q^{(3-2q)+}$ complexes as 'central ions' coordinating one or more F^- ion(s) as:

$$AlOx_q^{(3-2q)+} + pF^- \rightleftharpoons AlF_pOx_q^{(3-p-2q)+} \qquad \text{(IV.2.5.)}$$

$$K^p_{AlOx_q} = \frac{[AlF_pOx_q^{(3-p-2q)+}]}{[AlOx_q^{(3-2q)+}][F^-]^p} \qquad \text{(IV.2.6.)}$$

$K^p_{AlOx_q}$ constants can be calculated from values of $\beta_{p,q}$ and stability constants of $AlOx_q^{(3-2q)+}$ complexes. For example, $\log K^1_{AlOx} = \log\beta_{AlFOx} - \log\beta_{AlOx} = 11.53 - 5.97 = 5.56$. This value is only less than one order of magnitude smaller than the value of the formation constant $\log\beta_1 = 6.1$ of binary AlF^+. Stepwise coordination of the second F^- to $AlOx^+$ has a value of $\log\beta_{AlF2Ox} - \log\beta_{AlFOx} = 4.14$. This is still a quite high value compared to $\log\beta_2 = 5.4$ of AlF_2^+. It can be concluded, that the presence of one or two oxalates in the coordination sphere of Al^{3+} does not influence too much the binding of fluoride ligands. This is not a unique feature, thinking of the similar behaviour of aluminium – EDTA – fluoride system.[104] All these findings emphasize the special strength of the aluminium – fluoride interaction.

The next step is the identification of ternary species in NMR. NMR experiments can make the model selection of potentiometric studies more reliable, furthermore, analysis of NMR spectra bring us closer to the structural and dynamic features of the species identified by titrations. We have two useful NMR nuclei in the complexes (^{13}C and ^{19}F), and in both cases all of the four ternary species can be found. Assignation is done by performing concentration variation measurements. In ^{19}F NMR the situation is easier, as binary and ternary species are distanced (see Figure IV.2.6b.). At 298 K the signal of AlFOx is broadened to baseline. In ^{13}C NMR (these samples are prepared from ^{13}C labeled oxalate) signals are overlapping. The situation is complicated by the presence of free oxalate, which has a substantial shift with small variations of pH. Knowing the positions of binary species and the free oxalate, all peaks are finally identified as shown on figure IV.2.7. It is also evident, that the ternary species do not indicate protonation effects. This is underlined in ^{13}C spectra, Figure IV.2.7., where vertical lines illustrate the invariance of the ternary peak positions with pH changes. On the other hand the binary $AlOx_2^-$ shows two peaks (*cis*/*trans*), while each of the $AlFOx_2^{2-}$ and $AlF_2Ox_2^{3-}$ species present only one broad peak. This means, that

oxalate is more labile in mixed complexes, than in binary ones. Chemical shift values for the four ternary complexes are presented in Table IV.2.4.

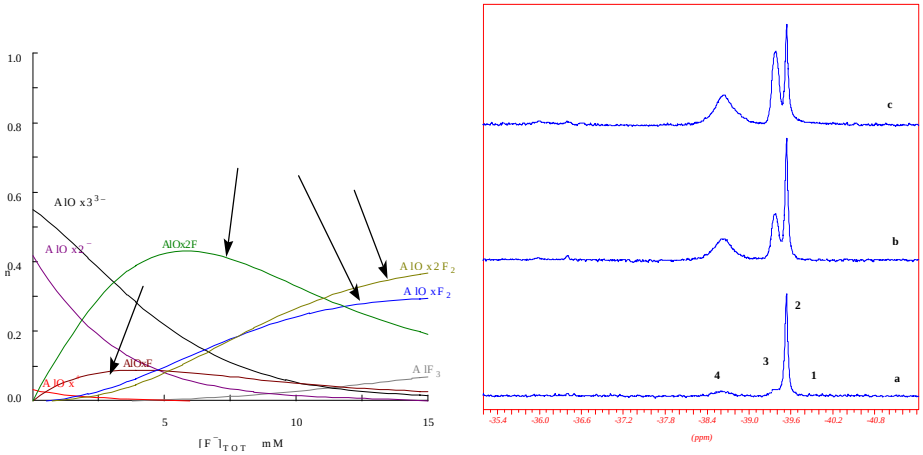

Figure IV.2.6. ***a)*** Concentration distribution (Al fraction) of a solution with c_{Al} = 5 mM, c_{Ox} = 15 mM, pH = 2.4 in 0.6 M NaCl media at 298 K. Arrows point out the four ternary species; ***b)*** ^{19}F NMR spectra of a solution with composition defined at ***a)*** at 298 K with varying c_F: (a) 3 mM, (b) 7 mM, (c) 9 mM. Numbers 1,2,3,4 mean complexes AlFOx, $AlFOx_2^{2-}$, $AlF_2Ox_2^{3-}$ and AlF_2Ox^-, respectively. Peak 1 is broadened, see text.

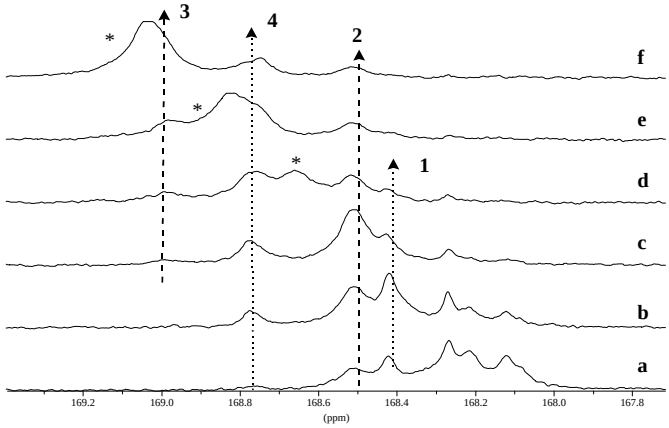

Figure IV.2.7. ^{13}C NMR spectra (99% enriched ^{13}C) of a sample with c_{Al} = 5 mM, c_{Ox} = 7 mM, c_H = 7.2 mM, pH = 2.2–2.7 with varying fluoride concentration c_F : (a) 2.5 mM, (b) 5.0 mM, (c) 7.5 mM, (d) 10.0 mM, (11) 12.5 mM, (e) 15.0 mM. Numbers 1,2,3,4 mean complexes AlFOx, $AlFOx_2^{2-}$, $AlF_2Ox_2^{3-}$ and AlF_2Ox^-, respectively.* stays for HOx^-/Ox^{2-}, binary $AlOx_i^{(3-2i)+}$ species are not numbered.

Dynamics. A striking characteristic of these spectra is that all species have broad signals. This may not be surprising if we think of the possible Werner type isomers, which are not distinguished by potentiometry, but they may be detected in NMR. In a recent study[105] several isomers were identified by ^{31}P and ^{19}F NMR in the Al^{3+} –pyrophosphate – F^- system. Generally, our signals narrow with increasing temperature, indicating that the isomers are in the 'fast exchange regime'. This must be the consequence of intra–molecular isomerisation reactions, as we detect as many peaks as the number of species found by independent experiments. The number of different isomers is indicated in Table IV.2.4. The temperature variation study (Figure IV.2.8a) shows peculiarities. Lowering the temperature the AlFOx peak narrows, while the signal of $AlF_2Ox_2^-$ broadens. This attitude is a result of complicated inter – and intra–molecular exchange reactions. Unfortunately, these exchange reactions can not be separated by temperature variation in the ternary system, in contrary to the binary aluminium – fluoride complexes. Therefore, direct detection of the isomers fails. Moreover, it is known that exchange processes which are hidden on T_2 time scale, (*i.e.* do not cause line broadening) may come to light on T_1 scale by incoherent magnetization transfer experiments. Recording 2D EXSY spectra has the advantage that a fast overview is obtained, strengthening the statements made on the nature of the identified species. A closer investigation of the 2D EXSY spectra (shown on Figure IV.2.8b.) requires explanation of cross peaks between AlF_2^+ and AlF_3. We have to note, that a small quantity of HF/F⁻⁻exists, but it is out of the measuring window. In chapter IV.1.2. we demonstrated that the formation rate of AlF_3 from AlF_2^+ and F (F means HF/F^-) is a slow process (eq. IV.1.17.) therefore, this reaction can not be responsible for these cross peaks. Direct F exchange between AlF_3 and AlF_2 was ruled out also. However, it can be shown that during the mixing time of 0.3 s the following chain of exchange reactions (follow the route of $^*F$) can produce magnetization transfer betwen the two binary complexes:

$$Al^*FF^+ + F \rightleftharpoons AlF_2^+ + {}^*F$$

$$AlF_3 + {}^*F \rightleftharpoons Al^*FF_2 + F$$

Another interesting feature is that cross peaks are present between the complexes with different number of oxalate ligands in the inner coordination sphere. E.g. AlF_2Ox^- and AlF_2^+, or AlF_2Ox^- and $AlF_2Ox_2^{3-}$. It means, surprisingly, that oxalate exchange, which is very slow in the binary oxalate complexes at room temperature, occurs in this case. This situation may be similar to that one where the coordination

of one fluoride ligand labilizes the coordinated water molecule.[61] However, no exchange is detected between AlFOx and AlF_2Ox. This means that the coordinated water is not enough labile. Thus, complex formation even for the ternary complexes is a slow process on the T_1 ^{19}F NMR time scale. Of course, the F assisted indirect exchange can also happen on the basis of the following reactions:

$$Al^*FFOx + F \rightleftharpoons AlF_2Ox + {}^*F$$

$$AlF_2Ox_2^{3-} + {}^*F \rightleftharpoons Al^*FFOx_2^{3-} + F$$

In order to clarify the dynamics in the ternary system more experimental work is needed.

In conclusion, several inter– and intra–molecular exchange reactions can be detected by ^{13}C and ^{19}F NMR, which indicate that compared to the binary complexes both F^- and Ox^{2-} ligands seem to be labilized in the ternary species.

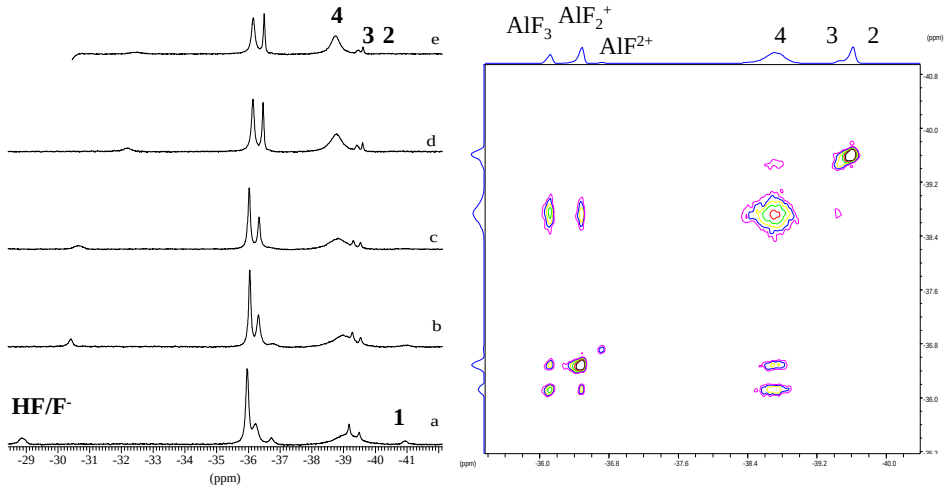

Figure IV.2. 8. ***a)*** ^{19}F NMR spectra of a solution with $c_{Al} = c_{Ox} = 5$ mM, $c_F = 7$ mM, pH = 2.2 in 0.6 M NaCl media at varying temperatures: (a) 278 K, (b) 238 K, (c) 288 K, (d) 293 K, (e) 298 K. ***b)*** 2D EXSY spectra for a sample with $c_{Al} = 5$ mM, $c_{Ox} = 6$ mM, $c_F = 8$ mM, pH = 2.4 in 0.6 M NaCl media at 298 K. Mixing time is 300 ms. Numbers 1,2,3,4 refer to species AlFOx, $AlFOx_2^{2-}$, $AlF_2Ox_2^{3-}$ and AlF_2Ox^- respectively. Binary complexes and HF/F^- are also indicated.

IV.3. The Aluminium – Citrate System

IV.3.1. Equilibrium and Structure

The equilibration of this system as stated in the introduction is very slow. A reliable model describing the existent species is accepted as being the one proposed by Öhman using potentiometric titrations. Usually the validity of an equilibrium model is checked by spectroscopic measurements. In our case NMR spectroscopy is applied in order to detect these species and to assign the peaks in the spectra to the corresponding complexes. Once these done it is possible to step further in order to elucidate the solution structure and the kinetic behaviour. In addition to the chemical shift, structural information is obtained mainly from two characteristics: the coupling pattern and the nuclear Overhauser effect (nOe). The first one is a consequence of scalar 'through bond' interaction , the second one is a 'through space' dipole–dipole interaction between spins.

The values of coupling constants indicate hybridization states and sterical arrangements. One-bond $^1J_{CH}$ couplings depend on the hybridization of the C atom. The higher is the *s* character of the bond, the higher is the coupling constant. Thus, for sp^3 hybridization state this value is ~125 Hz, for sp^2 ~156 Hz and for *sp* ~250 Hz. One has to remember, that here the tendency is important, as substituent effects can cause dramatic variations $^1J_{CH}$ in values.[106]

Geminal two-bond $^2J_{HH}$ couplings are highly sensitive to structural arrangements. The value of $^2J_{HH}$ depends on the largeness of the torsion angle Ψ. For the $R–H_2C^{\alpha}–COO$ molecular fraction Ψ is the angle between the projection in plane of the C^{α}–R bond (fixed) and the projection in the same plane of the C–O bond (rotating). The situation is depicted in Figure IV.3.1. with representative Ψ angle in the inset diagram.[107]

Two-bond heteronuclear $^2J_{CH}$ coupling constants are small compared to $^1J_{CH}$ values. Couplings through a carbonyl group result in $^2J_{CH}$ three times as large as in other cases, because of the lone-pair electrons of the carbonyl oxygen. Thus, in acetaldehyde $^2J(C,CO,H)$ = 26.6 Hz and in ethane $^2J(C,C,H)$ = 4.8 Hz. In several amino acids and carboxylic acids (α-alanine, β-alanine, N-acetylhistidine, aspartic acid, 3 methyl butanoic acid, propanoic acid) the value of $^2J(COOH,C,H)$ ~ 6.7-7.0 Hz.[3]

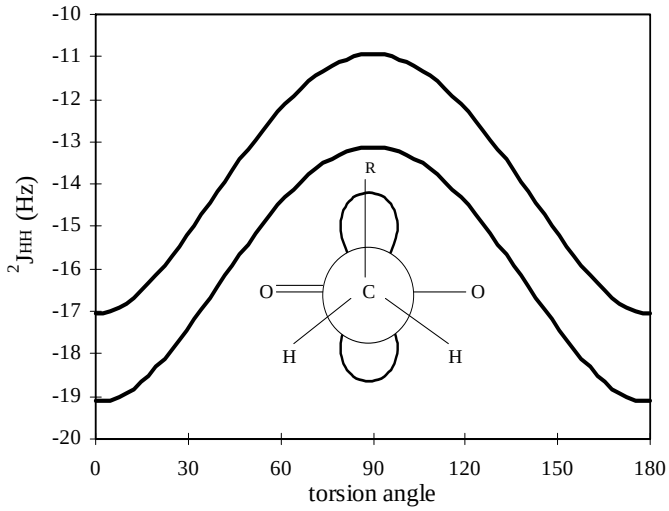

Figure IV.3.1. Proposed dependence of the H–C–H' geminal coupling constant, $^2J_{HH}$, on the torsion angle, Ψ. The bordered region represents the dependence of the coupling on the orientation of the π orbital. The inset diagram shows the position obtained for Ψ = ±90°.

The most important structural informations in this work are obtained from the three-bond $^3J_{CH}$ values. These values on the basis of the semiempirical Karplus equation give the torsion angle, Φ, between the coupled spins:[108]

$$^3J = A \cos^2\Phi + B \cos \Phi + C \qquad \text{(IV.3.1.)}$$

where constants A, B, C are determined both theoretically and experimentally. The Newman projection for the definition of a torsion angle, Φ, as a rotation of the bond in the back in clockwise direction, is shown on the following scheme:

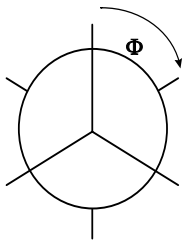

Small torsion angles, when coupled spins are in *gauche* position, give rise to a small $^3J_{CH}$, while *trans* orientation results in a large coupling. The $^3J(60°)$ *gauche* values vary over a range of 0 – 3.3 Hz and $^3J(180°)$ *trans* values vary from 4 to 10 Hz. For sp^2 hybridization the disposition of the oxygen atoms on the coupling path seems to play some role as well.

Aydin and Gunther derived the following Karplus type equation taking into account different substituent effects:[107]

$$^{3}J_{C,H} = 4.50 - 0.87 \cos\Phi + 4.03 \cos 2\Phi \qquad \text{(IV.3.2.)}$$

Considering the uncertainity of ± 1 Hz the graphical representation of this relation is as shown on Figure IV.3.2.

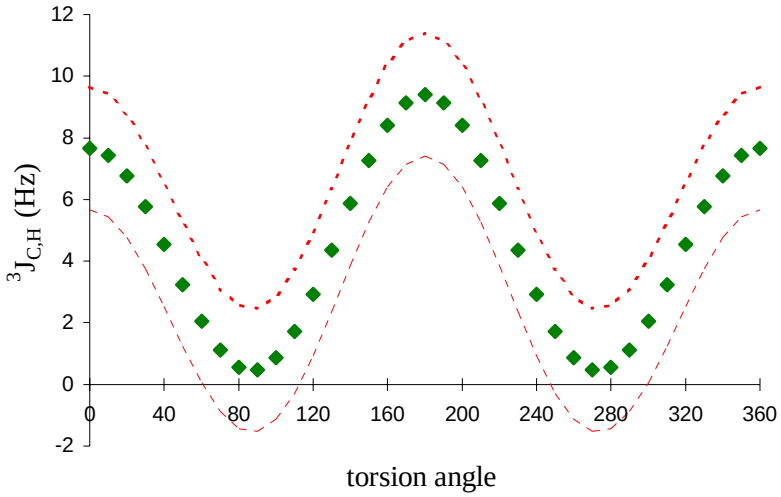

Figure IV.3.2. Variation of three-bond C, H coupling constant, $^{3}J_{CH}$, as a function of the torsion angle, Φ, based on equation IV.3.2.

Couplings over four, or more bonds are rare. Nevertheless there are special sterical arrangements where these couplings appear. Thus, four-bond $^{4}J_{HH}$ couplings are invariably observed for H–C–C–C–H fragments with a planar W conformation. This coupling can be as large as 2.5 Hz. In most cases its value is < 1 Hz. In one dimensional spectra it is almost impossible to detect, as the normal line width of the NMR peak hides it. This coupling comes 'to light' in the finely tuned two dimensional COSY spectra.

Besides these precious spin-spin couplings, the other important structural characteristic in NMR is the nOe. The basic phenomena responsible for its appearance is the cross relaxation. nOe depends on the internuclear distance and on the rapidity of molecular tumbling. Experimentally one can measure the equilibrium nOe, i.e. the change in the intensity of an NMR resonance when the

transition of another one is perturbed. Suppose the normal intensity of a resonance (at thermal equilibrium and without perturbing the system) is I_0 and the intensity observed while saturating some other related resonance (and waiting for the new equilibrium to be established) is I, then we define nOe as:

$$\eta = (I-I_0)/I_0$$

These data point out which spins are close in space. Extra information about molecular geometry can be obtained by measuring not the value of η, but the rate at which it arises. Measuring the rate of growth of the nOe internuclear distances can be obtained. Technically this is realised by 2D NOESY experiment (see experimental session). The signal of nOe is positive for small organic molecules and it becomes negative for large biomolecules. In the vicinity of molecular mass ~1000 this effect is not observed.[77]

Returning to the Al-citrate system the scope of this work is to obtain the encountered data from the NMR spectra and in the light of the aforementioned characteristics to give the solution structure of the appearing species.

Accepting the equilibrium constants determined by Öhman, we tried to prepare solutions in which only one species is dominant. Thus, $Al(Cit)_2^{3-}$ is dominant at a c_{cit}/c_{Al} ratio 4/1, while the trinuclear $Al_3(OH)(H_{-1}Cit)_3^{4-}$ (referred to from now on as *As*) and $Al_3(OH)_4(H_{-1}Cit)_3$ (referred to from now on as *Sy*) are dominant at ratios $c_{cit}/c_{Al} > 1$ at higher pH values. Concentration distribution curves are shown on figure IV.3.3. and IV.3.4.

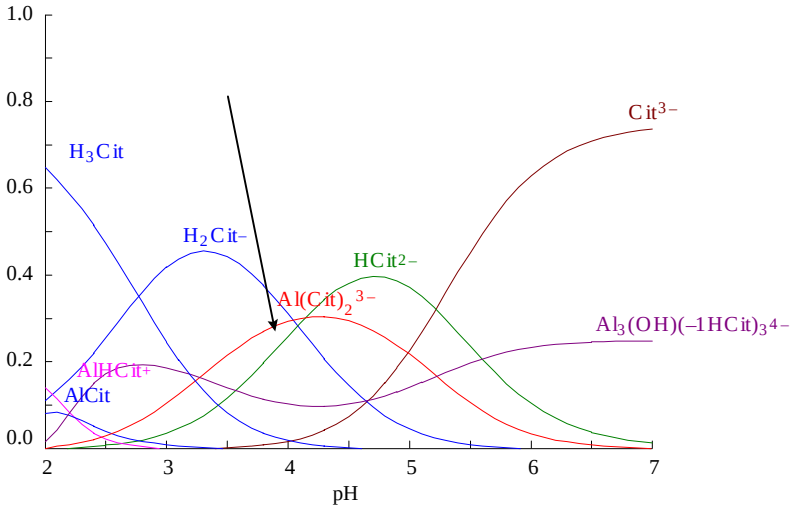

Figure IV.3.3. Concentration distribution (shown for citrate fraction) as a function of pH in a solution with c_{Al} = 250 mM and c_{Cit} = 1.00 M. The arrow points the curve corresponding to species $Al(Cit)_2^{3-}$

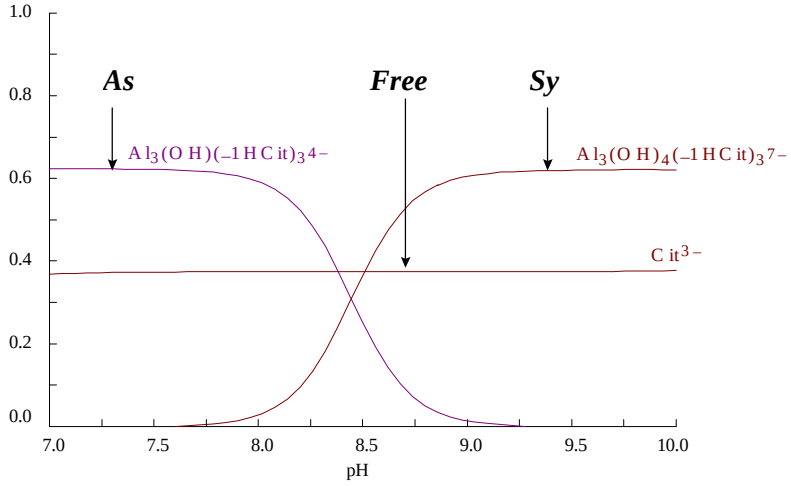

Figure IV.3.4. Concentration distribution (shown for citrate fraction) as a function of pH in a solution with c_{Al} = 500 mM and c_{Cit} = 800 mM. The arrows point curves corresponding to species *As*, *Sy* and Free citrate.

In the followings the enumerated species, free citrate, $Al(Cit_2)^{3-}$, *Sy*, and *As* will be characterized.

Assignation of species. Prior to analyzing the system, the terminology of several parts of the citrate ligand and the referred coupling constants are drawn on scheme:

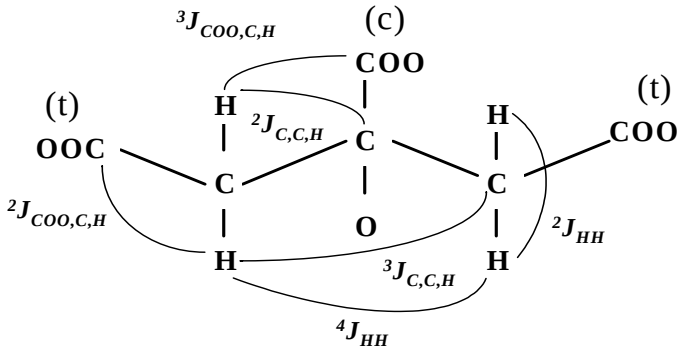

The terminal carboxyl groups are labeled as –COO(t), the central one as –COO(c). One-bond $^1J_{CH}$ exist in the $–CH_2–$ group, between a H and the C atom (not shown on figure); between the two H atoms a geminal $^2J_{HH}$ appears. Two-bond $^2J_{CH}$ are observed between the quaternary C and one H of the $-CH_2-$ group, with symbol $^2J_{C,C,H}$ and between the –COO(t) carbon and one proton of the $–CH_2–$ group, with symbol $^2J_{COO,C,H}$. Three-bond $^3J_{CH}$ couplings are present between one $–CH_2–$ carbon and one proton of the other $–CH_2–$ group, with symbol $^3J_{C,C,H}$; and between the –COO(c) carbon and the H of a $–CH_2–$ group, with symbol $^3J_{COO,C,H}$. Four-bond $^4J_{HH}$ coupling is present between one H of one $–CH_2–$ group and the H of the other $–CH_2–$ group.

It is obviuos to start the assignation with the free citrate. Both ^1H and ^{13}C spectra were recorded at different pH values. This is useful, as besides chemical shift, the coupling constants and line width values have already been determined, which vary with pH.[6] The ^1H NMR spectrum of the free citrate is an asymmetric doublet. This is expected on the basis of the Newman projection, which points out that the 2 H (*a*, *b*) atoms of a $–CH_2–$ group are magnetically unequivalent:

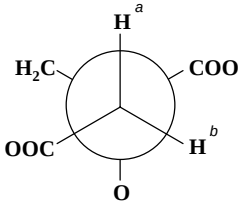

The ^{13}C NMR spectra shows 4 resonances of the six carbon atoms present in the molecule. The distribution of these is as follows: one resonance for the two $-CH_2-$ groups, which are equivalent, one peak for the quaternary carbon; one peak for the two equivalent -COO(t) groups and one for the -COO(c) group. NMR data at different pH values are collected in table IV.3.1.

Table IV.3.1. NMR data of 0.5 M free citrate solution at different pH values

pH[a]	^{1}H NMR		^{13}C NMR δ (ppm)			
	δ(ppm)	$^2J_{HH}$ (Hz)	CH_2	Cquat.	COO(t)	COO(c)
4.2	2.83 2.70	15.7	47.28	77.09	179.38	182.8
10.4	2.62 2.46	15.4	48.60	77.97	182.18	184.8

[a] at 4.2 $HCit^{2-}$ and H_2Cit^- are present in ratio 1:1, at 10.4 deprotonated Cit^{3-} is present.

$Al(Cit)_2^{3-}$. In a sample with c_{Al} = 0.25 M, c_{Cit} = 1.00 M at pH = 4.2 (prepared by mixing Al^{3+}, H_3Cit and Na_3Cit in corresponding ratio and waiting at least one day for equilibration) $HCit^{2-}$, H_2Cit^-, $AlCit_2^{3-}$ and little *As* complex is present on the basis of the equilibrium model (Figure IV.3.3.). In ^{1}H NMR spectra $HCit^{2-}/H_2Cit^-$ appear as one signal due to the fast H^+ exchange, the concentration of the *As* complex is small and signals of this species are almost negligible. The main interest is focused on detecting the signals of $AlCit_2^{3-}$. It turns out that ^{1}H NMR is unavailable for our purposes as only the asymmetric doublet of the free citrate is observed, all other signals are under it. ^{13}C NMR is suitable, besides free citrate signals the peaks of the $AlCit_2^{3-}$ complex appear as well. The assignation resulting from integration of the quantitative spectra is summarised in the following table:

Table IV.3.2. NMR data of $Al(Cit)_2^{3-}$ present in a sample with c_{Cit} = 1M, c_{Al} = 0.25M, pH = 4.2

^{13}C NMR δ (ppm)			
CH_2	C quat	COO(t)	COO(c)
~45.6 broad	77.14	179.37	185.25

From these data it is obvious, that $Al(Cit)_2^{3-}$ shows a simple spectra, very similar to that of the free citrate. Interestingly the ^{13}C chemical shift of –COO(t) coincides with that of the free citrate at pH ~ 4, whilst the position of –COO(c) is very similar to that of free citrate at pH = 10.4. A peculiarity of the spectra is, that while the signals of free citrate show their natural line width the signals of $Al(Cit)_2^{3-}$ are broader, especially in the $–CH_2–$ region. It seems that this mononuclear complex is fluxional, i.e., it has some intramolecular dynamic

processes with permuting atomic positions, which at the same time may result in chemically non–distinguishable species (see chapter IV.3.2. for details). It is certainly appearing in ^{1}H NMR as well, but due to overlapping with free citrate signals it is impossible to observe. On the basis of these spectra a tentative solution structure can be drawn, with the two citrate ligands positioned symmetrical around the octahedral Al and acting tridentate. $Al(Cit)_2^{3-}$ can be the diprotonated form of $Al(Cit)_2^{5-}$ crystallised as its NH_4^+ salt at pH ~ 8. Both ligands are coordinated to Al^+ via the deprotonated alcoxy group, the central and one terminal carboxylate group.[67] The unbound other terminal carboxylate is protonated, explaining the above mentioned chemical shift values. In conclusion the following tentative structure can be suggested:

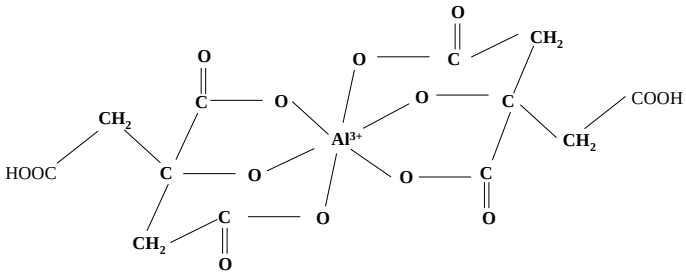

$Al_3(OH)_4(H_{-1}Cit)_3^{7-}$ (*Sy*). At pH > 8 this complex begins to form. At a ratio c_{Cit}/c_{Al} = 1 in a narrow pH region it is possible to obtain only this species. Samples where free citrate is present as well can be prepared either by addition of citrate, or by increasing the pH. The advantage of these samples is the possibility of studying intermolecular processes. The obtained NMR data are collected in table IV.3.3.

Table IV.3.3. NMR data of *Sy* present in a sample with c_{Cit} = c_{Al} = 0.46 M, pH=10.59

^{1}H NMR		^{13}C NMR							
δ_H (ppm)	$^{2}J_{HH}$ (Hz)	δ_{CH2} (ppm)	$^{1}J_{CH}$ (Hz)	$\delta_{C,\ quat}$ (ppm)	$^{2}J_{C,C,H}$ (Hz)	δ_{COO}(t) (ppm)	$^{2}J_{COO,C,H}$ (Hz)	δ_{COO}(c) (ppm)	$^{3}J_{COO,C,H}$ (Hz)
2.60	16.9	48.38	126.4	76.87	6.17	182.38	4.63	190.07	4.6
2.49					4.62		6.16		quintet

As the ^{1}H NMR spectrum consists of a single asymmetric doublet and the ^{13}C spectrum also has the simplicity of the free citrate it is obvious to assume that the three citrate ligands with all $–CH_2–$ and –COO(t) groups are equivalent. The notable difference with the signals of free citrate is that the peaks of the *Sy* complex are broad. It is understandable to assume a fluxionality of the molecule. This property will be discussed in details in chapter IV.3.2. The remarkable high field shift of –COO(c) in ^{13}C NMR is in accordance with Öhman's tentative structure having the non coordinated, deprotonated central –COO.

As far as coupling constants are concerned the $^{2}J_{C,C,H}$ and $^{2}J_{COO,C,H}$ values are the same. One can not draw hasty conclusions from these values, as it is known that that $^{2}J_{COO,C,H}$ of carboxylic acids behave irregularly. The three-bond coupling constant, $^{3}J_{COO,C,H}$, and the quintet structure from the ^{1}H coupled ^{13}C spectra obtained for the central carboxylate indicate that the four H atoms are displayed equivalently around –COO(c) carbon. Still, as the $–CH_2–$ groups have a flip flop movement, only some limit projections can be drawn, as shown on Scheme IV.3.1. *a), b).* As referred to the 16.9 Hz value of geminal H-H coupling constant the approximative orientation can be sketched by analysing diagram IV.3.1.

Altogether, it can be stated that in the *Sy* complex all three bounded citrates show a similar sterical orientation, pendulating between the limit conformations as drawn on scheme IV.3.1. *a*), *b*). IV.3.1. *c*) shows the orientation of the p_z orbital of the –COO(t) carbonyl.

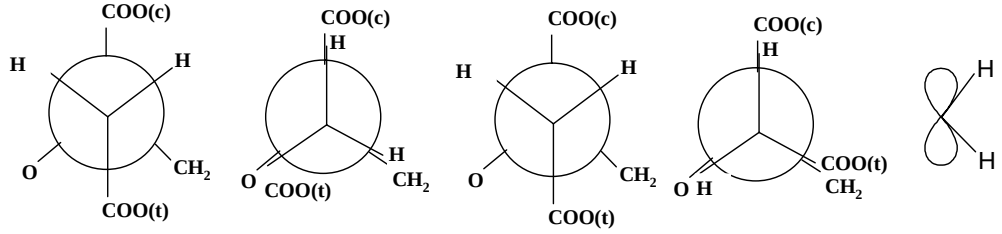

Scheme IV.3.1. Limit Newman projections for the two$–CH_2–$ *a)* , *b*) groups of one citrate in *Sy*, *a)* corresponding ϕ values for the orientation of the H atoms referred to –COO(c) (60°, 300°) and (120°, 360°); *b)* (60°, 300°) and (240°, 360°); *c*) positions of H atoms of $–CH_2–$ towards the p_z orbital of –COO(t).

$Al_3(OH)(H_{-1}Cit)_3^{4-}$ (*As*). The *As* species was prepared in solid form either as its Na^+, or NH_4^+ salt. The X ray structure shows that it is a non symmetric molecule. The question is whether this asymmetry is maintained in solution, or this structure collapses as do several Al complexes in solution? There is a good chance that spectrum analysis will give the informative $^nJ_{HH}$, $^nJ_{CH}$ values for a tentative solution structure to be obtained. One can ask why did not we use the nOe information in addition to the J coupling? Unfortunately in the vicinity of molecular mass ~1000 the nOe is not detectable. Our *As* complex has M = 859 and the recorded NOESY spectra were not able to give any information. We tried to invoke the ROESY spectra, but even that one was useless.

Sketching the assembly for this trinuclear species is a good starting point for structure elucidation. Keeping in mind the solid structure a schematic view of 3 Al and 3 citrate ligands can be drawn as follows, where to complete the octahedral geometry around one of the three Al atoms one OH and one H_2O enters the co-ordination sphere.

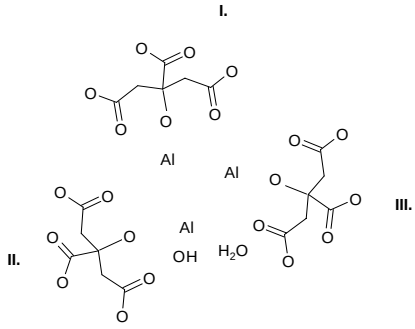

Let's start with the assignation of the NMR peaks. Dissolving the solid a very complicated pattern in the ^1H spectrum is resulted, with several overlappings, as seen on Figure IV.3.3 *a*). An association of three citrates around three aluminium atoms may result in a very ordered or disordered form. The ^1H NMR spectrum in the most complicated case is a mixture of 6 asymmetric doublets, giving 6 x 4 = 24 signals. A COSY experiment allows the neighbouring protons to be located. The appearing cross peaks represent the coupling patterns, and the values of $^2J_{HH}$ coupling constants are obtained at the same time.

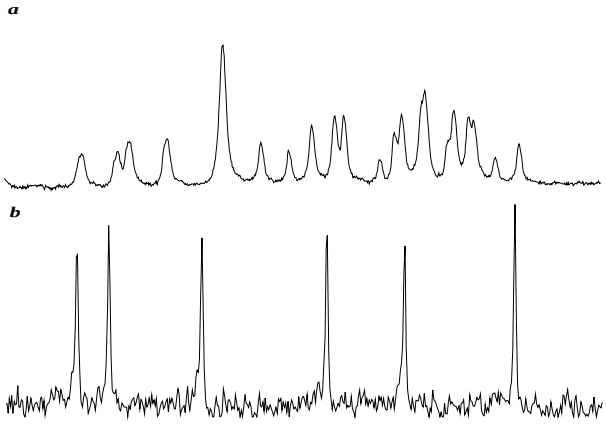

Figure IV.3.3. ***a)*** ^{1}H NMR (500 MHz) spectrum of the *As* complex with $c_{Al} = c_{cit}$ = 0.5 M at pH=7.2 and ***b)*** – CH_2 – region of the ^{13}C NMR (125 MHz) inverse gated spectrum of the same sample measured at 298 K.

As seen from Figure IV.3.4, in our case we have 5 asymmetric doublets and one singlet, marked with *1,2,3,4,5,6*. This suggests that on five – CH_2 – groups the H atoms have different environments. In the case of the sixth one they are equivalent. On the other hand between 2.80 – 2.88 ppm there are some cross peaks with low intensity, marking connectivity between one H of *1* and one H of *2* showing a $^{4}J_{HH}$ coupling. This is possible only if these H atoms belong to the two – CH_2 – groups of the same citrate, **I**.

The next step is to assign the H atoms to the corresponding carbons. A decoupled, quantitative {H}^{13}C spectrum showed that in the – CH_2 – region we have six separate resonances (Figure IV.3.3.*b*) therefore a 2D heteronuclear ^{1}H - ^{13}C correlation spectra should point out directly the corresponding protons. The result is shown on Figure IV.3.5. In this way every symbol *1,2,3,4,5,6* was assigned to the corresponding H atoms and –CH_2– carbons.

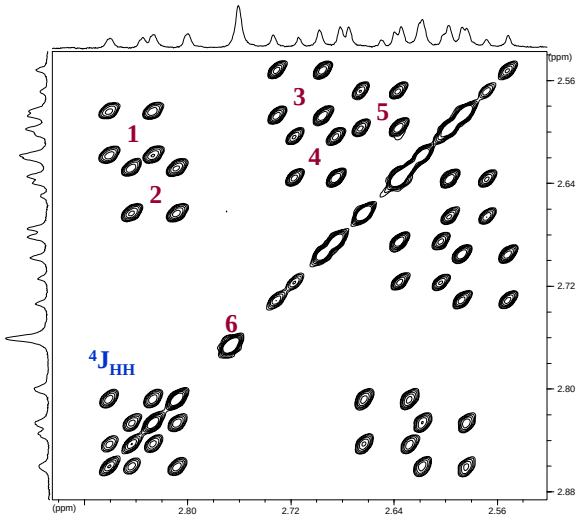

Figure IV.3.4. 500 MHz COSY 45 spectra of the *As* complex

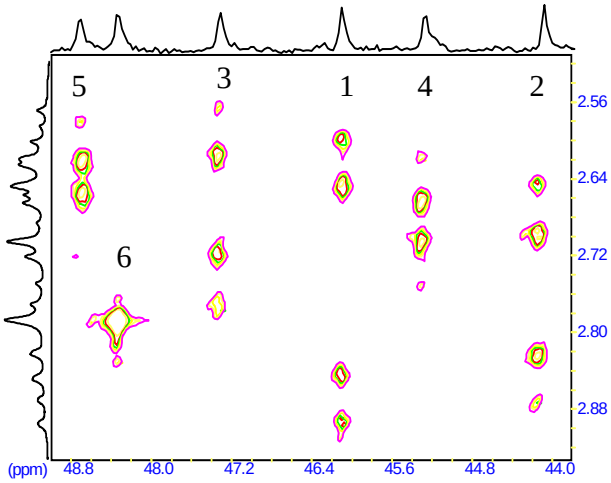

Figure IV.3.5. ^{13}C detected HETCOR (360 MHz) spectra of the *As* complex

To trace the complete framework of the molecule, one has to identify which signals belong to the same citrate. The connectivities are clarified by measuring long range heteronuclear correlation spectra, which give the 2 and 3 bond distanced H and C atoms. The most reasonable is to start the identification in the quaternary carbon range. We have 3 quaternary carbons in the molecule and by 2 bond distances they should point out those H atoms which are on the

neighbouring – CH_2 – groups and naturally on the same citrate. The result is shown on Figure IV.3.6.

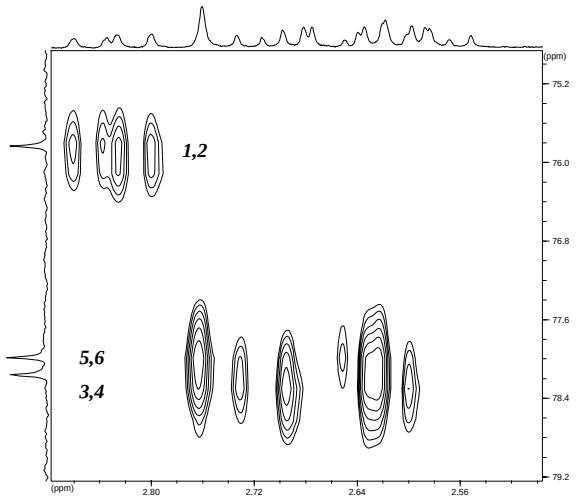

Figure IV.3.6. Gradient pulse, inverse (^{1}H) detected, long range HMQC spectra (500 MHz), with incremented delay D6 = 50 ms, corresponding to $^nJ_{CH}$ = 10 Hz of the *As* complex , zoomed for quaternary carbon region

It is not surprising that *1* and *2* belong to the same ligand **I**, confirming at the same time our previous statement from the COSY experiment. Groups *3,4* belong to **II** and *5,6* to **III**. Thus, this can be a preliminary assignation of which signals belong to which ligand.

Further, the -COO region has to be clarified. The {H}^{13}C 1D spectrum shows that there are 9 resonances, from which 6 signals belong to terminal and 3 to central -COO groups. An assignation on the basis of the LR HETCOR (Figure IV.3.7 a) spectra is not trivial as the cross peaks are overlapping. Only little help is given if the spectra are tuned for different ^nJ values.

The lowest field resonance at 185.39 ppm is the signal of the central –COO of citrate **II** with the *3* and *4* –CH_2– groups as both *3* and *4* H signals show a cross peak. The next resonance at 185.21 ppm points out only H atoms of *2*, thus being a terminal –COO of citrate **I**. Resonance at 183.28 ppm is connected to all four signals of *4*, and it is one terminal –COO of citrate **II**. The situation becomes complicated when reaching the 180.95 – 179.69 ppm region. For assignation another experiment was performed. As the *6* H peak stays a little bit further from the other signals in the ^{1}H spectrum it is possible to decouple it selectively.

Meantime a ^{1}H coupled ^{13}C spectrum is recorded and on the carbonyl region only those signals will appear as decoupled ones which are in this $–CH_2–$ group's vicinity, namely one terminal, and one central –COO. In this way resonances at 180.95 and 180.12 are pointed out. This indication leads to the conclusion that the peak at 180.95 ppm corresponds to a H *5* in the long range HETCOR. Combining these results, the signal at 180.95 ppm is the central –COO for citrate **III**, finally 180.12 ppm signal is the terminal –COO for *6*. Thus, by this technique all carbonyl signals are identified, see Figure IV.3.7 b.

a)

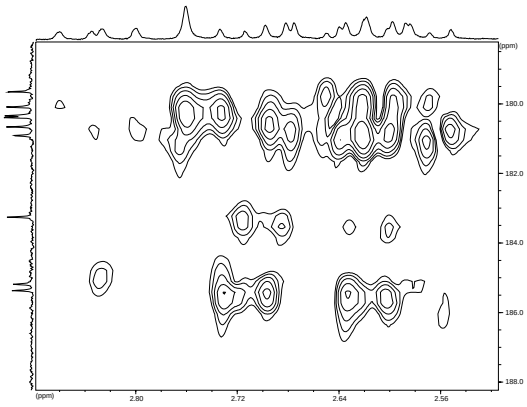

b)

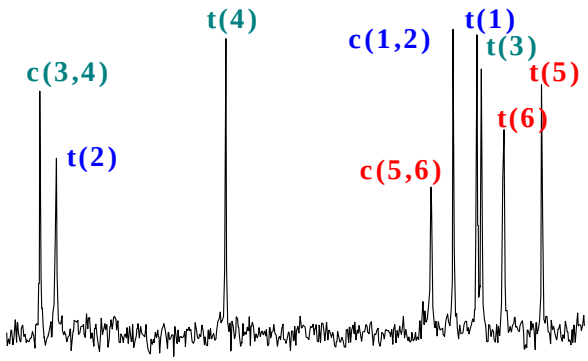

Figure IV.3.7. a) Gradient pulse, inverse (^{1}H) detected long range HMQC spectra (500 MHz) with incremented delay D6 = 200 ms, corresponding to $^{n}J_{CH}$ = 2.5 Hz of the *As* complex , zoomed for carboxyl region. **b)** ^{13}C (125 MHz) power gated spectrum of the same sample.

For obtaining the C-H coupling constants the coupled ^{13}C spectrum was recorded and it is shown on Figure IV.3.8.

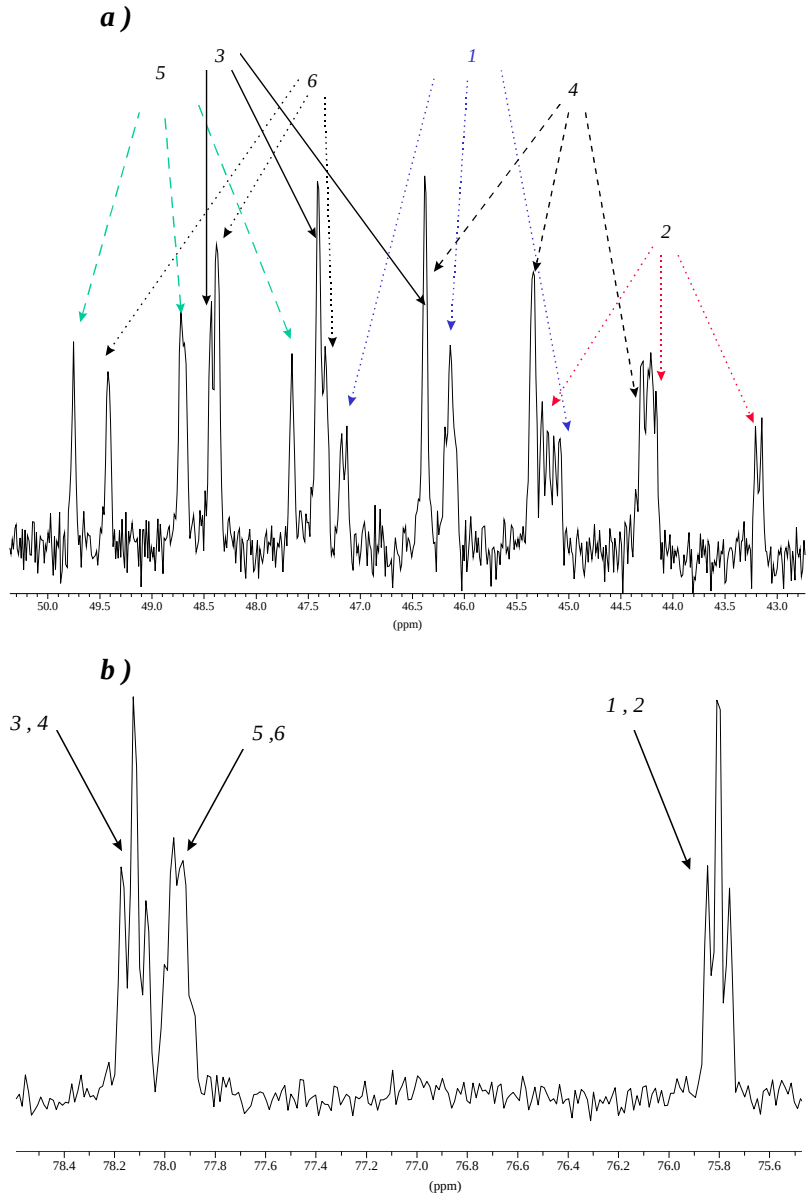

Figure IV.3.8. Coupled ^{13}C NMR (125 MHz) spectrum of a 0.8 M *As* solution at pH = 7.3; **a)** $-CH_2-$ region, **b)** quaternary C region, **c) –**COO region, indicating the assignation as well (continued on the next page).

c)

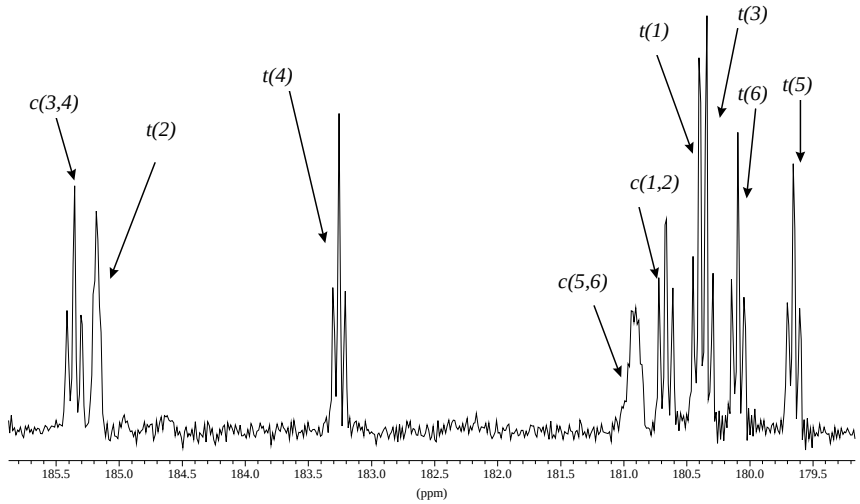

Figure IV.3.8. Coupled ^{13}C NMR (125 MHz) spectrum of a 0.8 M *As* solution at pH = 7.3; **a)** $-CH_2-$ region, **b)** quaternary C region, **c) –**COO region, indicating the assignation as well (see also previous page).

Thus, as a result of a proper use of some considerable and not quite cheap NMR time, and of a great deal of (financially non manifested) intellectual effort it is possible to give the complete assignation. In this way we solved the spectral identification of 18 C and 12 H atoms belonging to a strongly coupled system of a complicated polynuclear coordination compound.

Table IV.3.4. NMR data of the *As* complex

Citrate	Nr[a]	^{1}H			^{13}C									
		δ (ppm)	$^2J_{HH}$ (Hz)	$^4J_{HH}$ (Hz)	δ_{CH2} (ppm)	$^1J_{C,H}$ (Hz)	$^3J_{C,C,H}$ (Hz)	δ_C (ppm)	$^2J_{C,C,H}$ (Hz)	$\delta_{COO\ t}$ (ppm)	$^2J_{COO,C,H}$ (Hz)	$\delta_{COO\ c}$ (ppm)	$^3J_{COO,C,H}$ (Hz)
I	*1*	2.843 2.602	17.03	~ 2	46.19	124.85	6.16 7.71	75.85	4.62	180.43	6.16	180.69	6.17
I	*2*	2.817 2.636	17.64	~ 2	44.26	131.01	6.16 7.71	75.85	4.62	185.21	3.08	180.69	6.17
II	*3*	2.716 2.570	17.85	–	47.47	127.92	–	78.16	6.16	180.37	6.17	185.39	7.71 6.16-7.71
II	*4*	2.698 2.618	16.41	–	45.39	131.01	–	78.16	6.16	183.28	6.16	185.39	7.71 6.16-7.71
III	*5*	2.658 2.584	14.56	–	48.75	131.47	–	77.99	4.62	179.69	6.16	180.95	3.08
III	*6*	2.761	–	–	48.43	131.01	–	77.99	4.62	180.12	6.16	180.95	3.08

[a] Nr. represents the symbols used for the six $–CH_2–$ groups, see text.

In the followings each bounded citrate will be discussed separately, considering the informations from Table IV.3.4. and Figures IV.3.1. and IV.3.2.

Citrate I. The presence of the $^4J_{HH}$ coupling constant suggests a W disposition as shown on Figure IV.3.9. *a*).

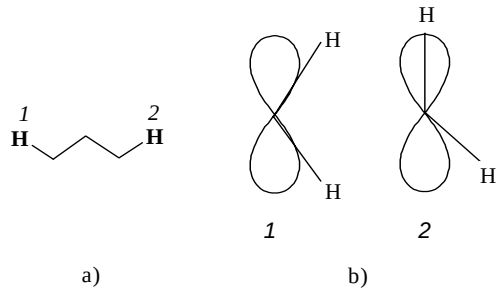

Figure IV.3.9. Structural arrangement of citrate **I.** ***a)*** W disposition of two H atoms *1, 2*; ***b)*** positions of H atoms with respect to the p_z orbital of –COO(t) group.

On the other hand, according to Figure IV.3.8. *a*) the coupling pattern for $–CH_2–$ *1* is a 'triplet' with $^1J_{CH}$ = 124.85 Hz. It is probably not a real triplet, but rather a combination of two doublets with very similar coupling constants, originating from the two non equivalent protons attached to the carbon atom at one bond distance. This is supported also by the fact that the central signal appears to be broader than the two smaller peaks. These latter ones are splitted in doublets with couplings of 6.16 and 7.72 Hz, respectively. The central signal is splitted to a pseudo triplet with couplings of 6.16 Hz at one side and 7.72 Hz at the other side. This coupling pattern is a consequence of measurable long range coupling to one H *2* proton. The same pseudo triplet pattern is obtained when measurable $^3J_{COO,C,H}$ coupling appears (see Figure IV.3.8c).

Now, taking into account the W arrangement we can draw four pairs of orientations A, B, C, D (two in each case because the orientation of both H–C–C(quaternary)–C units in the citrate has to be considered). It is obvious, that all these possibilities give raise to an above described coupling pattern in the $–CH_2–$ region. The table under the pictures contains the coupling constants for each case. Each box contains the coupling constants for the left hand conformation in the first line, while those in the second line are the values for the right hand conformation, according to Figure IV.3.2.

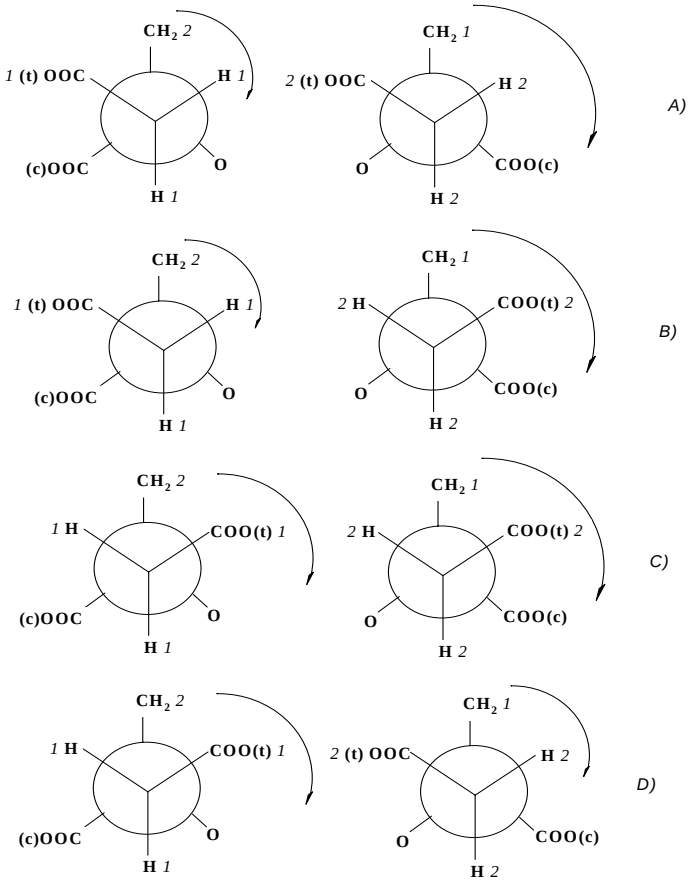

Possibility	Angle referred to –CH_2–	$^3J_{C,C,H}$ (Hz)	Angle referred to –COO (c)	$^3J_{COO,C,H}$ (Hz)
A	(60, 180) (60, 180)	(2, 7) (2, 7)	(180, 300) (60, 300)	(7, 2) (2, 2)
B	**(60, 180)** **(180, 300)**	**(2, 7)** **(7, 2)**	**(180, 300)** **(60, 180)**	**(7, 2)** **(2, 7)**
C	(180, 300) (180, 300)	(7, 2) (7, 2)	(60, 300) (60, 180)	(2, 2) (2, 7)
D	(180, 300) (60, 180)	(7, 2) (2, 7)	(60, 300) (60, 180)	(2, 2) (2, 7)
measured value		6.16 7.71		6.17 6.17

Figure IV.3.10. Possible Newman orientations for the W arrangement of the H atoms. The table includes the corresponding angles and coupling constants and the measured coupling constant values, respectively.

It is easy to deduce that while all eight conformers satisfy the coupling pattern in the $–CH_2–$ region, only case B) satisfies the requirement for central –COO coupling pattern as well.

Finally, the orientation of the H atoms towards the terminal –COO has to be clarified on the basis of $^2J_{HH}$ data. Analysing Figure IV.3.1. the values of 17.03 and 17.64 indicate the orientation for H *1* atoms at ~ 0° and for H *2* atoms at ~ ±30° angle from the p_z orbital, as perceived generally on figure IV.3.9.*b*).

Citrate II. In the absence of observable $^3J_{C,C,H}$ coupling an arrangement of (60°, 300°) for *3,4* methylene H atoms is supposed, as this orientation yields a hardly detectable constant, $^3J_{C,C,H}$ < 2 Hz (see Figure IV.3.11.*a*). In this case with respect to the –COO(c) group H *3* atoms will possess a (180°, 300°) and H *4* atoms a (60°, 180°) position. This will end up in ^3J values ~7, and < 2 Hz for H *3*; and in < 2 and ~ 7 Hz for H *4*. Following the argumentation presented for citrate **I** a pseudo–triplet is expected for –COO(c) (*3,4*). This pattern appears indeed at 185.39 ppm (see Figure IV.3.8.*c*). The orientation of the geminal H atoms for $^2J_{HH}$ values of 17.85 and 16.41 is ~ ±25° for H *3* and ~ ±15° angle for H *4* from the p_z orbital of –COO(t). Concluding these findings citrate **II** looks like:

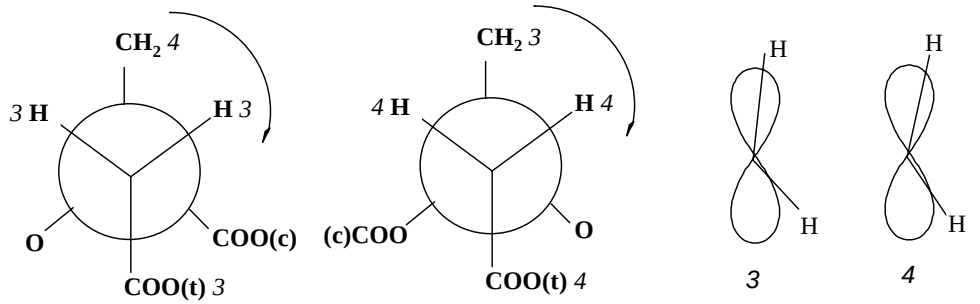

a) b)

Figure IV.3.11. Structural arrangement of citrate **II.** ***a)*** Newman projection with ~ (60°, 300°) and ~ (60°, 300°) orientations of H *3, 4* atoms; ***b)*** positions of H *3, 4* atoms with respect to the p_z orbital of –COO(t).

Citrate III. With no detectable $^3J_{C,C,H}$ an analogous situation with citrate **II** is met. The difference here is the appearance of two almost equivalent H atoms in the case of H *6*. This will result in a multiple splitting of –COO(c), first in a triplet, than

from one H *5* each resonance will split in a doublet. This pattern is really present at 180.95 ppm. (see Figure IV.3.8c.)

The geminal $^2J_{HH}$ coupling for H *5* is smaller than those values found at *1,2,3,4*. The orientation of the H atoms for the value of 14.56 is a symmetric one around the p_z orbital (see figure IV.3.12.*b*) Thus, the sterical arrangement of the third bounded citrate is:

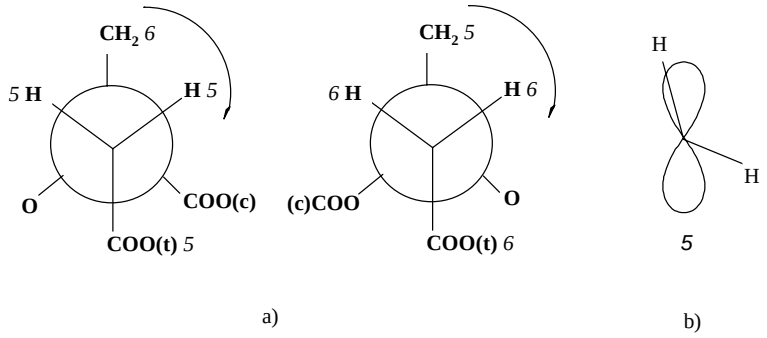

Figure IV.3.12. Structural arrangement of citrate **III**. *a*) Newman projection with ~ (60°, 300°) and ~ (60°, 300°) orientations of H *5*, *6* atoms; *b*) positions of H atoms with respect to the p_z orbital of –COO(t) group for H *5*.

The values of one-bond couplings were left out from this discussion. It is useful to analyse them together. The value of 127.92 Hz for *3* from citrate **II** is the same as the value obtained for free citrate. Thus, in this $–CH_2–$ group the bond orientations for the C atom are the same as those in free citrate. For other $–CH_2–$ groups there is a distorsion of bond orientation from this position.

Now we are at a point that we possess a remarkable amount of different torsion angles. These help us to build up the fragments of the molecule, i.e. the three coordinating citrate ligands. On the other hand using X ray data we can draw the stick model of the solid state structure of *As*, shown on Figure IV.3.13. Analysing our solution structure results, those fragments are unambiguously recognised and identified on the solid structure. Here we can state safely that the two structures are very similar. Hydratation plays some role: the C backbone of citrate **I** is distorted from a perfect W conformation in solid state, but this shape becomes more emphasised in solution. In Figure IV.3.13. the fragments of citrate **I**, **II** and **III** characterised by solution NMR are recognised; moreover, the identification of the separate *1*, *2*, *3*, *4*, *5* and *6* $–CH_2–$ groups is done.

As a final argument one can state that in the case of such a polynuclear assembly it is possible to trace the framework of the molecule on the basis of informations obtained from NMR measurements.

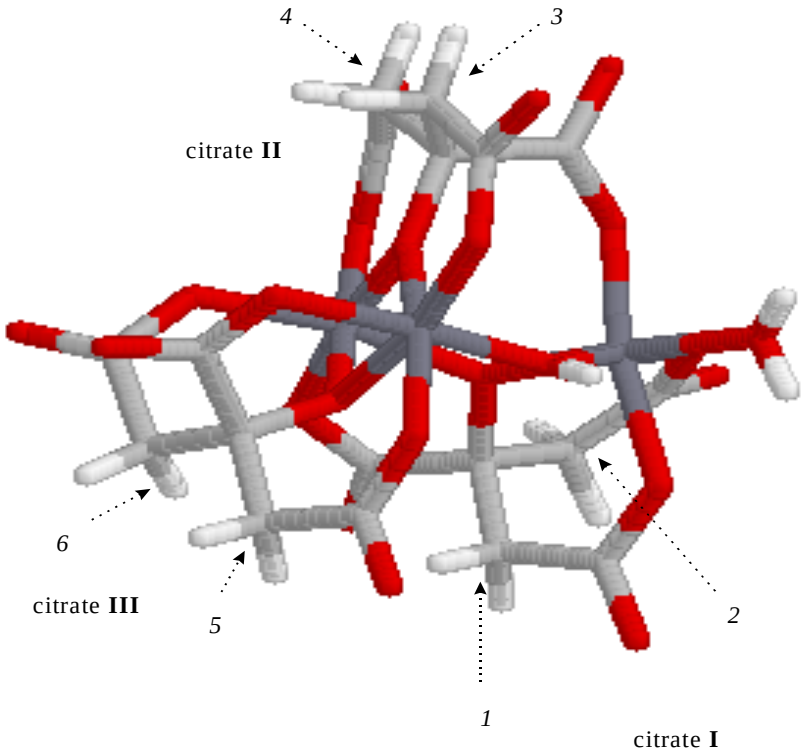

Figure IV.3.13. The solid structure of *As* calculated from X ray data and presented using the sticks model of the RasMol molecule drawing software package. The solution structure is almost identical to this one. Figures *1,2,3,4,5,6* indicate the corresponding $–CH_2–$ groups. The central Al atoms are dark grey, and the H atoms are light grey.

IV.3.2. Dynamics

In this part the kinetic behaviour of the structurally characterized species, $Al(Cit)_2^{3-}$, *Sy*, *As* is presented. We discuss the *intra*- and *inter*-molecular exchange reactions starting from the acidic region of the system following with the alkaline region.

$Al_3(OH)(H_{-1}Cit)_3^{4-}$ (*As*). The *As* complex is the major species in a wide range of pH ≈ 3-8 at total aluminum concentration $c_{Al} \geq 1$ mM at ratio $c_{Al}/c_{Cit} \geq 1$. Both ^1H and ^{13}C NMR signals of *As* are narrow (LW ≤ 2 Hz) in the whole pH region in accordance with earlier findings.[68] A variable temperature study showed that this line width is invariant up to 80 °C in solutions prepared either from Na^+ or from NH_4^+ salts of the complex. These experimental findings state that intra–molecular exchange does not happen on the actual NMR time scale between the three non–equivalent citrate ligands of *As*. It is easy to visualise this on the ^{13}C NMR spectra, where all resonances are separated. If one considers 1 Hz as a measurable line broadening, than in accordance with the above presented results the exchange broadening is absent here. Still, if exchange exists, than this broadening must be LB ≤ 1 Hz. This means that $k_{obs} = LB \cdot \pi \leq 3\ s^{-1}$ and the average life time at a given site is $\tau = 1/k_{obs} \geq 0.3$ s for all the three different citrate sites of *As*. Thus, T_2 spectroscopy gave only this limit value, but the longitudinal T_1 relaxation time scale provides a tool to follow slower processes by using magnetisation transfer technique.

T_1 values for the free citrate ligand are ranging 2-6 s, being smaller for the $-CH_2-$ and larger for the other carbons of citrate. Experiments were done inverting selectively one of the 9 carbonyl signals of *As*. Step by step each peak was inverted. No magnetisation transfer (MT) could be detected up to 80 °C. Again, even on this time scale, only a limiting value for $k_{obs} \leq 0.03\ s^{-1}$ and $\tau \geq 3\text{-}5\ T_1 \approx 30$ s can be calculated for the *intra*-molecular exchange reactions between the three different citrate sites of *As.* All these data prove that there is no fluxional site-exchange in *As* within about 30 s.

This kind of inertness of the μ_2 and μ_3 tetradentate bridging ligands of *As*, or in other words, its non–fluxional behaviour does not mean *a priori* a same inertness of one of the three ligands against *inter*-molecular exchange with a free ligand. However a ^{13}C NMR MT experiment at 80 °C using a sample prepared by adding excess citrate to the solution of *As* (c_{As}=0.30, c_{cit}= 0.10 at pH = 4.0)

showed, that this *inter*-molecular exchange was also unmeasurably slow, $k^{obs}_{As,Free} \leq 0.03\ s^{-1}$. It is important to mention, that this system was in metastable state during the experiment (about 6 hours), but no measurable transformation of *As* to $Al(Cit)_2^{3-}$ was observed. However, after one week the measured ^{13}C spectra showed the formation of some $Al(Cit)_2^{3-}$. This inertness in aqueous solution is in accordance with earlier studies for $Al(acac)_3$ in organic solvents (having $k^{inter} = 10^{-5} - 10^{-6}\ s^{-1}$ rate constants at room temperatures,[109] see also Table IV.3.7.). The reality of any comparison is very much limited here by the different denticity of the ligands and the different polarities of the solvents. Moreover, bearing in mind the very asymmetric structure of *As* both in solution and solid state these results are not surprising.

$Al(Cit)_2^{3-}$. As stated before, the formation of the $Al(Cit)_2^{3-}$ complex is preferred at large excess of citrate over Al^{3+} at pH ≈ 4. There was already mentioned that the signals of this complex are broadened at room temperature. This broadening is a consequence of exchange reactions and temperature variation may result in varying the corresponding line width values. Recording the spectra at different temperatures the following data were obtained:

Table IV.3.5. ^{13}C NMR data of a solution with $c_{Al} = 0.25$ M, $c_{Cit} = 1.0$ M at pH = 4.3 at different temperatures. Missing values are due to the fact, that the spectra were not recorded in the respective region.

Temp (K)	Free citrate		$Al(Cit)_2^{3-}$		k_{02}^{obs} (s^{-1})
	δ (ppm)	LW (Hz)	δ (ppm)	LW (Hz)	
298	COO(c) 182.8	1.01	COO(c) 185.22	13.8	
	COO(t) 179.4	1.12	COO(t) 179.52	10.1	1.1 ± 0.9[a]
	C(q) 77.1	1.59	C(q) 77.24	3.7	
	CH_2 47.28	1.45	CH_2 45	~ 150	
323	C(q) 77.41	1.56	C(q) 77.65	1.9	2.6 ± 0.4[a]
348	COO(c) 183.0	5.05	COO(c) 185.35	6.0	
	COO(t) 179.8	4.30	COO(t) 180.05	6.5	14.5 ± 0.3[a]
	C(q) 77.58	4.83	C(q) 77.86	5.5	(12 ± 3)[b]
	CH_2 48.00	15.62	CH_2 45.66	23.6	

[a] from MT measurements; [b] from line broadening calculation using the data from this table

***Intra*–molecular exchange.** It is obvious from the above presented figures that at room temperature the free citrate signals show their natural line width while the peaks of the complex are broad. This is a certain indication that the reaction responsible for broadening is an intra–molecular exchange. There might be conformers of the complex in solution.[69] Gregor and Powell have not specified the structures of these conformers, they might differ in their chelate ring conformations, similar as discussed below for *Sy* in some details. A more plausible explanation can be based on the fluxional site exchange of the $Al(Cit)_2^{3-}$. Simultaneous exchange between the coordinated and the unbounded, protonated terminal carboxylate groups of both citrate ligands (see chapter IV.3.1.) results in identical structures. If the rate of the fluxional rearrangement is fast enough, only one signal of the non equivalent terminal carboxylates and methylene groups can be observed, which are in fact broadened.[67] A closer look at the data of Table IV.3.5. shows that the broadenings of the different peaks are different, in accordance with the structure of $Al(Cit)_2^{3-}$. The smallest broadening of the quaternary carbon atom indicates, that the position of these atoms in $Al(Cit)_2^{3-}$ is very similar during the rearrangement. In contrary, the –COO and especially the $–CH_2–$ groups (with LW = 150 Hz) have somewhat different environments, i.e. different chemical shifts. The line broadening values of the time averaged signals depend among others on the chemical shift difference between the exchange sites,[110] so the exchange broadening can be different for different atoms of the ligand involved in the same exchange process.

***Inter*–molecular exchange.** $Al(Cit)_2^{3-}$ is fluxional in solution, but what about the exchange with free citrate? T_2 spectroscopy indicates inter–molecular exchange only at 348 K, see for example the LW for free citrate in Table IV.3.5.. Therefore, we turn to the longitudinal time scale. In the sample discussed already in Table IV.3.5. both bounded and free citrates exist, which make possible the analysis of inter–molecular processes:

$$Al(Cit)_2^{3-} + {}^*Cit \underset{k_{0,2}}{\overset{k_{2,0}}{\rightleftharpoons}} Al(Cit)({}^*Cit)^{3-} + Cit$$

where $k_{2,0}$ is the rate constant for the exchange from $Al(Cit)_2^{3-}$ to free Cit, and $k_{0,2}$ is the constant referring to exchange from the free citrate to the complex. As at this pH citrate is present in protonated forms, charges are omitted for clarity.

Magnetisation transfer experiments were done in the quaternary carbon range as other peaks were too broad. In this way inverting the free citrate signal (77.09 ppm) only a small decrease in the intensity of $Al(Cit)_2^{3-}$ (77.14 ppm) appears at a delay time of ~0.5 s after inversion at 298 K. This exchange is speeded up with temperature, so at 348 K negative magnetisation is transferred already at 0.06 s duration. Integration of the resonances at each delay time give a plot similar to that from Figure IV.3.12. The measured points are fitted in MATLAB for evaluating the pseudo first order rate constants. Calculated k_{02}^{obs} values figure in the last column of Table IV.3.5. The value from line broadening comes from relation $k_{obs} = LB \cdot \pi$. As this species is present in detectable amount only in a narrow pH range at large excess of free citrate it is impossible to measure the H^+ concentration dependence in order to determine the rate equation; but it is possible to consider some routes for the ligand exchange reaction.

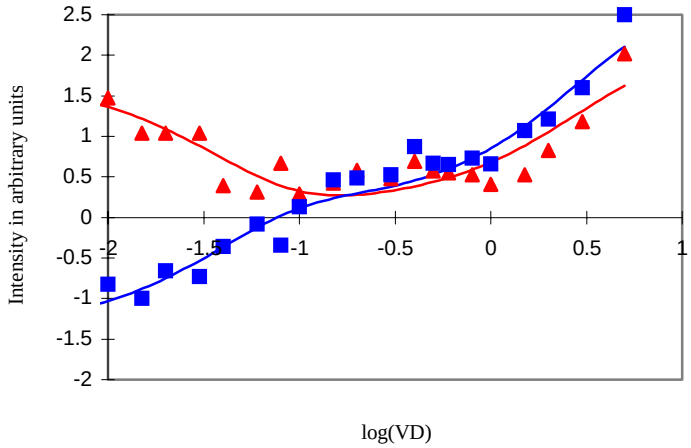

Figure IV.3.12. Intensity in arbitrary units vs. logarithm of the variable delay time in a sample of c_{Al} = 0.25 M, c_{Cit} = 1.0 M at pH = 4.3 at 348 K. Free citrate signal (■) was inverted, and negative magnetisation was transferred to $Al(Cit_2)^{3-}$ (⬧). Continuous line represents fitted curve, while symbols correspond to measured values.

Comparing the k_{02}^{obs} = 14.5 s^{-1} measured at 348 K with the upper limit of the same constant k_{obs} = 0.03 s^{-1} measured at 353 K for the *As* complex, the difference is at least three orders of magnitude. It is not surprising that the tridentate non-bridging citrate ligands of $Al(Cit)_2^{3-}$ are much more labile against

ligand exchange compared to μ_2 and μ_3 tetradentate bridging ligands of *As.* Moreover, the increase in lability for $Al(Cit)_2^{3-}$ is even more, about six – seven orders of magnitude higher compared to that of $Al(acac)_3$ (see Table IV.3.7.). Knowing the bidentate nature of acac in $Al(acac)_3$, the much larger lability of the tridentate citrate must be related to the large polarity of water in our case compared to Hacac or tetrahydrofurane (THF) solvents used for $Al(acac)_3$.[109]

The activation parameters of the inter–molecular exchange can be roughly estimated using the measured three points. Inverting the free citrate signal the rate equation has to be:

$$v = k_{02}^{obs} \cdot [Cit] \qquad \text{(IV.3.3.)}$$

and the complete form is:

$$v = k_{02} \cdot [Al(Cit)_2^{3-}] \cdot [Cit]^x \qquad \text{(IV.3.4.)}$$

the pseudo first order rate constant is:

$$k_{02}{}^{obs} = k_{02} \cdot [Al(Cit)_2^{3-}] \cdot [Cit]^{(x-1)} \qquad \text{(IV.3.5.)}$$

where k_{02} is the real rate constant and x is the reaction order of Cit^{2-}, with possible values of 0 and 1 in this case. On the other hand the dependence of pseudo–order rate constant from temperature is expounded by the Eyring relation as:

$$k_{02}^{obs} = \frac{k_B \cdot T}{h} \cdot e^{\Delta S^{\neq}/R} \cdot e^{-\Delta H^{\neq}/(R \cdot T)} \cdot [Al(Cit)_2^{3-}] \cdot [Cit]^{(x-1)} \qquad \text{(IV.3.6.)}$$

where k_B is the Boltzmann constant, h is the Planck constant, R is the universal constant for gases. Divison of equation IV.3.6. by T and taking the natural logarithm of the expression the following relation is obtained:

$$\ln \frac{k_{02}^{obs}}{T} = \ln \frac{k_B}{h} + \frac{\Delta S^{\neq}}{R} + \ln[Al(Cit)_2^{3-}] + (x-1) \cdot \ln[Cit] - \frac{\Delta H^{\neq}}{R \cdot T} \qquad \text{(IV.3.7.)}$$

Representing graphically $\ln \frac{k_{02}^{obs}}{T}$ as a function of $\frac{1}{T}$ the value of $\Delta H^{\neq}$ is calculated from the slope, while the intercept gives the value for $\Delta S^{\neq}$, if the corresponding x and concentration of $Al(Cit)_2^{3-}$ and Cit (obtained from the ^{13}C NMR spectra) values are substituted. The result is ΔH^* = 43 ± 1 kJ mol^{-1} and ΔS^* = –96 ± 29 J mol^{-1} K^{-1} for x=0 and ΔS^* = –90 ± 29 J mol^{-1} K^{-1} for x = 1. One has to treat these numerical values with precaution. Although the estimation of ΔS^* may have large error because of the only three data points and because of the far extrapolation of 1/T to zero; still, it means a definite loss of entropy during the formation of transition state, irrespective if x = 0, or 1 is set.

x = 0 means, that the rate is independent of the free citrate concentration and a dissociative mechanism could be operative. Furthermore, with x = 0 a so called water assisted I_a mechanism can also be imagined. Both are contradicted by the obtained loss of entropy and the relatively small ΔH^*. Although there is not enough information to decide equivocally, these activation parameters may support a mechanism with associative character, probably an I_a in this aqueous solution, with x = 1. The same mechanism was proposed by Saito and Nagasawa for the inter-molecular ligand exchange reaction of $Al(acac)_3$ in organic solvents, where the activation parameters were ΔH^* = 85 kJ mol^{-1} and ΔS^* = –38 J mol^{-1} K^{-1}, ΔV^* = +10 cm^3.[109]

$Al_3(OH)_4(H_{-1}Cit)_3^{7-}$ (*Sy*). Increasing the pH in the Al^{3+} – citrate system the trinuclear complex *As* can be transformed into an other trimer, $Al_3(OH)_4(H_{-1}Cit)_3^{7-}$ (*Sy*). The reaction was found to be very slow, the equilibration might take one week.[72] The slowness of this reaction, which was found by us also using NMR, can be attributed to a major change in the structure, as shown already at the structure elucidation.

***Intra*-molecular exchange.** ^1H and ^{13}C NMR signals of *Sy* were found to be substantially broadened compared to that of other species, i.e. *As* and/or free citrate, coexisting in the equilibrium system. This kind of broadening can be attributed to an *intra*-molecular rearrangement of *Sy*, similarly to $Al(Cit)_2^{3-}$ mentioned above. This dynamic system was studied by ^1H NMR.

A temperature dependence study has been performed in a sample with c_{Al} = c_{Cit} = 0.23 M at pH=10.7. The ^1H NMR spectrum of this solution consists of the asymmetric doublets of free citrate and *Sy* complex. A small quantity of $Al(OH)_4^-$ is also present under these circumstances, but it is not detectable by ^1H or by ^{27}Al NMR. Let's assume that the broadening of the *Sy* signals is caused by the rearrangement between two limit conformations of the molecule: *Sy(A)* and *Sy(B)*, both showing an asymmetric doublet. Furthermore, the inter–molecular ligand exchange between *Sy* and free citrate is expected to occur as well. Thus, for performing a simulation of the spectra at different temperatures a 12 site system has to be considered. Two pseudo first order rate constants were introduced: k_{03}^{obs} for inter-molecular exchange, and k_{intra}^{obs} for intra-molecular exchange. Schematically these processes can be represented as in Scheme IV.3.13.

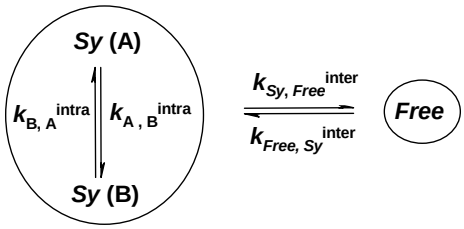

Scheme IV.3.13.

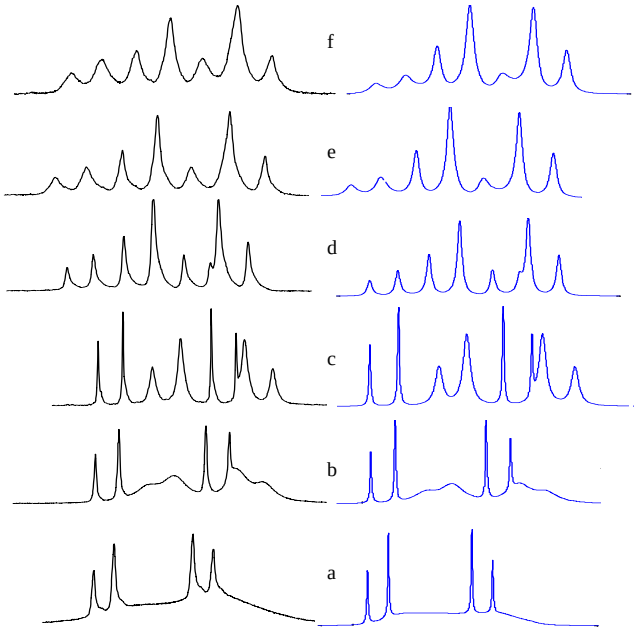

Figure IV.3.13. Recorded (left) and simulated (right) ^{1}H NMR spectra of a solution with $c_{Al} = c_{Cit} = 0.23$ M at pH=10.7 at different temperatures: (a) 285 K, (b) 298 K, (c) 315 K, (d) 325 K, (e) 345 K, (f) 355 K.

Analysing first qualitatively the spectra from figure IV.3.13., one can see that at T ≤ 315 K the signals of free citrate show their natural line width of ~ 1 Hz. So, up to this temperature only the intra–molecular exchange is operative. The two forms of *Sy* are in fast exchange regime at 315 K and lowering the temperature to 298 K a broadening, and then a coalescence situation is attained at 285 K. The separation of the two forms into two asymmetric doublets was hardly detectable, as the solution was frozen at lower temperatures. Although this splitting was possible to observe on another sample at 273 K. From this spectrum the chemical shifts of *Sy(A)* and *Sy(B)* could be determined. On the other hand the variation of

chemical shift is linear with temperature. These two informations helped to calculate the positions of *Sy(A)* and *Sy(B)* at each temperature. Populations of *Sy(A)* and *Sy(B)* were set as equal. The values of rate constants had to be varied for obtaining simulated spectra with the same parameters as those of the measured spectra (intensity, line width). Data are collected in Table IV.3.6.

Table IV.3.6. Pseudo first order rate constant values obtained for intra– and inter–molecular exchange reactions of *Sy* at different temperatures, and the corresponding measured line broadenings.

Temp.(K)	k_{intra}^{obs} (s^{-1})	k_{03}^{obs} (s^{-1})	LB(free citrate) (Hz)	LB (*Sy*) (Hz)
273	–	0	1.1	–[a]
285	80	0	1.1	–[a]
298	200	0	1.1	–[a]
315	822	0	1.1	4.7
325	2800	1.1	3.1	3.1
345	15000	2.7	6.0	4.1
355	15000	3.7	7.0	5.2

[a] Missing values are due to the fact that the correct broadenings are impossible to give at those temperatures, the system being at coalescence.

Increasing the temperature the fast exchange regime for the intra-molecular exchange is reached and the averaged signals narrow. Above 315 K, besides this rearrangement the exchange between the bounded and free citrate is launched, and a value for $k_{03}^{obs} \neq 0$ can be fitted. As a consequence, a broadening appears on the free citrate signals, and this exchange results in a broadening on the *Sy* signals, too. At 355 K the fitted value for k_{intra}^{obs} is the same as at 345 K, indicating that the intra–molecular exchange became too fast to be observed. The line width at 355 K is determined by the inter-molecular exchange, with $k_{03}^{obs} = 1.1 \cdot 10^{1}\ s^{-1}$.

The values of the rate constants at different temperatures can be used for calculation of the activation parameters using $\ln(k/T)$ vs. $1/T$ graph. In the case of k_{intra}^{obs} the activation parameters are: $\Delta H^{*} = 70 \pm 5$ kJ mol^{-1} and $\Delta S^{*} = 34 \pm 15$ J $mol^{-1}\ K^{-1}$. Taking into account the good linearity and the fact that these data were based on measurements spanning as wide range as $\Delta T = 80$ K, these values can surely be trusted. The obtained value of ΔS^{*} does not differ greatly from zero, as it is normal for a pure *intra*–molecular exchange process. Energy barriers of fluxional processes are preferably expressed as ΔG^{*}. The obtained value at 300 K

is ΔG^* = 59.4 kJ mol^{-1}. This is slightly over the middle of the wide range, ΔG^*= 5 – 100 kJ mol^{-1}, stated in the literature[103] for fluxional rearrangements. It is difficult to rationalise this rearrangement, because we do not know the structure of the conformers, *A* and *B* in details. Several conformers of *Sy* can be drawn which are different in the conformation of the possible 6 chelate rings. As we discussed in chapter IV.3.1. the two – CH_2 – groups of one citrate in *Sy* could have two different limit conformations. The splitting of the signals to two asymmetric doublets with equal intensity at low temperatures suggests, that the two – CH_2 – groups become non equivalent. *Sy(A)* and *Sy(B)* are identical, the exchange is a fluxional rearrangement which consists of the simultaneous change in conformation of the – CH_2 – groups of all three ligands. Detailed study of the symmetry is out of the scope of this work. Similar values, ΔH^* = 114 kJ mol^{-1} and ΔS^* = 68 J mol^{-1} K^{-1} were published for fluxional site exchange of Al(tfac)$_3$ (tfac = trifluor-acetylacetonate)[111] in $CDCl_3$, see Table IV.3.7. The relatively large ΔG^* in our case might suggest that this stereochemical rearrangement is going via a bond – rupture mechanism, as it was proposed also for mixed Al^{3+}-β-diketonate complexes, in which one Al^{3+}–oxygen bond (of three) reptures to give a five-coordinate intermediates.[112] We believe, that the hydroxyl oxygens acting as anchor donors remain coordinated, whilst one of the terminal carboxylate oxygens leaves the coordination sphere of Al^{3+}.

One can expect a similar rearrangement mechanisms for the Al(cit)$_2^{3-}$ discussed above. In the contrary, there is no fluxionality and or stereochemical rearrangement for *As* having tetradentate bridging ligands. A same rupture of one Al^{3+}–oxygen bond might happen in that complex also, but it does not give "enough freedom" to the citrate carbon-backbone to change its conformation.

***Inter*-molecular ligand exchange.** The inter–molecular exchange has already been discussed briefly when talking about analysis of ^{1}H spectra. Thus, we evaluated this process starting with temperature dependence by performing a band shape analysis. Still, we would like to give a rate equation. In this way the concentration and pH dependencies were studied. In order to detect slow exchange processes the aforementioned magnetisation transfer technique was used applying ^{13}C NMR. The exchange reaction is:

$$Al_3(H_{-1}Cit)_3(OH)_4^{7-} + {}^*Cit^{3-} \underset{k_{0,3}}{\overset{k_{3,0}}{\rightleftharpoons}} Al_3(H_{-1}Cit)_2({}^*H_{-1}Cit)(OH)_4^{7-} + Cit^{3-}$$

where $k_{3,0}$ is the rate constant for the exchange from *Sy* to free Cit^{3-}, and $k_{0,3}$ is the constant referring to exchange from the free citrate to the complex.

On a sample with c_{Al} = 0.80 M, c_{cit} = 1.38 M at pH = 7.8 and T = 298 K where species *As*, *Sy* and free citrate are present MT experiment was performed. Typical results are shown on Figure IV.3.15.

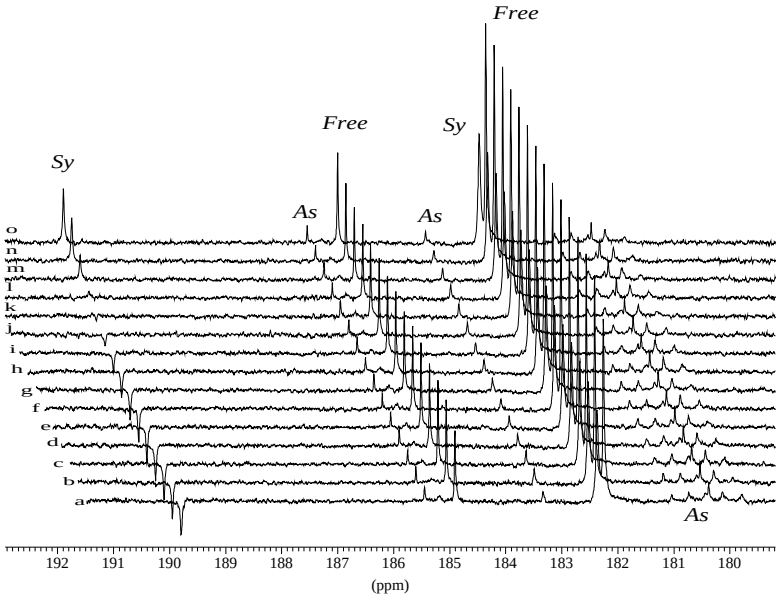

Figure IV.3.15. ^{13}C NMR serial plot, –COO region, in a sample with c_{Al} = 0.80M, c_{cit} = 1.38M at pH = 7.8 and T = 298K. The variable delays were set as: (a) 0.001s, (b) 0.005 s, (c) 0.01 s, (d) 0.05 s, (e) 0.1 s, (f) 0.2 s, (g) 0.4 s, (h) 0.6 s, (i) 1.0 s, (j) 1.5 s, (k) 2.0 s, (l) 3.0 s, (m) 5.0 s, (n) 10.0 s, (o) 20.0 s. The –COO(c) peak of *Sy* was inverted, using a DANTE pulse train.

The –COO(c) signal of *Sy* at 189.07 ppm was selectively inverted. If exchange takes place, than one –COO(c) peak, either corresponding to *As*, or of free citrate has to 'answer'. Indeed, an almost unobservable, very small inversion of negative magnetisation was transferred to the free citrate resonance at 184.8 ppm at a delay time around 3 s, see spectra k–m on Figure IV.3.15. One has to note that no MT was observed to any of the three –COO(c) of the *As* at 185.39, 180.69 or 180.95 ppm. This experimental finding was expected reminding that there was

no magnetisation transfer between *As* and free ligand up to 80 °C, and the time of transformation of *As* to *Sy* was well over the time scale of the MT experiment.

The *inter*-molecular exchange between *Sy* and *Free* was studied further as a function of c_{cit}, c_{Al} and $[H^+]$. Citrate and aluminium concentrations did not influence the exchange rate. The lack of contribution of a bimolecular reaction between the -7 charged *Sy* and the –3 charged free citrate was not a surprise, because of a large electrostatic repulsion between the reactants, and the quite saturated coordinated sphere of the Al^{3+} centers in *Sy*.

Even though variation of k_{obs}^{inter} with pH was clearly observable. The obstacle here was the pH measurement in solutions. Therefore, the application of HCN/CN^- "*in situ* ^{13}C NMR pH-meter" seemed to be the most reliable method. MT measurements were performed in samples with different $[OH^-]$ concentration. The graphical representation of the calculated pseudo first order rate constants as a function of $[OH^-]$ is shown on Figure IV.3.16. The rate equation was obtained by the least square fitting of a straight line to the k_{obs}– $[OH^-]$ data-pairs. The values obtained for the slope and intercept yielded the corresponding k_1 and k_2. Thus, the expression for the pseudo first order rate constant is:

$$k_{30}^{obs} = d[Sy]/dt[Sy] = k_1 + k_2 \cdot [OH^-] \qquad \text{(IV.3.8.)}$$

where $k_1 = 0.08 \pm 0.01\ s^{-1}$ and $k_2 = 59 \pm 10\ M^{-1}s^{-1}$. So, the rate equation is:

$$v = k_1[Sy] + k_2[Sy] \cdot [OH^-] \qquad \text{(IV.3.9.)}$$

This two term rate equation for the *inter*-molecular ligand exchange can be explained by the existence of two different parallel steps: (a) a non-hydroxide catalyzed or water assisted dissociation of the coordinated citrate, (b) a second order, hydroxide catalyzed reaction. According to our knowledge, this kind of ligand exchange reaction for Al-complexes was not described in the literature so far, although similar phenomena were observed for bismuth–citrate in basic solutions.[113-115] The activation parameters would help to comment the mechanism. Their values are possible to obtain from the results presented earlier.

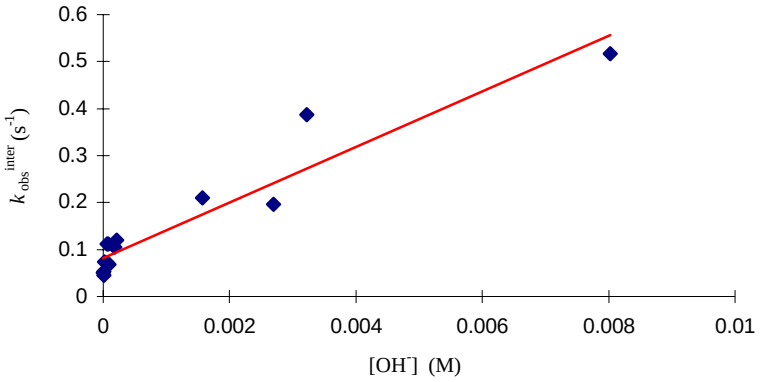

Figure IV.3.16. Graphical representation of the k_{30}^{obs} values obtained from MT experiments as a function of [OH^-]. Dots represent measured points, and the continuous line is the fitted curve.(R^2 = 0.9064)

We have a variation of k_{30}^{obs} with temperature based on four measured points (three from ^{1}H NMR shown in Table IV.3.6. at 325, 345 and 355 K, and one from ^{13}C NMR MT at 298 K) in a 57 °C interval for which ΔH^* = 55 ± 7 kJ mol^{-1} and ΔS^* = – 78 ± 21 J mol^{-1} K^{-1} are calculated. In the light of these information a discussion of the mechanism can be done taking separately the two steps:

(a) for this step a $v = k_1 \cdot [Sy]$ first order rate equation has to be valid, meaning this follows a pure dissociative (D) mechanism. In other words the rate determining step is a slow process with the formation of a Sy^* complex followed by a fast citrate exchange. The scheme for this process is:

$$Sy \xrightarrow{\text{r.d.s.}} Sy^{\#}$$

$$Sy^{\#} + \text{Cit}^* \overset{\text{fast}}{\rightleftharpoons} Sy + \text{Cit}$$

The nature of complex $Sy^{\#}$ has to be clarified taking into account the value of ΔS^* as well.

(*i*) $Sy^{\#}$ is a complex with only two coordinated citrates. This is hardly probable, as for the supposed process: $Al_3(OH)_4(H_{-1}Cit)_3 \rightarrow Al_3(OH)_4(H_{-1}Cit)_2 + H_{-1}Cit$ the value of ΔS^* should be positive as the transition state should be more disordered.

(*ii*) if not a D, than an I mechanism is operative. But in this case a second order rate equation should have been obtained. This can be explained only by the

intervention of a H_2O molecule, which entering into *Sy* results a more ordered transition state for $Sy^{\#}$:

$$Al_3(OH)_4(H_{-1}Cit)_3 + H_2O \rightarrow Al_3(OH)_4(H_{-1}Cit)_3,H_2O$$

(*iii*) something between (*i*) and (*ii*). In the r.d.s. the rupture of one coordinative bond takes place and a H_2O molecule skips into the appearing free place. This new species ($Sy^{\#}$) will be more hydrated, consequently the entropy is decreasing. In the second step the labilized citrate will exchange rapidly.

The presented arguments lead to the conclusion that a water assisted dissociation of the coordinated citrate is happening.

(b) The contribution of the second order process exceeds the first order path only at $[OH^-] > 2\cdot10^{-3}$ M, i.e. pH > 11.3. At these pH values, even at excess of citrate over Al^{3+} the equilibrium system is getting shifted to the formation of $Al(OH)_4^-$. It seems that a hydroxide attack on the $Al_3(OH)_4$–core of *Sy* speeds up the ligand exchange reaction substantially. According to the (tentative) structure of *Sy*, all the three Al^{3+} in this trimer are coordinated by two μ_2 and one μ_3–OH^- groups, therefore the reaction of any of the Al-centers with an additional OH^- could readily result in the formation of an $Al(OH)_4$ unit in the intermediate. When this entire $Al(OH)_4$ unit leaves the intermediate, the rest of *Sy* should decompose in one or several fast elementary step(s). The overall reaction can be written as:

$$Al_3(H_{-1}Cit)_3(OH)_4^{7-} + OH^- + H_2O \rightleftharpoons Al(OH)_4^- + 2\ Al(H_{-1}Cit)(OH)^{2-} + Cit^{3-}$$

Interestingly the mixed hydroxo complex, $Al(H_{-1}Cit)(OH)^{2-}$, is identified in the equilibrium system by pH potentiometry in a narrow pH range as a minor species just before all Al^{3+} are transferred from *Sy* to $Al(OH)_4^-$. It is worth mentioning that this transformation of *Sy* to $Al(OH)_4^-$ was much faster than that of *As* to *Sy*, see above. Not more than a few minutes was needed for equilibration, checked qualitatively by NMR.

In addition, the values of the activation parameters for the inter–molecular ligand exchange of *Sy* are very similar to the corresponding results obtained for the citrate exchange between $Al(Cit)_2^{3-}$ and free ligand (and $Al(acac)_3$),[2] i.e the very large decrease of entropy supports an I_a mechanism for the water assisted dissociation of *Sy*.

Here we can attempt to compare the lability of *Sy* against ligand exchange with free ligand to the same process of *As* and $Al(Cit)_2^{3-}$. As a matter of fact the pH ranges of the formation of the three complexes are different. Unfortunately the rate equations of the exchange reaction for *As* and $Al(Cit)_2^{3-}$ could not be

measured, therefore we know only the values of pseudo first order constants for these two species. These rate constants probably do not involve large contribution of a proton–assisted dissociation, because the ligands in the *As* complex do not show any unbound site for proton attacks, and the unbound donor sites in $Al(Cit)_2^{3-}$ are already protonated. In contrary, there are two paths for the ligand exchange of *Sy*, see equation IV.3.8. Obviously, the rate constant of water assisted monomolecular dissociation (k_1) of *Sy* is a suitable constant for the comparison to the k_{02}^{obs} and $k_{As,Free}^{obs}$ values of $Al(Cit)_2^{3-}$ and *As*, respectively. The values at 298 K for $Al(Cit)_2^{3-}$, *Sy* and *As* are 1.1 ± 0.1 s^{-1} , 0.08 ± 0.01 s^{-1} and <0.03 s^{-1}, respectively. Using these constants the labilities can be ordered as follows: $Al(Cit)_2^{3-}$>*Sy*>> *As*. (*Sy* >> *As* relation is based on the fact that $k_{As} \leq 0.03$ s^{-1} at 353 K). The next question to be addressed is, if these differences can be attributed to the different chemical surroundings at the metal centers or to the different coordination modes of the ligands in the three complexes. In fact the surrounding of Al^{3+} ions in *As* all having 3 alcoholic and one hydroxide μ_2-O donors in the very asymmetric core is very different from that of the other two complexes. *Sy* has the central ions in an $Al_3(OH)_4^{5+}$ core with two μ_2 and one μ_3–OH^- groups, and the monomeric $Al(Cit)_2^{3-}$ has only two equivalent tridentate citrate ligands bounded to Al^{3+}. There are no enough experimental data to decide equivocally if the differences in the quality of neighbour donor sites in the inner sphere of Al^{3+} atom(s) have or have no dramatic influence on the lability of the (other) coordinated citrate ligand(s). In fact all donors are oxygens, thus this influence might not be very important. Using this rough simplification, we can consider a relation between the difference of the coordination mode and the lability of the ligand in the individual complexes. It is obvious, that the bridging μ_2- and μ_3-citrates of *As* are very inert against substitution. The lability of tridentate citrates of $Al(cit)_2^{3-}$ and *Sy* seems to be affected by the protonation of the unbound carboxyl groups: the protonated ligands in $Al(cit)_2^{3-}$ are more labile then the deprotonated ones in *Sy*. At the same time there is a hydroxide-catalysed dissociation of the ligands in *Sy*.

The gap between the time scale of ligand exchange reactions and the formation kinetics of *As* and *Sy* is still very large: second(s) or tens of second for the former one and hours or days for the latter one. Additional studies are needed to follow the rate of the trimer formation.[116] What is clear, that the rate of the formation reactions can not be determined by the water exchange rate of

Al(ligand)$(H_2O)_x$, rather the rate of chelate ring-clause could be sterically controlled [117] even for the monomeric citrate species. The formation of the trimers has to be a multistep process. As there is no indication of dimer formation in macroscopic scale,[72] it may suggest, that these intermediates are formed at low concentrations in fast pre–equilibria. The rate determining step could be the oligomerisation. Considering the extremely slow formation of the trimers, the high stability of these species requires a very slow dissociation of these complexes. Our results, the unmeasurably slow ligand exchange for the *As* and the quite slow reaction for *Sy* are in accordance with this condition.

Table IV.3.7. Activation parameters of exchange reactions measured in this work together with selected literature values

Complex/ type of exchange reaction	Solvent	ΔH^* (kJ mol^{-1})	ΔS^* (J mol^{-1} K^{-1})	k_{298} (s^{-1})	Mechanism	Reference
$Al(H_2O)_6^{3+}$/ solvent exchange	water	85	+42	1.29	D/I_d	[24]
$Al(acac)_2$ (hfac)/ intra-molecular rearrangement	CH_2Cl_2	(90)[b]	(+45)[b]	0.86	bond-rupture	[112]
$Al(acac)_3$ / inter-m. ligand exchange	Hacac	85	–38	$9.1\cdot10^{-5}$	I_a	[109]
$Al(tfac)_3$ / intra-m. site exchange	$CDCl_3$	114	+68	0.65 at 84.5	bond-rupture	[111]
As / inter-m. ligand exchange	water	–	–	<0.03[a]	–	this work
As / intra-m.ster. rearrangement.	water	–	–	<0.03[a]	–	this work
$Al(cit)_2$ / inter-m. ligand exchange	water	43 ± 1	–90 ± 29	1.0 ± 0.1	I_a	this work,
Sy / water assisted inter-m. ligand exchange	water	65 ± 7	–78 ± 21	0.08 ± 0.01	I_a	this work
Sy / intra-m. rearrangement	water	70 ± 5	+ 34 ± 15	230	bond-rupture	this work

[a] $k_{353K} < 0.03\ s^{-1}$

[b] values in parentheses mean Arrhenius activation energies.

V. SUMMARY

In this thesis we report equilibrium, equilibrium dynamics and solution structure study of aluminium – fluoride, oxalate and citrate systems in aqueous solution by means of multinuclear (^{1}H, ^{19}F, ^{13}C and ^{27}Al) NMR and potentiometry. The following results were obtained.

We identified and re-determined the stability constants of $AlF_i^{(3-i)+}$ complexes (i = 1 – 5) using ^{19}F NMR. First time in the literature we directly detected the AlF_5^{2-} complex, but there was no spectroscopical evidence for the formation of AlF_6^{3-}. We proved that the stability constant of AlF_6^{3-}, if the limiting complex exists at all in aqueous solution, is $K_6 < 0.5$. We performed a complete dynamic analysis using the characteristic line broadening of the ^{19}F NMR signals and the incoherent magnetization transfer method. We detected only ligand substitution processes for which an associative interchange (I_a) mechanism was operative, while the H_2O substitution, *i.e.* complex formation, was much slower. We could identify *cis* and *trans* isomers of the AlF_2^+ species at lower temperatures.

In the aluminium – oxalate system we identified the $AlOx_i^{(3-2i)+}$ (i = 1 – 3) species by ^{13}C NMR measurements. Two signals were detected for $AlOx_2^{2-}$ and they were attributed to the *cis* and *trans* isomers. Dynamic NMR studies showed that the system was highly inert both for intra– and inter– molecular exchange reactions at room temperatures. At higher temperatures complete ^{13}C NMR band shape analysis was performed and the dynamic parameters of the *cis/trans* isomerization could be determined. We found that the rate determining step of this isomerisation was the breaking of one Al^{3+} - OOC bond.

Stability constants of four mixed complexes, AlFOx, AlF_2Ox^-, $AlFOx_2^{2-}$ and $AlF_2Ox_2^{3-}$, were determined in the Al^{3+} – fluoride – oxalate ternary system by potentiometric titrations. We confirmed and characterized these species by ^{19}F and ^{13}C NMR as well. The mixed complexes were dominant species at comparable concentration of fluoride and oxalate. Very complicated exchange phenomena were observed both in ^{19}F and ^{13}C NMR spectra. The lability of ligands was increased compared to those of the binary species.

We detected and characterized three Al^{3+} – citrate complexes: $Al(Cit)_2^{3-}$, $Al_3(OH)_4Cit_3^{7-}$ (*Sy)* and $Al_3(OH)(H_{-1}Cit)_3^{3-}$ (*As*) by ^{1}H and ^{13}C NMR. The first two species had symmetric structure, and they were fluxional. The *As* complex had

rigid structure and no fluxionality was observed on the T_1 time scale of the ^{13}C NMR up to 80 °C. The conformations for each citrate of *As* were described by using the $^2J_{HH}$ and $^3J_{CH}$ scalar coupling constant values. The solution stucture of *As* was found to be identical with the X-ray stucture is solid. Ligand exchange reactions between free citrate and the complexes, $Al(Cit)_2^{3-}$ and *Sy*, were investigated and on the basis of the rate equations and the activation parameters associative interchange (I_a) mechanism was proposed. The lability of the citrate ligand in the complexes could be ordered as follows: $Al(Cit)_2^{3-} > Sy >> As$.

Since a large amount of dynamic data was collected for the Al^{3+} – ligand (L) complexes, it is worth to compare their kinetic behaviour. An important similarity between the monodentate F^-, the bidentate oxalate (forming 5-membered chelate ring) and the tri- or tetradentate citrate (forming 5- or 6-membered chelates), was that the complex formation reactions, like $Al + L \rightleftharpoons AlL$, were too slow to be detected on the actual NMR time scales. This similarity can be rationalized by the existence of the same rate determining step, namely, the leaving of a water molecule from the inner sphere of Al^{3+}. Although the lability of the coordinated water could be increased by coordination of one or several donor atom(s) to the metal ion, it was still not enough to speed up the formation of higher complexes, *e.g.* $AlF_2^+ + F^- \rightleftharpoons AlF_3$, for dynamic NMR detection.

Different results were found for the ligand exchange reactions. *As* was very inert up to 80 °C. Ligand substitutions of type, $AlL^* + L \rightleftharpoons AlL + L^*$, were fast for AlF_2^+ and AlF_3 at room temperature, and an associative interchange mechanism (I_a) was suggested. This associative character might be related to the good penetration ability of the small sized F^- ligand. In the case of coordinatively saturated species, $Al(Cit)_2^{3-}$, *Sy* and $Al(Ox)_3^{3-}$, no bimolecular ligand exchange reactions were found. For these complexes the ligand exchange took place by the dissociation of the tridentate citrate or bidentate oxalate via dissociative interchange (I_d) mechanism. Isomerisations of the Werner type isomers, AlF_2^+ and $AlOx_2^-$ were intramolecular reactions. In case of the bidentate oxalate the rate determining step could not be the leaving of a H_2O molecule, it was rather the bond breaking of one arm of the coordinated oxalate.

In conclusion, the multinuclear NMR spectroscopy was found to be an exceptionally useful tool to collect different type of informations about the studied equilibrium systems.

VI. ÖSSZEFOGLALÁS

Az alumínium a XX század féme. Felfedezése a múlt század közepére esik, nagyobb tételben azonban csak a múlt század végén állították elő. Azidőtájt az ára az ezüstével vetekedett, annak ellenére, hogy a földkéregben előforduló leggyakoribb fém. Jelentősége a vaséval hasonlítható össze és alkalmazása is a vaséval együtt értékelhető. Ha az alumínium oldaláról vizsgálódunk, akkor könnyen észrevehetjük a következő előnyöket. Ötvözetei összevethető szilárdságúak az acélokéval, de jóval kevésbé korrodeálódnak (passziválódás) és jóval könnyebbek (7.8 g cm^{-3} és 2.7 g cm^{-3}). Ahol erős, de könnyű szerkezeti anyagra van szükség, mint pl. repülőgépipar, építőipar, ott az alumíniumot megtaláljuk. Az elektrotechnikai alkalmazás rávilágít az alumínium másik nagy előnyére, nevezetesen arra, hogy kicsi a fajlagos ellenállása, a drága réz helyett így az erősáramú elektrotechnika első számú fémes vezető anyaga. Az alumínium nem alattomos fém, a jelenlegi kutatási eredmények azt mutatják, hogy nem található meg az élő szervezetekben. Sem jelenléte, sem hiánya nem oka betegségeknek, legalábbis egyértelmű bizonyítékok ezt nem támasztják alá. A biokémiai és élettani ciklusban való megjelenése kizárólagosan az emberi tevékenység (ipari termelés) eredménye, következésképpen az élő szervezetekben nem fejlődött ki védekező rendszer ellene. Időről-időre felmerül toxikus volta. Az Alzheimer kór és az alumínium szervezetbeli jelenléte közötti kapcsolat nagyon valószínű, és az élő szervezetek kalcium és magnézium háztartásába való beépülésével is "alaposan gyanúsítható". Az alumínium biológiai szerepe az elmúlt évtizedek aktív kutatómunkája ellenére sem tekinthető tisztázottnak. Az azonban egyértelmű, hogy az Al^{3+} ion, hidrolízisre való erős hajlama miatt, csak komplex vegyületei formájában juthat el a "tetthelyre", ahol kedvező (gondoljunk terápiás alkalmazásaira) vagy káros hatását kifejtheti. A komplexképzésben a természetben előforduló fluorid és az oxigéntartalmú kismolekulák, például a citrát (Cit), oxalát (Ox) külön-külön és együttesen is szerepet játszanak, és a vizes oldatban elkerülhetetlenül jelenlévő OH^- ion hatása sem hanyagolható el. Az alumínium kémiájára vonatkozó ismereteink hiányosságának egyik oka az, hogy az alumínium igen nehezen vizsgálható. Az olcsó és könnyen hozzáférhető műszeres technikák számára rejtőzködő elem. A látható, infravörös és ultraibolya spektrofotometriai és az elektrokémiai módszerek csak igen közvetetten alkalmazhatók. Az NMR szempontjából a ^{27}Al atommag 100 %-os jelenlétével biztató lehetne, de az I=5/2 –

es értékű magspin és a belőle következő gyors kvadrupólus relaxáció, a széles jelek nem tették az NMR spektroszkópusok kedvelt mérési tárgyává. Így az alumínium komplexek oldatbeli szerkezetéről is keveset tudunk. Egyensúlyi kémiájának vizsgálata sem könnyű az előzőek szerint, amit még tetéz kinetikai inertsége is. Ennek következtében az alumíniumról szóló egyensúlyi tárgyú dolgozatok visszatérő gondja az "egyensúly elérése". Azt mondhatjuk, hogy az alumínium koordinációs kémiai vizsgálata kényszerűen mindig "kinetikával terhelt". A leírtak fényében a munkánk célja az volt, hogy:

1. megvizsgáljuk koordinációs kémiai igényességgel az Al^{3+} ion és néhány fémion – szállító ligandum (F^-, OH^-, oxalát, citrát) vizes oldatait az eddigi eredmények ellenőrzése céljából.
2. eszközként alkalmazva a multinukleáris NMR spektroszkópiát, elsősorban a ligandumok NMR aktív magjainak (^1H, ^{13}C és ^{19}F) mérésével közvetlen módszerrel igazoljuk az egyensúlyi modellekből következő részecskeeloszlást.
3. felhasználva az utóbbi évtized rohamos fejlődését a kismolekulák NMR spektroszkópiás szerkezetvizsgálatában, szerkezeti információkat gyűjtsünk a képződő komplexek oldatbeli szerkezetéről, és összevessük azt a szilárd komplexekre vonatkozó diffrakciós eredményekkel.
4. a dinamikus NMR teljes eszköztárát felsorakoztatva a gyakorlatilag hiányzó, vagy csak kvalitatív becsléseken alapuló egyensúlyi dinamikai információkat gyűjtsünk az Al^{3+} és az előzőekben felsorolt ligandumok vizes oldatbeli egyensúlyairól.

Legfontosabb kísérleti eszközünk a magmágneses rezonancia spektroszkópia (NMR) volt. A ^1H, ^{13}C, ^{19}F és ^{27}Al NMR spektrumokat Bruker 360 és 500 MHz–es készülékeken vettük fel és a WINNMR program segítségével dolgoztuk fel. Az egyszerű egydimenziós méréseken (^1H, ^{19}F) kívül ^{13}C NMR esetén a ^1H lecsatoláshoz az "inverse gated" és "power gated"; polarizáció átvitelhez a DEPT impulzusszekvenciákat alkalmaztuk. Szükség esetén a szerves kismolekulák tanulmányozásánál bevált két dimenziós korrelációs módszerekhez folyamodtunk: COSY, NOESY, ROESY, HETCOR, LR HETCOR. Ezek segítségével elvégezhető a jelazonosítás, esetenként a jelek intenzitásából a komplexek stabilitási állandói határozhatók meg. A csatolási séma és a $^2J_{HH}$ és $^3J_{CH}$ spin-spin csatolási állandók lehetővé teszik az oldatban lévő komplexek szerkezetének meghatározását.

VI. ÖSSZEFOGLALÁS

Az egyensúlyi rendszereinkben előforduló kémiai cserefolyamatokat mágnesezettség átviteli módszekkel tanulmányoztuk. A T_1 skálán történő méréseknél szelektív inverzióátvitelt egy dimenzióban a DANTE szekvenciával, két dimenzióban az EXSY impulzusszekvenciával végeztük. Az eredményeket a MATLAB programmal, a Gauss – Newton – Marquardt féle nem lineáris legkisebb négyzetek módszerével értékeltük. A T_2 skálán a jelszélesség mérése mellett a teljes jelalak analízist is alkalmaztuk. A spektrumokat a Bloch egyenletek mátrix formalizmusa alapján számoltuk ki, a mért és számolt spektrumokat jellegzetes adataik, a jelek szélessége, eltolódása és intenzitása alapján hasonlítottuk össze.

Egyensúlyi méréseket az alumínium – oxalát – fluorid rendszerben potenciometriás módszerrel, fluorid ionszelektív és kinhidron elektród együttes alkalmazásával végeztünk. A stabilitási szorzatokat, amelyek ún. sztöchiometriai állandók, a LETAGROP program alkalmazásával számítottuk ki.

Az oldatok pH-ját lehetőség szerint kombinált elektróddal mértük. Savas oldatokban az elektródot tönkretevő HF jelenlétében a F^-/HF ^{19}F NMR jelének, illetve nagy, nem állandó elektrolitkoncentráció elkerülhetetlensége folytán, lúgos oldatokban a CN^-/HCN ^{13}C NMR jelének kémiai eltolódását mérve "in situ" határoztuk meg a pH-t.

Munkánk során az alumínium és néhány fontos ligandum komplexének összetételét, oldatbeli szerkezetét és kinetikai sajátságait határoztuk meg multinukleáris NMR módszerekkel. Eredményeinkkel sikerült a korábban már vizsgált rendszerekre vonatkozó ismereteket kiegészíteni, pontosítani és az ellentmondások egy részét feloldani. Az egyensúlyok dinamikai jellemzésében gyökeresen új eredményeket értünk el.

Az alumínium – fluorid ^{19}F NMR vizsgálata során azonosítottuk a törzs komplexeket és a jelintenzitások segítségével kiszámoltuk ezek stabilitási állandóit. Az alkalmazott közegtől függően változott a részecskék száma. Így, 3 M KCl háttérelektrolit mellett az $AlF_i^{(3-i)+}$, i = 1 – 3, míg 0.6 M TMACl közegben az $AlF_i^{(3-i)+}$, i = 1 – 5 komplexek jelennek meg. Az irodalomban számos utalás történik az AlF_5^{2-} és AlF_6^{3-} részecskékre, ám létezésüket vizes oldatban eddig még nem igazolták. Az általunk felvett ^{19}F NMR spektrumok egyértelműen bizonyítják az AlF_5^{2-} komplex képződését, de nem utalnak AlF_6^{3-} jelenlétére még nagyon nagy F^- fölösleg mellett sem. Megállapítottuk, hogy ha ez a komplex mégis létezik vizes közegben, akkor stabilitási állandója, K_6 , < 0,5.

VI. ÖSSZEFOGLALÁS

Az alumínium – fluorid rendszerben megjelenő egyes törzskomplexek jelszélessége pH, illetve hőmérsékletfüggő. Teljes jelalak analízissel és mágnesezettség átviteli mérésekkel bizonyítottuk, hogy a rendszer egyensúlyi dinamikáját a F^- csere jellemzi és nem a komplexképződés. A fluoridcsere valószínűleg asszociatív interchange mechanizmussal írható le. Megállapítottuk, hogy a cseresebességi állandók értéke nagyobb a vízcserére vonatkozó állandókénál, és értékük a szubsztitúció mértékével nő. Alacsony hőmérsékleten az AlF_2^+ részecske *cisz* és *transz* izomerjei is azonosíthatóak.

Az alumínium – oxalát rendszerben ^{13}C NMR segítségével azonosítottuk a törzskomplexeket. Megállapítottuk, hogy szobahőmérsékleten nincs cserefolyamat sem a törzskomplexek, sem pedig ligandumcsere a komplexek és a szabad oxalát között. Az $AlOx_2^-$ komplexnek két azonos intenzitású jelét detektáltuk, ez a *cisz* és *transz* izomerekhez rendelhető. Vizsgáltuk az izomerizáció hőmérséklet függését, megállapítva, hogy az Al^{3+} belső koordinációs szférájában történik az átrendeződés. Az $AlOx_3^{3-}$ részecske és a szabad oxalát közötti csere csak magasabb hőmérsékleten észlelhető. A mágnesezettség átviteli kísérletek eredményeiből számolt aktiválási paraméterek D, vagy I_d mechanizmusra utalnak.

Az alumínium – fluorid – oxalát rendszerben négy vegyes ligandumú részecskét találtunk potenciometriásan ($AlFOx$, AlF_2Ox^-, $AlFOx_2^{2-}$, $AlF_2Ox_2^{3-}$) és kiszámoltuk a stabilitási állandókat. Összemérhető c_F és c_{Al} koncentrációviszonyok mellett a vegyes komplexek képződése meghatározó fontosságú. A komplexeket ^{13}C és ^{19}F NMR segítségével is azonosítottuk. Széles NMR jeleik és azok különös viselkedése a hőmérséklet növelésével bonyolult inter – és intra – molekuláris cserefolyamatok jelenlétére utal. Megállapítható, hogy akár a fluorid, akár az oxalát törzskomplexekhez viszonyítjuk, a vegyes ligandumú komplexekben a ligandumok labilisabbak.

Az alumínium – citrát rendszerben megjelenő egymagvú és hárommagvú komplexeket egyaránt azonosítottuk ^1H és ^{13}C NMR mérésekkel. Az $Al(Cit)_2^{3-}$ és a hárommagvú $Al_3(OH)_4(H_{-1}Cit)_3^{7-}$ (*Sy*) részecskék szerkezete oldatban viszonylag szimmetrikus, amint azt a jelszegény NMR spektrumok is alátámasztják. Elvégeztük a hárommagvú $Al_3(OH)(H_{-1}Cit)_3^{4-}$, (*As*), komplex esetén az igencsak jelgazdag ^1H és ^{13}C NMR spektrumok teljes hozzárendelését. A csatolási állandók értékeiből megadtuk a három különböző citrát ligandum térbeli elrendeződését. Eredményeinket összevetve az irodalomban közölt szilárd szerkezettel arra a következtetésre jutottunk, hogy vizes oldatban az *As* komplex megőrizte nem

szimmetrikus szerkezetét, és a ligandumok elrendezése igen hasonló a szilárd szerkezethez.

Tanulmányoztuk a már szerkezetileg is jellemzett három alumínium – citrát részecske kinetikai viselkedését. Az *As* komplex inert, nem vesz részt sem inter –, sem intra – molekuláris cserefolyamatokban. Megállapítottuk, hogy az $Al(Cit)_2^{3-}$ és *Sy* részecskék egyaránt fluxionálisak, ez utóbbi esetében kiszámítottuk az intra – molekuláris csere aktiválási paramétereit. Mindkét komplex cserekapcsolatban van a szabad citráttal. Az $Al(Cit)_2^{3-}$ esetén az aktiválási entrópia nagy negatív értéke asszociatív jellegű (I_a) mechanizmusra utal. A *Sy* komplex esetében a ligandumcsere dinamikáját leíró egyenlet: $w = k_1[Sy] + k_2[Sy][OH^-]$. Az első tag valószínűleg a víz koncentrációját is tartalmazza. Erre utal az aktiválási entrópia nagy negatív értéke. Az OH^- kinetikai szerepe magyarázható az egyik Al^{3+} – hoz való átmeneti koordinálódásával, ami a komplexet labilissá teszi. A komplexek labilitási sorrendje $Al(Cit)_2^{3-}$ > *Sy* >> *As*. A kinetikai sajátság változása jól értelmezhető a nem hídhelyzetű protonált háromfogú, illetve a deprotonált háromfogú citrát koordinációval a két első, valamint a négyfogú, hídhelyzetű ligandum jelenlétével a harmadik komplex esetében.

Az általunk vizsgált reakciók kinetikai adatait az alábbi táblázatban foglaltuk össze.

Cserefolyamat	ΔH^* (kJ mol^{-1})	ΔS^* (J mol^{-1} K^{-1})	k_{298} (s^{-1})	Mechanizmus
$AlOx_2^{2-}$ / intra	67 ± 5	–6 ± 6	5 ± 0,5	kötés felhasadás
$AlOx_3^{3-}$ / Ox	164 ± 17	225 ± 51	$6{,}6\cdot10^{-5}$	D/I_d
$Al(Cit)_2^{3-}$ / Cit	43 ± 1	–90 ± 29	1,0 ± 0,1	I_a
As / Cit	–	–	<0,03	–
As / intra	–	–	<0,03	–
Sy / intra	70 ± 5	34 ± 15	230	kötés felhasadás
Sy / Cit	65 ± 7	–78 ± 21	0,08±0,01	I_a

VII. REFERENCES

(1) *Chemistry of Aluminium, Gallium, Indium and Thallium*, A.J. Downs, Ed.; Blackie Academic & Professional: London, 1993.
(2) N. N. Greenwood, A. Earnshaw: *Chemistry of the Elements*, Butterworth – Heinemann: Oxford, 1997, 216 – 265.
(3) R. W. Smith: *Coord. Chem. Rev.*, **1996**, *149*, 81.
(4) N. Clarke: *PhD Thesis*, The Royal Institute of Technology, KTH, Stockholm, 1994.
(5) S. N. Mhatre, R. K. Iyer, P. N. Moorthy: *Magn. Res. Chem.*, **1993**, *31*, 169.
(6) B. D. LaZerte: *Can. J. Fish. Aquat. Sci.*, **1984**, *41*, 766.
(7) The Proceedings of a Symposium Organised by the Environment and Food Chemistry Groups of the Industrial Division of the Royal Society of Chemistry, London 17th May, 1988; Aluminium in Food and the Environment, J. R. Duffield, D. R. Williams p.1; W. K. Stewart, p. 6; J. A. Edwardson et al., p. 20.
(8) B. Corain, G. G. Bombi, A. Tapparo, M. Perazzolo, P. Zatta: *Coord. Chem. Rev.* **1996**, *149*, 11.
(9) J. W. Akitt: *Progress in NMR Spectrosc*., **1989**, *21*.
(10) A. Sparen: *PhD Thesis*, The Royal Institute of Technology, KTH, Stockholm, 1994.
(11) F. R. Venema: *PhD Thesis*, Technical University Delft, Delft, 1992.
(12) L.–O. Öhman: *PhD Thesis*, University of Umeå, Umeå, 1983.
(13) T. Hedlund: *PhD Thesis*, University of Umeå, Umeå, 1988.
(14) E. Marklund: *PhD Thesis*, University of Umeå, Umeå, 1990.
(15) M. Karlsson: *PhD Thesis*, University of Umeå, Umeå, 1998.
(16) A. Lakatos: *PhD Thesis*, University of Szeged, in preparation.
(17) L. – O. Öhman, W. Forsling: *Acta Chem. Scand. A.* , **1981**, *35*, 795.
(18) L. – O. Öhman, S. Sjöberg: *Acta Chem. Scand. A*, **1982**, *36*, 47.
(19) L. – O. Öhman, S. Sjöberg, N. Ingri: *Acta Chem. Scand. A*, **1983**, *37*, 561.
(20) L. – O. Öhman, S. Sjöberg: *Polyhedron*, **1983**, *2*, 1329.
(21) L. – O. Öhman, S. Sjöberg: *Acta Chem. Scand. A*, **1983**, *37*, 875.
(22) N. Herron, R. L. Harlow, D. L. Thorn: *Inorg. Chem.* **1993**, *32*, 2985.
(23) N. Herron, D. L. Thorn, R. L. Harlow, F. Davidson: *J. Am. Chem. Soc.*, **1993**, *115*, 3028.
(24) D. Hugi – Cleary, L. Helm, A. E. Mehrbach: *Helv. Chim. Acta*, **1985**, *18*, 545.

(25) J. Miceli; J. Stuehr: *J. Am. Chem. Soc.* **1968**, *90*, 6967.
(26) A. Walsleben, H. Strehlow: *J. Sol. Chem.* **1985**, *14*, 881.
(27) F. Secco, M. Venturini: *Inorg. Chem.* **1975**, *14*, 1978.
(28) B. Perlmutter–Haymann, E. Tapuhi: *Inorg. Chem.* **1977**, *16*, 2742.
(29) B. Perlmutter–Haymann, E. Tapuhi: *Inorg. Chem.* **1979**, *18*, 875.
(30) M. Eigen in *Advances in the Chemistry of Coordination Compounds*, S. Kirschner, Ed.; Macmillan: New York, 1961, p 371.
(31) R. B. Martin, *Coord. Chem. Rev.* , **1996**, *141*, 23.
(32) E. J. Martinez, J.–L. Girardet, C. Maerschalk, C. Morat: *Inorg. Chem.*, **1999**, *38*, 4765.
(33) J.–P. Issartel, A. Dupuis, C. Morat, J.–L. Girardet: *Eur. Biophys. J.* **1991**, *20*, 115.
(34) *Ullman's Encyclopaedia of Industrial Chemistry*, 5th completely revd. ed., VCH Verlag: Weinheim 1985, 566–568.
(35) C. Brosset, J. Orring: *Svensk Kem. Tidskr.*, **1943**, *5*, 101.
(36) M. Yamazaki, T. Takeuchi: *Kogyo Kagaku Zasshi*, **1967**, *70*, 656.
(37) S. P. Petrosyants, Y. A. Buslaev: *Koord. Khim.* **1979**, *5*, 163.
(38) S. P. Petrosyants, Y. A. Buslaev: *Koord. Khim.* **1981**, *7*, 907.
(39) D. Hass, S. P. Petrosyants, Y. A. Buslaev, I. Hartley: *Dokl. Akad. Nauk. SSSR* **1983**, *269*, 380.
(40) S. P. Petrosyants, Y. A. Buslaev: *Koord. Khim.* **1986**, *12*, 907.
(41) V. V. Kon'shin, B. N. Chernyshov, E. G. Ippolitov: *Dokl. Akad. Nauk. SSSR*, **1984**, *278*, 370 (Eng. ed.).
(42) E. J. Martinez, J. –L. Girardet, C. Morat: *Inorg. Chem.* **1996,** *35,* 706.
(43) V. V. Shurukin, Yu. A. Kozlov, V. V. Blochin, V. E. Mironov: *Russian J. of Phys. Chem.* **1976**, *50*, 145.
(44) B. J. Plankey, H. H. Patterson: *Inorg. Chem.* **1989**, *28*, 4331.
(45) P. Zbinden, *PhD Thesis*, University of Lausanne, Lausanne, Switzerland, 1994.
(46) M. Kesarwani, M. Azam, K. Natarajan, A. Mehta, A. Datta: *J. Biol. Chem.*, **2000**, *275*, 7230.
(47) T.E. Graedel: *J. Electrochem. Soc.*, **2000**, *147*, 1006.
(48) I. Hojgaard, H.G. Tiselius: *Urological Research,* **1999**, *27*, 397.
(49) M. Zysset, P. Blaser, J. Luster, A. Gehrig: *J. of Soil Science Soc. of America,* **1999**, *63*, 1106.

(50) W.C. Mahaney, K. Sanmugadas, R. Hancock: *Zeitschrift fur Geomorphologie*, **1999**, *43*, 393.
(51) R. Hamel, R. Levasseur, V.D. Appanna: *J. Inorg. Biochem.*, **1999**, *76*, 99.
(52) E. Bottari, L. Ciavatta *Gazz. Chim. Ital.* **1968**, 1004.
(53) S. Sjöberg, L.–O. Öhman, *J. Chem. Soc., Dalton Trans.* **1985**, 2665.
(54) L. Ciavatta, M. Iuliano, R. Porto: *Annali di Chimica*, **1999**, *89*, 51.
(55) D. Taylor: *Aust. J. Chem.*, **1978**, *31*, 1455.
(56) R. D. Gillard, S. H. Laurie, P. R. Mitchell: *J. Chem. Soc. A.* ,**1969**¸3006.
(57) N. Bulc, L. Golic, J. Siftar: *Acta Crystallogr. , Sect. C*, **1984**, *40*, 1829.
(58) P. Roman, C. Guzman – Miralles, A. Luque: *J. Chem. Soc., Dalton Trans.*, **1996**, 3985.
(59) P. Chaudhuri, H. Diebler: *J. Chem. Soc., Dalton Trans.*, **1977**, 596.
(60) P. M. Ehde, L. Pettersson, J. Glaser: *Acta Chem. Scand.* , **1991**, *45*, 998.
(61) B. L. Phillips, S. N. Crawford, W. H. Casey: *Geochim. Cosmochim. Acta*, **1997**, *61*, 4965.
(62) G. Smith, D. S. Sagatys, R. C. Bott, D. E. Lynch, C. H. L. Kennard: *Polyhedron* **1992**, *11,* 631.
(63) G. A. Banta, S. J. Rettig, A. Storr, J. Trotter: *Can. J. Chem.* ,**1985**, *63*, 2545.
(64) R. Job, P. J. Kelleher, W. C. Stallings, C. T. Monti, J. P. Glusker: *Inorg. Chem.*, **1982**, *21*, 3760.
(65) Z. H. Zhon, H. L. Wan, S. Z. Hu, K. R. Tsai: *Inorg. Chim. Acta* ,**1995**, *237*, 193.
(66) J. Strouse, S. W. Layten, C. E. Strouse: *J. Am. Chem. Soc.* ,**1977**, *19*, 562.
(67) M. Matzapetakis, C. P. Raptopoulou, A Terzis, A. Lakatos, T. Kiss, A. Salifoglou: *Inorg. Chem.* **1999**, *38*, 618.
(68) T. L. Feng, P. L. Gurian, M. D. Healy, A. R. Barron: *Inorg. Chem.* ,**1990**, *29*, 408.
(69) J. E. Gregor, H. K. J. Powell: *Aust. J. Chem.*, **1986**, *39*, 1851.
(70) R. J. Motekaitis, A. E. Martell: *Inorg. Chem.*, **1984**, *23*, 18.
(71) L.–O. Öhman , S. Sjöberg: *J. Chem. Soc., Dalton Trans.* **1983**, 2513.
(72) L.–O. Öhman: *Inorg. Chem.*, **1988**, *27*, 2565.
(73) H. M. Irving, M. G. Miles, L. P. Pettit: *Anal. Chim. Acta* , **1967**, *38*, 475.
(74) A. K. Covington, M. Paabo, R. A. Robinson, R. G. Bates: *Anal. Chem.*, **1968**, *40*, 700.
(75) J. Bene: *TDK Dolgozat*, Debrecen, 1996.

(76) L. van Geet Anthony: *Anal. Chem.* , **1970**, *42*, 679.
(77) A. E. Derome: *Modern NMR Techniques for Chemistry Research*, Pergamon: Exeter, 1987.
(78) F. J. M. van de Ven: *Multidimensional NMR is Liquids*, VCH Publishers: New York, 1995.
(79) S. Braun, H. – O. Kalinowski, S. Berger: *150 and More Basic NMR Experiments*, Wiley, VCH Verlag GmbH: Weinheim, 1998.
(80) *Two – Dimensional NMR Spectrospy*, W. R. Croasmun, R. M. K. Carlson, Ed.; VCH Publishers: New York, 1987.
(81) U. Weber, H. Thiele: *NMR Spectroscopy: Modern Spectral Analysis*, Wiley – VCH Verlag GmbH: Weinheim, 1998.
(82) P.Bigler: *NMR Spectroscopy: Processing Strategies*, VCH Verlagsgesellschaft mbH: Weinheim, 1997.
(83) M. T. Beck, I. Nagypál: *Chemistry of Complex Equilibria*, Akadémiai Kiadó: Budapest, 1989.
(84) G. Gran: *Analyst,* **1952**, *77*, 667.
(85) P. Brauner, L. G. Sillén, R. Whiteker: *Arkiv Kemi*, **1968**, *31*, 365.
(86) M. Braun, J. Posta, A. Löki: *XXXIX. Magyar Spektrokémiai Vándorgyűlés*, Mosonmagyaróvár, **1996**, Sept. 4–6, p.71–74.
(87) N. Parthasaraty, J. Buffle, W. Haerdi: *Can. J. Chem.*,**1986**, *64*, 24.
(88) B. R. Martin: *Biochem. Biophys. Res. Commun.* , **1988**, *155*, 1194.
(89) A. M. Bond, G. T. Hefter: *Critical Survey of Stability Constants and related Thermodynamic Data of Fluoride Complexes in Aqueous Solution*, IUPAC Chemical Date Series No. 27; Pergamon: Oxford, 1980.
(90) S. F. Lincoln, A. E. Mehrbach in *Substitution Reaction of Solvated Metal Ions,* A. G. Sykes Ed., Advances in Inorganic Chemistry, Vol 42, Academic Press: London, 1995, pp 2–78.
(91) R. M. Fuoss: *J. Am. Chem. Soc.* , **1958**, *80*, 5059.
(92) B. J. Plankey, H. H. Patterson: *Inorg. Chem.*, **1989**, *28*, 4331.
(93) S. T. Lo, T. W. Swaddle: *Inorg. Chem.*, **1975**, *14*, 1878.
(94) Z. Szabó, J. Glaser, I. Grenthe: *Inorg. Chem*., **1996,** *35*, 2036.
(95) W. G. Baldwin, D. R. Stranks: *Aust. J. Chem.*, **1968,** *21*, 2161.
(96) D. Pouli, W. M. Smith: *Can. J. Chem.*, **1960,** *38*, 567.
(97) H. R. Watling, P. Sipos, L. Byrne, G. T. Hefter, P. M. May: *Appl. Spectrosc.*, **1999**, *53,* 415.

(98) H. R. Watling, S. D. Fleming, W. von Bronswijk: *J. Chem. Soc., Dalton Trans.*, **1998**, 3911.
(99) C. F. Baes, R. E. Mesmer: *The Hydrolysis of Cations*, Wiley: New York, 1976, 112.
(100) P. Sipos, P. M. May, G. T. Hefter: to be published.
(101) (a) P. M. Ehde: *PhD Thesis*, University of Umeå, Umeå, 1991; (b) Z. Szabó, I. Grenthe: *Inorg. Chem*., **1998**, *37*, 6214.
(102) MATLAB®, The Mathworks, Inc.
(103) K. G. Orrell, V. Šik, D. Stephenson: *Progr.in NMR Spectr.*, **1990**, *22*, 141.
(104) J. Nemes, I Tóth, L. Zékány: *J. Chem. Soc., Dalton Trans.*, **1998**, 2707.
(105) E. J. Martinez, J. – L. Girardet, C. Maerschalk, C. Morat: *Inorg. Chem*., **1999**, *38*, 4765.
(106) L. Szilágyi: *Mágneses Rezonancia*, Tankönyvkiadó, Budapest, 1977.
(107) W. A. Thomas: *Progr. Nucl. Magn. Res. Spect.*, **1997**, *30*, 183.
(108) P. E. Hansen: *Progr. Nucl. Magn. Res. Spect.*, **1981**, *14*, 175.
(109) K. Saito: *Polyhedron*, **1990**, *9*, 215.
(110) J. Sandsröm: *Dynamic NMR Spectroscopy*, Academic Press: London, 1982.
(111) D. L. Grossmann, D. T. Haworth, *Inorg. Chim. Acta*, **1984**, *84*,217.
(112) D. A. Case, T. J. Pinnavaia: *Inorg. Chem.*, **1971**, *10*, 482.
(113) E. Asato, W. L. Driessen, R. A. G. de Graaff, F. B. Hulsbergen, J. Reedijk: *Inorg. Chem.*, **1991**, *30*, 4210.
(114) E. Asato, K. Katsura, M. Mikuriya, T. Fujii, J. Reedijk: *Inorg. Chem.*, **1993**, *32*, 5322.
(115) E. Asato, K. Katsura, M. Mikuriya, U. Turpeinen, I. Mutikainen, J. Reedijk: *Inorg. Chem.*, **1995**, *34*, 2447.
(116) J. Burgess: *Ions in Solution*, Ellis Horwood Limited: Chichester, 1988.

ACKNOWLEDGEMENT

I would like to thank Imre Tóth for supervising me during these years and never giving up to deepen my coordination chemistry ‘sense’ and my chemical thinking; not even in my stubborn periods. I appreciate very much your corrections, suggestions and help in improving this thesis.

I am grateful to István Bányai that I finally learnt to feel and handle a kinetic system. Thanks for the cool NMR lessons and for our long discussions.

Köszönöm Zékány Lászlónak számítógépes ismereteim elmélyítését, az illesztéseknél nyújtott segítségét és a hibaszámoláshoz viszonyuló nézeteim alakítását.

I would like to thank prof. Ingmar Grenthe for giving me the possibility to discover the complicated world of easy looking potentiometry.

Vanka Jutka and Rózsa Béla are deeply acknowledged for the inevitable morning news and their help in laboratory work.

I am grateful to all members of the ‘rare elements group’ for the friendly atmosphere, for the daily teas and the unforgettable aqua regia.

Finally I want to thank my previous and present colleagues from Debrecen and Stockholm for the pleasant environment during these years.

Much of this of work was supported financially by the Hungarian Science Research Foundation, Project T 261115.